Monitoring the efficacy of aseptic sterilization processes by means of calorimetric and impedimetric sensing principles

Dissertation

zur

Erlangung des Doktorgrades

der Naturwissenschaften

(Dr. rer. nat.)

dem
Fachbereich Pharmazie
der Philipps-Universität Marburg
vorgelegt von
Jan Oberländer
aus **Düsseldorf**

Marburg/Lahn **2018**

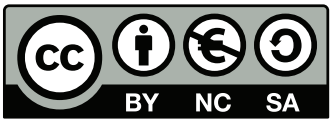

Gutachter: Prof. Dr. Michael J. Schöning

Gutachter: Prof. Dr. Michael Keusgen

Eingereicht am 30.05.2018

Tag der mündlichen Prüfung am 11.07.2018

Hochschulkennziffer: 1180

Erklärung

Ich versichere, dass ich meine Dissertation

"Monitoring the efficacy of aseptic sterilization processes by means of calorimetric and impedimetric sensing principles"

selbständig und ohne unerlaubte Hilfe angefertigt und mich dabei keiner anderen als der von mir ausdrücklich bezeichneten Quellen bedient habe. Alle vollständig oder sinngemäß übernommenen Zitate sind als solche gekennzeichnet.

Die Dissertation wurde in der jetzigen oder ähnlichen Form noch bei keiner Hochschule eingereicht und hat noch keinen sonstigen Prüfungszwecken gedient.

Marburg, den 30.05.2018 Jan Oberländer

Abstract

Package sterilization is an essential step during aseptic packaging of food, pharmaceuticals or medical instruments to prevent microbiological contamination of the product. In food industries, the main objective is to produce consumer-safe and long-term stable food products. In recent years, the favored method to sterilize package material is by use of gaseous hydrogen peroxide (H_2O_2) at concentrations up to 10% v/v and elevated temperatures up to 300 °C. These process parameters enable a fast and effective sterilization of packages prior to filling with sterile products within a process chain. Monitoring of this sensitive process is performed by predefined machine settings and laborious microbiological challenge tests, with earliest results after 72 hours. In previous works different sensors to monitor the packaging sterilization process have been developed, but till now there is no commercial system available to continuously monitor the final gas concentration or the microbial sterilization efficacy online within the package.

In the present work, as a first approach the sensing principle of a calorimetric H_2O_2 gas sensor has been studied in more detail. The sensor is based on a differential set-up of one catalytically activated and one passivated temperature-sensing element. Surface characterizations have been performed to reveal the chemical reaction of H_2O_2 at the applied catalyst manganese(IV) oxide (MnO_2). The surface characterization depicted a transition of the manganese oxidation state. Moreover, the treatment with H_2O_2 eliminates the polymeric layer on top of the catalyst, which has been applied as polymer matrix to attach the catalyst onto the sensing element. The calorimetric gas sensor has been further described by analytical expressions in order to evaluate the theoretical temperature rise. Thereby, different sensor scenarios (steady-state process, gas diffusion process and convective gas flow) have been described by the sensor's thermochemistry and physical transport mechanisms. These theoretical assumptions have been accompanied by surface and thermal characterizations of polymers applied as passivation materials. The characterizations demonstrate the suitability of the three investigated polymers (SU-8 photoresist, Teflon derivatives PFA and FEP), to act as a passivation against gaseous H_2O_2.

As second approach of this work, a novel biosensor has been developed. This biosensor is based on interdigitated electrodes (IDE) on which a standardized test organism is immobilized. This test microorganism, spores of *Bacillus atrophaeus*, is commonly applied in industrial microbiological challenge tests to evaluate the efficacy of sterilization processes. Impedance measurements are applied to characterize the microbiological samples at the sensor surface before and after the gaseous H_2O_2 sterilization process. Thereby, a remaining change in impedance and phase has been observed. Numerical simulation tools have been employed to analyze the sensor signal, and to gather material parameters of the spores. Finally, the impedimetric and calorimetric sensor have been

combined to serve as a miniaturized sensor system to analyze the efficacy of the gaseous sterilization process.

Contents

Acronyms

AC: alternating current

AFM: atomic force microscopy

APTES: 3-aminopropyltriethoxysilane

ATCC: American type culture collection

ATR-FTIR: attenuated total reflection Fourier transform infrared spectroscopy

cfu: colony forming unit

DC: direct current

DMSO: dimethyl sulfoxide

DNA: deoxyribonucleic acid

DSC: differential scanning calorimetry

DSMZ: Deutsche Sammlung von Mikroorganismen und Zellkulturen

FDA: Food and Drug Administration

FEM: finite element method

FEP: fluorinated ethylene propylene

H_2O_2: hydrogen peroxide

IDE: interdigitated electrode

LCR-meter: measurement system to analyze inductive (L), capacitive (C), and resistive (R) elements

LCR: logarithmic cycle reduction

LSE: least square error

MnO_2: manganese(IV) oxide

Pd: palladium

PE: polyethylene

PET: polyethylene terephtalate

PFA: perfluoralkoxy

ppm: parts per million

PS: polystyrene

Pt: platinum

RIE: reactive ion etching

RTD: resistance temperature detector

SEM: scanning electron microscopy

SiO_2: silicon dioxide

TEM: transmission electron microscopy

TGA: thermogravimetric anlysis

Ti: titanium

UV: ultraviolet

VDMA: Verband Deutscher Maschinen- und Anlagenbau e.V.

VOC: volatile organic compound

XPS: X-ray photoelectron spectroscopy

1 Introduction

1.1 Aseptic processing

Aseptic processing and packaging is widely applied in pharmaceutical, medical and food industries. The aseptic process defines the ability to process and produce commercially sterile products and preventing recontamination by microorganisms, as well as their enduring forms, such as exo- or endospores [1–3].

In aseptic processing, sterilized products are packaged under sterile conditions into separately sterilized packages. In food industries, aseptic processing facilitates extended product shelf-life without adding preservative to the goods. Moreover, aseptic processing enables a fast product sterilization applying moderate thermal processes, as compared to canned food with a subsequent autoclaving process. Thereby, food nutrients, such as heat-sensitive vitamins, can be preserved [4].

Liquid food products, like dairy products, are mainly sterilized by thermal treatment between 70 °C and 150 °C for a defined period of time. Depending on the applied time and temperature, the process can be classified, according to [4–7] as given in Tab. 1.1. For dairy products the thermal sterilization is mostly combined with microfiltration, whereby a high level of sterility can be assured [8].

Tab. 1.1: Different temperature and time conditions applied for food sterilization and preservation.

Process	Temperature (°C)	Time (s)
Pasteurization	70–75	15–30
Extended shelf-life (ESL)	120–134	1–4
Ultra high-temperature (UHT)	135–143	1–4

1.2 Packaging sterilization processes

In aseptic food packaging the most critical process to prevent products' recontamination is by package sterilization. Since, storage and handling of package prior to filling can result in a microbial load between 2–8 cfu cm^{-2} (cfu: colony forming unit) [9]. The required logarithmic cycle reduction (LCR) for the sterilization is predefined by the type of product, the storage temperature and the shelf-life. For sterile, low-acid products (pH $>$ 4.5) a six-fold decimal reduction of bacterial spores is required. If *Clostridium botulinum* spores might grow in the product, then a full 12-fold decimal reduction must be achieved [10].

In dependence of the packaging material, different sterilization processes are currently employed; either: heat, chemical or physical treatment or a combination thereof [11,

12]. The sterilization process needs to be compatible with the packaging material; typical materials are: glass bottles, bottles made of polyethylene terephthalate (PET), polystyrene (PS) cups and composite packages made out of different layers of polyethylene (PE), paper board and aluminum. Moreover, the package sterilization need to fulfill the following criteria:

- high microbicidal and sporicidal activity at short exposure times;
- volatile compound, resulting in a minimum of sterilant residues on the packaging material;
- not harmful towards the packaging material nor to the product to be filled;
- applicability of the sterilization method in-line of a process chain or in a batch process;
- non-toxicity for the technician as well as the product consumers (minimized occupational hazards).

The different package sterilization methods will be described subsequently.

1.2.1 Heat sterilization

Thermal sterilization is one of the state-of-the-art methods to sterilize surfaces or materials. The process can be divided into dry heat and steam (moist heat). Dry heat is a hot air treatment without present water molecules, whereas steam is gaseous water with or without air or gas. It has been demonstrated, the sterilization by applying steam is more efficient than with dry air. For example, a steam sterilization at 121 °C for 20 min has the same efficiency as compared to dry heat sterilization at 170 °C for 60 min [10]. Nonetheless, dry heat sterilization is applied for aseptic glass vials in pharmacy, at air temperatures of 300–330 °C. Additionally, dry heat is applied during extrusion processes of package foil (temperatures up to 200 °C), which achieves a sterile packaging material within seconds.

The sterilization by applying steam is quite more challenging, especially to apply saturated steam, which is highly efficient in short exposure times. For this application the steam and packaging material must be under pressure in a specially designed chamber. Thus, the sterilization process is usually applied as a batch process. In food industries thermal sterilization is a common process applied for canned food products. During aseptic processing this method is applied to sterilize e.g., aluminum lids, metal cans or glass bottles. For this, the material to be sterilized need to withstand this thermal stress. Additional cooling systems on the outside of the packaging material have been implemented to enlarge the applicability, for example, to deep-drawn polystyrene (PS) cups [10, 12].

The principle of thermal sterilization differs by the sterilization method: dry heat causes mainly a dehydration of microorganisms following by coagulation and oxidation of proteins of the microorganisms. Whereas beside the protein coagulation, moist heat induces irreversible denaturation of essential enzymes, structural proteins and DNA (deoxyribonucleic acid), which causes inactivation of microorganisms [12, 13].

1.2.2 Irradiation

Sterilization by irradiation is performed by electromagnetic wave applied to the device to be sterilized. In general, electromagnetic waves are characterized by wavelength (λ) and resultant energy (E) as shown in Eqs. (1.1) and (1.2).

$$\lambda f = c \tag{1.1}$$

$$E = hf = \frac{hc}{\lambda} \tag{1.2}$$

Here, f is the frequency, c is the speed of light in vacuum ($3 \cdot 10^8$ ms^{-1}) and h is the Planck's constant (4.135^{-15} eV $\cdot$ s) [14].

Ultraviolet light

Ultraviolet (UV) light is a relatively low energetic radiation, which is differentiated by its wavelength/energy into UV-A to UV-C. For sterilization purposes the high energetic UV-C radiation is applied with a wavelength of 100–280 nm. The radiation energy is sufficient to excite electrons of molecules in a higher energy orbital resulting in more reactive molecules. The absorption of the UV light energy by microorganisms can result in DNA mutations. In addition, the absorbed energy is responsible for covalent binding between adjacent thymine bases, which inhibits the reproduction of the microorganism [14]. Main drawback of this method is the low penetration depth of UV light. In which, shadowing effects caused by dust particles or multilayered microorganisms, as well as cavities in pre-formed packages, result in insufficient sterility.

In aseptic systems UV light is commonly applied in combination with a chemical medium such as hydrogen peroxide or peracetic acid. In this combination, UV irradiation results in reactive radical formation, where a high microbicidal and sporicidal efficiency can be achieved. Additionally, UV irradiation results in reduced H_2O_2 residuals on the package material [5, 10, 12, 15].

Ionizing radiation

Ionizing radiation is a highly efficient sterilization method, which penetrates deep into objects to be sterilized. It can be differentiated by the type of radiation; for sterilization mainly α-, β-, γ-, X-rays and electron beam are of interest. Commercially, sterilization with γ-rays from a cobalt-60 or cesium-137 source is applied to sterilize sealed products in food, medical and pharmaceutical industries, as well as equipment for biotechnology.

The mode of action of ionizing radiation relies on the structural modification of the genome of microbiological organisms such as bacteria, viruses, molds and spores. The radiation can directly interact with the DNA. The irradiation can cause single-strand breaks, which can be repaired by using the second strand as template. Moreover, it can also induce the more severe double-strand break. The both DNA damages result in reproduction failures, which can cause mutations [16]. A further effect can be allocated to electron displacement of the irradiated product, i.e. water molecules, which generates free radicals, such as $OH^{\bullet}$, that can induce DNA damage [17].

Main drawback of these method is the complexity of the system design. The radiation source needs to be specially shielded from the environment and operating personal. Furthermore, the sterilization of food products and packages by radiation is still disputable, due to adverse effects and thereby consumers are reluctant to purchase irradiated food [18–20]. The interaction with packaging material and the resulting effects toward the filled product are still under investigations, for example, the molecular modification of the polymeric structure of packaging materials [17].

1.2.3 Chemical sterilization methods

Beside thermal or irradiation sources applied for sterilization, different chemical media are applied in package sterilization processes. The application form of the medium varies between the companies and the type of packaging and surface materials to be sterilized.

Hydrogen peroxide H_2O_2

The discovery of hydrogen peroxide (H_2O_2) is assigned to L. J. Thenard in 1818; he studied reactions by combining nitric acid with barium peroxide; after precipitation of barium nitrate he received an oxygen-rich solution, firstly he concluded that the acid became oxygenated [21]. Thenard later improved the production of H_2O_2 by use of hydrochloric and sulfuric acid instead of nitric acid [22]. Right after discovery and industrial production of H_2O_2 the antiseptic effects and application as wound disinfectant as well as microbicidal agent have been described [23, 24].

H_2O_2 is a clear, colorless liquid; it is the simplest peroxide compound, consisting of oxygen and hydrogen. H_2O_2 is weakly acidic and has strong oxidizing properties [25]. It is highly reactive and produces different kinds of radicals during decomposition, like hydroxyl and hydroperoxyl ($HO^\bullet$, $HO_2{}^\bullet$), and further reactive species of oxygen and hydrogen, such as $O_2{}^{\bullet-}$, $O^\bullet$ and $H^\bullet$, finally only the environmentally friendly end-products water and oxygen remain [24, 26]. Beside the application as sterilant or disinfectant, H_2O_2 is widely applied as reactive oxidant, for example, as bleaching agent, cleaning agent during thin-film processing in semiconductor industries or in high concentrations as a propellant of aeronautics and space rockets [27].

In recent years, package sterilization by applying hydrogen peroxide as chemical sterilization medium in food and pharmaceutical industries has become very favorable. In case of semi-rigid composite packages in food industries, H_2O_2 is either applied as a liquid at temperatures between 60–80 °C or at elevated temperatures (140–300 °C) as vapor-phase medium. Both methods are combined with a latter thermal or radiation (e.g., UV light) treatment to remove the excess of H_2O_2, whereby the decomposition of H_2O_2 accompanied by reactive species is accelerated [1, 12, 28]. The efficiency of the sterilization by H_2O_2 is mainly dependent on the concentration, temperature and exposure time. In case of the vapor-phase application humidity, gas flow and condensation are further factors [29–31]. After the sterilization process the residual concentration of H_2O_2 must be less than 0.5 parts per million (ppm), as recommended by the Food and Drug Administration (FDA, USA), to avoid off-flavor or oxidation of the food product [32].

A multitude of investigations has been performed to unravel the mechanism of microbicidal and sporicidal actions of liquid- and vapor-phase H_2O_2 and is still in focus of ongoing research [24, 33]. The microbicidal activity is associated to the oxidizing properties of H_2O_2, whereby oxidation of various structural macromolecules, such as proteins, lipids, carbohydrates and nucleic acids, occurs [24, 26]. This results in damage of the protective cell membrane, loss of outer structural integrity and thereby, increase in cell permeability [34]. The final cell death is believed to occur by the localized generation of short-lived hydroxyl radicals and the strand break of DNA [35, 36].

In case of the more resilient microbiological spores, a slightly different mechanism is discussed in literature. The spores are consisting of a more complex membrane structure of multiple layers (Fig. 1.1), whereby the penetration of liquid H_2O_2 is inhibited for a certain time [37]. One of the layers, the so-called coat, plays a major role in the resistance. Enzymes loosely attached to this coat, such as superoxide dismutase and catalase, can inactivate toxic chemicals [38, 39]. Additionally, the DNA of spores is protected by small-acid soluble proteins (SASP) against oxidizing agents [40–43]. Thereby, the mechanism of H_2O_2 is believed to inactivate spores by oxidizing essential proteins. This results in the damage of the spore's inner membrane, thus creating pores and channels, causing loss of spore and cell integrity and leakage of inner substances [39, 44].

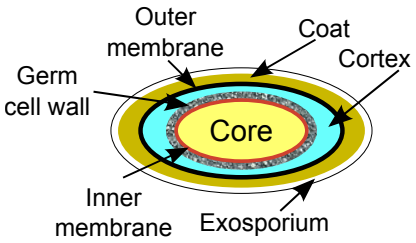

Fig. 1.1: Schematic structure of *Bacillus* spore layers (not to scale). The given exosporium is not present for all spore species; adapted from [45], with permission from Elsevier.

The mode of action of gaseous or vapor-phase H_2O_2 is also a topic of current research [26, 46–48]. The higher kinetic energy of the molecules and the higher availability of radicals at elevated temperature are some factors, which are responsible for irreparable damage of resilient microorganisms and spores [26, 49]. Additionally, the effect of H_2O_2 condensation needs to be taken into account during vapor sterilization. By vaporization of a 30% aqueous H_2O_2 solution, the molar fraction of condensed H_2O_2 during sterilization of aseptic packages has been evaluated to be 120 times higher compared to the present gas phase [50]. The enriched H_2O_2 concentration of the condensate originates from the zeotropic mixture of H_2O_2 and water, each of a different vapor pressure [51–53]. Thereby, H_2O_2 condenses earlier than the water and higher sporicidal activity can be achieved in short exposure time [50].

In conclusion, the sterilization with H_2O_2 is a well-established and approved process. The precise mechanism, however, is still missing, especially the effect of H_2O_2 and resulting radicals on the protected DNA or interactions on molecular level are not identified at the present time [54]. The knowledge of these factors would be helpful to develop highly efficient sterilization systems.

Peracetic acid (PAA)

Peracetic acid (PAA) is an organic peroxyacid consisting of an equilibrium mixture of H_2O_2 and acetic acid. Due to its oxidizing and corrosive properties it is an efficient sterilization and bleaching agent with a high reactivity [55]. PAA rapidly breaks down to oxygen, water and acetic acid. Compared to pure H_2O_2, the sterilization efficiency against bacteria, spores and fungi can be reached at lower temperatures (40–60 °C) [4, 56, 57]. In aseptic systems PAA is applied to sterilize bottles made from PET or low-density polyethylene (LDPE). The bottles can be rinsed with liquid PAA for a certain period of time, and subsequently rinsed with sterile water to avoid product contamination and off-flavor of the product [15]. Further application forms of PAA are spraying as aerosol or heated vapor [4]. The mode of action of PAA is mainly described by oxidative damage of microbiological macromolecules such as proteins, carbohydrates, lipids and nucleic acids [56, 58]. PAA additionally possesses the ability to denature proteins and enzymes by disruption of proteinaceous sulfhydryl (−SH) and sulfur (S−S) bonds and thereby increasing the cell wall permeability to PAA [26, 58].

The presented sterilization technologies are all applied in food industries. This work is focused on the sensor development and characterization to monitor the sterilization process by means of gaseous H_2O_2. Beside the sterilization of packages in food industries, gaseous H_2O_2 becomes of interest to sterilize vessels or isolators in pharmaceutical industries as well as tubes and devices for medical applications. Thereby, a fast and reliable method to monitor this gaseous sterilization process is of great interest.

1.3 Validation methods of industrial food package sterilization processes

In terms of quality control, the set-up of new sterilization systems or the optimization procedures it is necessary to validate the sterilization efficiency: on the one hand, to fulfill governmental requirements of aseptic packaging, on the other hand, to guarantee consumer safe products. The currently applied methods as well as governmental regulations will be described in this section.

1.3.1 State-of-the-art validation of food package sterilization processes

The state-of-the-art method to validate and quantify sterilization efficiencies relies on microbiological challenge tests. The following two methods are the standards recommended by the FDA (USA), Institute for Thermal Processing Specialists (IFTPS) (Canada), Verband Deutscher Maschinen- und Anlagenbau e.V. (VDMA) and Verein Deutscher Ingenieure (VDI) (Germany) to prove the effectiveness of industrial filling machines [2, 59–61]:

- count-reduction test;
- end-point test.

For both methods, test packages are artificially contaminated with a known number of microorganisms, resilient against the applied sterilization process. To evaluate sterilization processes with vaporized H_2O_2, spores of *Bacillus atrophaeus* are applied as resilient bioindicator [62–64]. The artificial contamination is either performed by spray inoculation of the overall package surface or by spot inoculation on positions within the package, which are critical to sterilize, the so-called: cold spots.

Count-reduction test

In case of the count-reduction test, contaminated packages (at least 10^5 colony forming units (cfu) per package) are fed to the aseptic filling machine. After the sterilization process, the packages are filled with a sterile test medium (e.g., skimmed milk or pipettable, filterable liquid). The test medium is applied to rinse the package and to recover the microorganisms from the package material. In case of flat packaging the microorganisms might also be recovered by swabs as described in [65]. In order to enumerate the surviving microorganisms of control (non-sterile) packages and after the sterilization process, samples of the test medium are distributed on plate count agar and incubated at prescribed temperature and time (e.g., 30 °C, 2-3 days for *B. atrophaeus*). After incubation the grown colonies are counted, and the difference between the number before N_0 and after N_s the sterilization process defines the count reduction rate. The effectiveness of the sterilization process is determined by at least $j = 20$ packages fed to the sterilization process and a control of $i = 5$ non-sterile packages to consider statistical fluctuations. The resulting mean logarithmic count reduction ($\mathrm{mLCR_{cr}}$) can be calculated by Eq. (1.3) [60].

$$\mathrm{mLCR_{cr}} = \log(\frac{1}{i}\sum_i N_{0,i}) - \log(\frac{1}{j}\sum_j N_{s,j}) \tag{1.3}$$

End-point test

To validate the sterilization efficiency based on the end-point test, the packages are artificially contaminated as before, but with three graduated infection stages, each stage a power of ten higher than the one before, for example an initial count $N_0 = \{10^3; 10^4; 10^5\}$ cfu. At least 100 packages of each stage are fed to the aseptic filling machine, performing a full filling process, including sterilization, filling and hermetical sealing. During the filling step a sterile incubation medium suitable for the applied microorganism is filled (e.g., skimmed milk or aseptic validation medium with pH indicator). These filled and sealed packages are incubated at least one week at 30 °C. After the incubation phase, the ratio between sterile and non-sterile packages can be determined to calculate the mean logarithmic count reduction ($\mathrm{mLCR_{ep}}$) by Eq. (1.4) [60].

$$\mathrm{mLCR_{ep}} = \log(N_0) - \log(\ln\left(\frac{\text{number of packages tested}}{\text{number of sterile packages}}\right)) \tag{1.4}$$

A further method to determine the mean logarithmic count reduction of the end-point test has been described by applying the most probable number (MPN) method, which

is based on statistic data evaluation of microbiological growth [66].

Both methods are valuable challenge tests, to determine the effectiveness of the sterilization process. Moreover, the count-reduction test can be used to identify cold spots within the packages. Thereby, a mapping of the package can be performed. Whereas, the end-point test is able to reveal weaknesses of the overall aseptic filling process, for example, sterility assessment of the product tank, product filler and packaging material. The difference of the test results can be assigned to the diverse post-processing after package sterilization. In both cases, the packages are guided through the aseptic filling machine, in case of the count-reduction test the surviving colonies can be recovered by a rinsing method or using swabs, which can be performed without applying the filler and sealer station of the aseptic packaging machine. Whereas, during the end-point test the packages are filled and sealed on the aseptic filling machine.

The disadvantages of both methods is the time- and lab-consuming procedure, especially to enable statistical evaluation a large number of test packages is necessary. Thereby, the sterilization efficiency during filling processes is only evaluated by retained samples of the filled products. The described challenge tests are mainly applied during periodic maintenance or after part exchange or repair [67].

Thereby, a sensor-based solution to monitor critical parameters, such as H_2O_2 concentration and temperature within the packages, would be beneficial to enable a higher throughput and time-to-market release. Moreover, a sensor which can detect the impact of the sterilization process directly on resilient microorganism would enable an increased process control and reliability at the production site.

1.3.2 Sensor-based validation

In order to overcome the limitations of the time-consuming and costly test methods introduced in the last section, there is a need for a sensor-based validation, to facilitate a parametric product release and to reduce the costly storage of filled products at production sites.

Commercially available H_2O_2 sensors are either based on electrochemical detection (e.g., Dräger AG & Co. KGaA) or on absorption spectroscopy of infrared light (e.g., Picarro, Inc.). These devices are not applicable as inline monitor, due to the size, the applicable temperature range, but most critically, the limited H_2O_2 concentration range up to 1000 ppm, whereas the concentration in aseptic filling machines might reach up to 10% v/v ($\hat{=}10\times10^4$ ppm) [68, 69]. Since no such commercial system is available, the H_2O_2 concentration can only be monitored in sample packages filled with sterile water and applying colorimetric test strips (e.g., peroxide test, Merck KGaA, Germany), whereby no online process control is possible. Additionally, the machine operating companies rely on monitoring the set-values of H_2O_2 dosage and measured parameters of e.g., H_2O_2 flow, air flow and temperature. But, monitoring of these parameters cannot predict the successful application of H_2O_2 within the package, for example, due to leakage of H_2O_2 after flow controller.

In order to overcome these limitations and to increase the parametrization of the sterilization processes applying gaseous H_2O_2 at elevated temperature, different sensor-

based methods have already been proposed and developed [31, 70–72]. One of these methods relies on the calorimetric detection of H_2O_2 vapor at elevated temperatures. The calorimetric measurement principle will be described in more details in Sec. 2.1. In these previous works an approach was presented to correlate the measurement signal with microbiological kill rate studies [73, 74].

Regarding the microbiological evaluations various commercial system are available to observe bacterial growth during incubation in media, e.g., BacTrac®, SY-Lab GmbH; R.A.B.I.T.®, Don Whitley Scientific Ltd. [75]. With these systems the storage and product release time can already be reduced. The principle of these systems are differentiated between direct and indirect impedance measurement.

The direct impedimetric detection of cell growth is based on electric conductivity changes within the culture medium, which is a result of the metabolic conversion of nutrition, thereby the conductivity of the medium is increasing. This conductivity increase is detected by electrodes directly immersed into the culture medium [76].

The indirect impedimetric method detects the metabolic CO_2 production. Therefore, impedance electrodes are placed, for example, in a potassium hydroxide (KOH) solution, which are in a sealed container with the culture medium to be monitored. The increased CO_2 concentration within KOH solution results in a decrease of electric conductivity [77]. Both detection methods are also described in industry standards to enumerate microorganisms in food samples [78, 79].

Furthermore, a current trend of research focuses on sensors, which are able to detect microorganisms or their growth within complex media such as food substances [80–82]. In which, the most promising principle is based on electrochemical impedance measurements, beside others such as optical or piezoelectric technologies [83]. In order to detect cells of various origin impedance spectroscopy is combined with interdigitated electrodes (IDE), whereby a label-free detection can be realized [84–88]. For example, this type of sensors is applied to characterize morphology changes during growth of mammalian cells [89]. The impedance spectroscopy of IDEs can be also used to characterize and typecast erythrocytes [86].

But all of these state-of-the-art techniques are not able to directly detect interactions between the gaseous H_2O_2 sterilization process and the microorganisms as bioindicator. Therefore, a novel sensor, which captures these interactions will be developed in this thesis (see Chapters 5–9). Due to the previously described advantageous application of IDEs, this kind of electrode structure has been chosen to characterize the impact of the gaseous H_2O_2 sterilization process towards the microbiological spores of *B. atrophaeus* by means of impedance analysis. A fundamental introduction of the impedance measurement principle will be given in Sec. 2.2.

1.4 Outline of this work

1.4.1 Aim of this work

The increasing amount of aseptically produced goods demands a better process control, towards a parametric product release. As introduced above, vaporized H_2O_2 at temperatures up to 300 °C is the medium of choice to sterilize food packages. A sensor-

based method is necessary to capture process parameters, especially at the last point of the process chain, within the package. In recent works, different types of gas sensors, especially calorimetric gas sensors, have been developed to enable monitoring of critical factors such as concentration of H_2O_2 and temperature within the process for the first time [31, 70–72]. Further material characterizations and theoretical considerations of these previously developed calorimetric gas sensors will be performed within this thesis, to reveal additional information about the sensing principle. Even though a correlation between these sensor results and microbiological tests has been performed, the challenge remains that these sensors do not additionally allow to detect interactions on microbiological samples at the same time.

In order to overcome this limitation, the main focus of this work was to develop, fabricate and characterize a novel sensor, which is able to monitor the sterilization effects on microbiological indicator organisms. The sensor should facilitate a fast method to analyze the effectiveness of gaseous sterilization processes with respect to H_2O_2 by delivering an electrical read-out signal. The sensor should be able to characterize the process without further incubation or reagents. Thereby, the sensor captures not only one single parameter, but the overall interactions on the immobilized microorganisms. In future, these sensors might be implemented in special test packages and fed through the sterilization process, in order to evaluate the sterilization efficacy in-line without requiring a production stop. In parallel to this thesis, Julio Arreola works on the immobilization strategy of the microbiological compartment onto the sensor surface and studies the microbiological impact of the sterilization process towards the microbiological spores.

1.4.2 Content of this work

In **Chapter 2**, the fundamental, applied principles of the sensors will be introduced, namely calorimetric gas sensing and impedance spectroscopy. The further content of this thesis can be divided into two main parts:

- Part I: characterization and theoretical considerations of calorimetric H_2O_2 gas sensors for aseptic sterilization processes.
- Part II: developing and characterization of an impedimetric biosensor to validate aseptic sterilization processes.

In the first part of this thesis, further analyses, characterizations as well as theoretical modeling of the calorimetric gas sensors to monitor gaseous sterilization processes applying H_2O_2 are presented; these sensors have been introduced by [31, 70–72].

In order to increase the fundamental knowledge about the decomposition mechanism of H_2O_2 in combination with one of the common catalysts, manganese(IV) oxide (MnO_2), characterizations of the catalyst have been performed. X-ray-induced photoelectron spectroscopy (XPS) has been applied to reveal the oxidation states of MnO_2 before and after exposure to H_2O_2 at process conditions. Thereby, a pathway of H_2O_2 decomposition on MnO_2 has been proposed and discussed in **Chapter 3**.

In **Chapter 4**, theoretical considerations of the calorimetric gas sensor have been performed. The thermochemistry of the calorimetric sensor has been considered with respect to the endothermal reaction of H_2O_2. Furthermore, different aspects of physical

transport phenomena, such as diffusion and forced convection, have been taken into account. Additionally, material characterizations of three polymers (SU-8 photoresist, perfluoralkoxy (PFA), fluorinated ethylene propylene (FEP)) have been performed. These polymer materials have been applied as passivation layer to avoid interaction of the sensor electrodes with the sterilization medium, like corrosion and deterioration of their structure. In the presented studies, their thermal stability and resistance against the harsh sterilization conditions have been investigated by differential scanning calorimetry (DSC), thermogravimetric analysis (TGA) and attenuated total reflection Fourier transform infrared spectroscopy (ATR-FTIR).

In the second part of this thesis, a novel sensor set-up to monitor interactions between the H_2O_2 sterilization process and the bioindicator, spores of *Bacillus atrophaeus*, will be introduced. The developed sensor consists of a differential set-up of interdigitated electrodes (IDE). One IDE serves as a reference (blank structure) to capture or study effects of the sterilization process on the sensor materials. On the second IDE, the microbiological indicator, spores of *B. atrophaeus*, have been immobilized.

In **Chapter 5**, theoretical models, analytical and numerical, are generated and applied to evaluate the sensor response. Comparisons with sensor measurements have been performed. The numerical model of the 3D sensor geometry could be reduced due to symmetry to a 2D model, which reduces the computational time. To increase the accuracy of the numerical simulation, profilometric investigations of the sensor geometry have been examined.

In **Chapter 6**, a finite element method (FEM) model has been extended by introducing a porous layer being representative for the immobilized spores. The model has been adjusted by literature values of the substrate material. Three different sensor states have been investigated: blank electrode structure, immobilized spores and after sterilization process. By applying FEM optimization routines, the tool has been applied to derive electrical material properties of the spore layer at different states.

The FEM-based simulations within these chapters have been performed in cooperation with Zaid B. Jildeh.

In **Chapter 7**, the development, fabrication process and application of the spore-based biosensor in industrial sterilization processes has been demonstrated for the first time. The sensor was in-house fabricated by applying standard lithography and lift-off techniques. First analyzes applying impedance spectroscopy were performed. Moreover, physical characterizations of the sensor by atomic force microscopy (AFM) and scanning electron microscopy (SEM) have been performed.

In **Chapter 8**, a strategy to functionalize the developed transducer structures (sensor surface) by means of an organosilane (3-aminopropyltriethoxysilane (APTES)) has been investigated. Focus of this study was to enhance the immobilization of the resilient spores onto to the sensor surface. Therefore, different sensor materials were characterized independently, namely silicon dioxide (SiO_2) and platinum (Pt) as well as their combination on chip level. The functionalized surfaces have been characterized by physical methods such as contact angle measurement, AFM, SEM and ellipsometry in order to reveal the morphology and surface properties. Impedance spectroscopy of the sensor has been applied to characterize the functionalization on sensor level. Moreover,

the immobilization of spores has been studied by microbiological methods, thereby the number of attached spores has been evaluated. The immobilization strategy has been developed by Julio Arreola.

In **Chapter 9**, a sensor-based study accompanied by microbiological reduction tests as well as calorimetric H_2O_2 measurements have been overviewed. Morphological characterizations, SEM and transmission electron microscopy (TEM), of *B. atrophaeus* spores have been conducted to investigate the impact of the sterilization process at different H_2O_2 concentrations. Finally, the results of the impedimetric, spore-based biosensor have been combined with both the calorimetric H_2O_2 measurement and the microbiological validation: thereby, an approach with two different sensing principles enables prediction of the kill rate.

References

[1] B. A. H. von Bockelmann and I. L. I. von Bockelmann. *Long-Life Products: Heat-Treated, Aseptically Packed: A Guide to Quality*. Åkarp, Sweden: B. von Bockelmann, 1998.

[2] Institute for Thermal Processing Specialists. *Guidelines for microbiological validation of the sterilization of aseptic filling machines and packages, including containers and closures (Doc no. G.005.V1)*. Guelph, Canada. 2011. URL: `http://www.iftps.org`.

[3] T. Sandle. "Sterility, sterilization and microorganisms". In: *Sterility, Sterilization and Sterility Assurance for Pharmaceuticals*. Ed. by T. Sandle. Vol. 32. Woodhead Publishing Series in Biomedicine. Oxford, UK: Elsevier, 2013, 1–20.

[4] E. M. A. Willhoft, ed. *Aseptic Processing and Packaging of Particulate Foods*. Boston, MA, USA: Springer US, 1993.

[5] G. Rysstad and J. Kolstad. "Extended shelf life milk – advances in technology". *International Journal of Dairy Technology* 59 (2006), 85–96.

[6] H. Deeth and M. Lewis. *High Temperature Processing of Milk and Milk Products*. Hoboken, NJ, USA: John Wiley & Sons, Inc., 2017.

[7] Verein Deutscher Ingenieure. *Hygienic requirements for the production and aseptically filling of beverage products: principles and design criteria*. Beuth Verlag GmbH. Berlin, Germany. VDI 4066-1. 2013.

[8] W. Hoffmann, C. Kiesner, I. Clawin-Rädecker, D. Martin, K. Einhoff, P. C. Lorenzen, H. Meisel, P. Hammer, G. Suhren, and P. Teufel. "Processing of extended shelf life milk using microfiltration". *International Journal of Dairy Technology* 59 (2006), 229–235.

[9] N. S. Buchner. *Verpackung von Lebensmitteln: Lebensmitteltechnologische, verpackungstechnische und mikrobiologische Grundlagen*. 1st ed. Berlin, Germany: Springer-Verlag GmbH, 1999.

[10] G. L. Robertson. *Food Packaging: Principles and Practice*. 3rd ed. Boca Raton, FL, USA: CRC Press, 2013.

[11] R. T. Toledo. "Overview of sterilization methods for aseptic packaging materials". In: *Food and Packaging Interactions: Developed from a Symposium Sponsored by the Division of Agricultural and Food Chemistry at the 193rd Meeting of the American Chemical Society, Denver, Colorado, April 5-10, 1987*. Ed. by J. H. Hotchkiss. Vol. 365. ACS symposium series. Washington, DC, USA: American Chemical Society, 1988, 94–105.

[12] I. A. Ansari and A. K. Datta. "An overview of sterilization methods for packaging materials used in aseptic packaging systems". *Food and Bioproducts Processing* 81 (2003), 57–65.

[13] T. Sandle, ed. *Sterility, Sterilization and Sterility Assurance for Pharmaceuticals: Technology, Validation and Current Regulations*. Vol. 32. Woodhead Publishing Series in Biomedicine. Oxford, UK: Elsevier, 2013.

[14] M. R. Adams and M. O. Moss, eds. *Food Microbiology*. 3rd ed. Cambridge, UK: Royal Society of Chemistry, 2008.

[15] J. R. D. David, R. H. Graves, and T. Szemplenski, eds. *Handbook of Aseptic Processing and Packaging*. 2nd ed. Boca Raton, FL, USA: CRC Press, 2012.

[16] K. Valerie and L. F. Povirk. "Regulation and mechanisms of mammalian double-strand break repair". *Oncogene* 22 (2003), 5792–5812.

[17] K. A. da Silva Aquino. "Sterilization by gamma irradiation". In: *Gamma Radiation*. Ed. by F. Adrovic. Rijeka, Croatia: InTech, 2012.

[18] K. M. Morehouse and V. Komolprasert. "Irradiation of food and packaging: an overview". In: *Irradiation of Food and Packaging*. Ed. by V. Komolprasert and K. M. Morehouse. Vol. 875. ACS symposium series. Washington, DC: American Chemical Society, 2004, 1–11.

[19] R. F. Eustice and C. M. Bruhn. "Consumer acceptance and marketing of irradiated foods". In: *Food Irradiation Research and Technology*. Ed. by C. H. Sommers and X. Fan. Vol. 68. Institute of Food Technologists Series. Ames, IA, USA: Wiley-Blackwell, 2012, 173–195.

[20] Y.-K. Ham, H.-W. Kim, K.-E. Hwang, D.-H. Song, Y.-J. Kim, Y.-S. Choi, B.-S. Song, J.-H. Park, and C.-J. Kim. "Effects of irradiation source and dose level on quality characteristics of processed meat products". *Radiation Physics and Chemistry* 130 (2017), 259–264.

[21] L. J. Thenard. "Observations sur des nouvelles combinaisons entre l'oxigène et divers acides". *Annales de Chimie et de Physique* 8 (1818), 306–312.

[22] W. C. Schumb, C. N. Satterfield, and R. L. Wentworth. *Hydrogen Peroxide: Part One*. Cambridge, MA, USA: Massachusetts Institute of Technology, 1953.

[23] C. Marchand. *The Therapeutical Applications of Peroxide of Hydrogen (medicinal), Glycozone and Hydrozone*. 9th ed. New York, NY, USA, 1895.

[24] G. McDonnell. "The use of hydrogen peroxide for disinfection and sterilization applications". In: *PATAI'S Chemistry of Functional Groups*. Ed. by Z. Rappoport. Chichester, UK: John Wiley & Sons, Ltd, 2009, 1–34.

[25] G. Goor, J. Glenneberg, and S. Jacobi. "Hydrogen peroxide". In: *Ullmann's Encyclopedia of Industrial Chemistry*. Weinheim, Germany: Wiley-VCH Verlag, 2007.

[26] M. Finnegan, E. Linley, S. P. Denyer, G. McDonnell, C. Simons, and J. Y. Maillard. "Mode of action of hydrogen peroxide and other oxidizing agents: differences between liquid and gas forms". *The Journal of Antimicrobial Chemotherapy* 65 (2010), 2108–2115.

[27] Evonik Resource Efficiency GmbH. *Hydrogen peroxide application areas*. Essen, Germany. 2016. URL: `http://h2o2.evonik.com`.

[28] E. L. Mitchell. "A review of aseptic processing". In: *Advances in Food Research*. Advances in Food Research. New York: Academic Press, 1988, 1–37.

[29] B. Wilke. "Wirkung von Wasserstoffperoxid in flüssiger und gasförmiger Phase bei der Sterilisation von Packmitteln". PhD thesis. Hohenheim, Germany: Universität Hohenheim, 1992.

[30] B. Unger-Bimczok, V. Kottke, C. Hertel, and J. Rauschnabel. "The influence of humidity, hydrogen peroxide concentration, and condensation on the inactivation of *Geobacillus stearothermophilus* spores with hydrogen peroxide vapor". *Journal of Pharmaceutical Innovation* 3 (2008), 123–133.

[31] P. Kirchner, S. Reisert, and M. J. Schöning. "Calorimetric gas sensors for hydrogen peroxide monitoring in aseptic food processes". In: *Gas Sensing Fundamentals*. Ed. by C.-D. Kohl and T. Wagner. Springer Series on Chemical Sensors and Biosensors. Heidelberg, Germany: Springer-Verlag GmbH, 2014, 279–310.

[32] Food and Drug Administration. *Code of federal registrations: food and drugs: indirect food additives: adjuvants, production aids, and sanitizers*. Code of Federal Regulations (CFR). 2011. URL: `http://www.fda.gov`.

[33] J. R. Rickloff. "Hydrogen peroxide gas decontamination". In: *Advanced Aseptic Processing Technology*. Ed. by J. Agalloco and J. E. Akers. Drugs and the Pharmaceutical Sciences. Boca Raton, FL, USA: CRC Press, 2010, 289–308.

[34] S. Baatout, P. de Boever, and M. Mergeay. "Physiological changes induced in four bacterial strains following oxidative stress". *Prikladnaia Biokhimiia i Mikrobiologiia* 42 (2006), 418–427.

[35] S. E. Wallen. "Sporicidal action of hydrogen peroxide". PhD thesis. Ames, IA, USA: Iowa State University, 1976.

[36] J. Cadet, T. Delatour, T. Douki, D. Gasparutto, J.-P. Pouget, J.-L. Ravanat, and S. Sauvaigo. "Hydroxyl radicals and DNA base damage". *Mutation Research* 424 (1999), 9–21.

[37] A. W. Friedline, M. M. Zachariah, A. N. Middaugh, R. Garimella, P. A. Vaishampayan, and C. V. Rice. "Sterilization resistance of bacterial spores explained with water chemistry". *The Journal of Physical Chemistry. B* 119 (2015), 14033–14044.

[38] P. Setlow. "Spores of *Bacillus subtilis*: their resistance to and killing by radiation, heat and chemicals". *Journal of Applied Microbiology* 101 (2006), 514–525.

[39] P. Setlow. "Resistance of bacterial spores". In: *Bacterial Stress Responses*. Ed. by G. Storz and R. Hengge. Monograph, ASM Press. Washington, DC, USA: ASM Press, 2011, 319–332.

[40] B. Setlow and P. Setlow. "Binding of small, acid-soluble spore proteins to DNA plays a significant role in the resistance of *Bacillus subtilis* spores to hydrogen peroxide". *Applied and Environmental Microbiology* 59 (1993), 3418–3423.

[41] P. Setlow. "Mechanisms for the prevention of damage to DNA in spores of *Bacillus* species". *Annual Review of Microbiology* 49 (1995), 29–54.

[42] B. Setlow, C. A. Setlow, and P. Setlow. "Killing bacterial spores by organic hydroperoxides". *Journal of Industrial Microbiology and Biotechnology* 18 (1997), 384–388.

[43] E. Melly, A. E. Cowan, and P. Setlow. "Studies on the mechanism of killing of *Bacillus subtilis* spores by hydrogen peroxide". *Journal of Applied Microbiology* 93 (2002), 316–325.

[44] D. E. Cortezzo, K. Koziol-Dube, B. Setlow, and P. Setlow. "Treatment with oxidizing agents damages the inner membrane of spores of *Bacillus subtilis* and sensitizes spores to subsequent stress". *Journal of Applied Microbiology* 97 (2004), 838–852.

[45] D. Paredes-Sabja, P. Setlow, and M. R. Sarker. "Germination of spores of *Bacillales* and *Clostridiales* species: mechanisms and proteins involved". *Trends in Microbiology* 19 (2011), 85–94.

[46] P. Engelhard. "Inaktivieren von Mikroorganismen auf festen Oberflächen mittels Atmosphären aus feuchter Luft/Wasserstoffperoxid und IR-Behandlung". PhD thesis. München, Germany: Technische Universität München, 2006.

[47] P. Engelhard and U. Kulozik. "Packstoffentkeimung mittels Wasserstoffperoxid – Methoden und Kombinationsverfahren". *Chemie Ingenieur Technik* 78 (2006), 1717–1722.

[48] S. Spanu and G. Vignali. "Modelling and multi-objective optimization of the VHP pouch packaging sterilization process". *International Journal of Food Engineering* 12 (2016), 739–752.

[49] J. Wang and R. T. Toledo. "Sporicidal properties of mixtures of hydrogen peroxide vapor and hot air". *Food Technology* 40 (1986), 60–67.

[50] K. Pruss, S. Stirtzel, and U. Kulozik. "Influence of the surface temperature of packaging specimens on the inactivation of *Bacillus* spores by means of gaseous H_2O_2". *Journal of Applied Microbiology* 112 (2012), 493–501.

[51] K. Hatanaka and Y. Shibauchi. "Sterilization method and apparatus therefor". US 4,797,255. 1989.

[52] D. Watling, C. Ryle, M. Parks, and M. Christopher. "Theoretical analysis of the condensation of hydrogen peroxide gas and water vapor as used in surface decontamination". *PDA Journal of Pharmaceutical Science and Technology* 56 (2002), 291–299.

[53] S. L. Manatt and M. R. R. Manatt. "On the analyzes of mixture vapor pressure data: the hydrogen peroxide/water system and its excess thermodynamic functions". *Chemistry - A European Journal* 10 (2004), 6540–6557.

[54] E. Linley, S. P. Denyer, G. McDonnell, C. Simons, and J. Y. Maillard. "Use of hydrogen peroxide as a biocide: new consideration of its mechanisms of biocidal action". *The Journal of Antimicrobial Chemotherapy* 67 (2012), 1589–1596.

[55] M. Baldry. "The bactericidal, fungicidal and sporicidal properties of hydrogen peroxide and peracetic acid". *Journal of Applied Bacteriology* 54 (1983), 417–423.

[56] G. McDonnell. "Peroxygens and other forms of oxygen: their use for effective cleaning, disinfection, and sterilization". In: *New Biocides Development*. Ed. by P. C. Zhu. Vol. 967. ACS symposium series. Washington, D.C, USA: American Chemical Society, 2007, 292–308.

[57] I. Grand, M. N. Bellon-Fontaine, J. M. Herry, D. Hilaire, F. X. Moriconi, and M. Naitali. "The resistance of *Bacillus atrophaeus* spores to the bactericidal activity of peracetic acid is influenced by both the nature of the solid substrates and the mode of contamination". *Journal of Applied Microbiology* 109 (2010), 1706–1714.

[58] G. McDonnell and A. D. Russell. "Antiseptics and disinfectants: activity, action, and resistance". *Clinical Microbiology Reviews* 12 (1999), 147–179.

[59] Food and Drug Administration. *Guide to Inspections of Aseptic Processing and Packaging for the Food Industry*. 2001.

[60] Verband Deutscher Maschinen- und Anlagenbau e.V. "Code of practice: filling machines of VDMA hygiene class V: testing the effectiveness of packaging sterilization devices". *VDMA-Fachverbandsschriften* 6 (2008), 1–16.

[61] Verein Deutscher Ingenieure. *Hygiene requirements for the production and aseptic filling of beverages and dairy products: hints to microbiological performance tests*. Beuth Verlag GmbH. Berlin, Germany. VDI 4066-3. 2014.

[62] D. Fritze and R. Pukall. "Reclassification of bioindicator strains *Bacillus subtilis* DSM 675 and *Bacillus subtilis* DSM 2277 as *Bacillus atrophaeus*". *International Journal of Systematic and Evolutionary Microbiology* 51 (2001), 35–37.

[63] P. Muranyi and J. Wunderlich. "Mikrobiologische Validierung von hygienischen und aseptischen Abfüllanlagen mit resistenzgeprüften Testorganismen". *Pharma und Food* (2015), 1–4.

[64] S. R. Sella, L. P. S. Vandenberghe, and C. R. Soccol. "*Bacillus atrophaeus*: main characteristics and biotechnological applications - a review". *Critical Reviews in Biotechnology* 35 (2015), 533–545.

[65] Deutsches Institut für Normung e.V. *Bestimmung des Oberflächenkeimgehaltes auf Einrichtungs- und Bedarfsgegenständen im Lebensmittelbereich*. Beuth Verlag GmbH. Berlin, Germany. DIN 10113-1-3. 1997.

[66] G. Moruzzi, W. E. Garthright, and J. D. Floros. "Aseptic packaging machine pre-sterilization and package sterilization: statistical aspects of microbiological validation". *Food Control* 11 (2000), 57–66.

[67] Verband Deutscher Maschinen- und Anlagenbau e.V. "Hygenische Abfüllmaschinen für die Nahrungsmittelindustrie: Checkliste Qualitätssicherung und Wartung". *VDMA-Fachverbandsschriften* 3 (2008), 1–32.

[68] Dräger. *DrägerSensor®- und Gasmessgeräte-Handbuch*. Lübeck, Germany: Dräger Safety AG & Co. KGaA, 2011.

[69] Picarro, Inc. *H_2O_2 analyzer*. Santa Clara, CA, USA. 2017. URL: `http://www.picarro.com`.

[70] N. Näther. "Entwicklung eines H_2O_2-Messverfahrens für die Überwachung der mikrobioziden Wirksamkeit bei der Sterilisation aseptischer Verpackungen". PhD thesis. Marburg, Germany: Philipps-Universität Marburg, 2009.

[71] P. Kirchner. "Thin-film calorimetric gas sensors for hydrogen peroxide monitoring in aseptic food processes". PhD thesis. Marburg, Germany: Philipps-Universität Marburg, 2013.

[72] S. Reisert. "Novel strategies for evaluating the effectiveness of aseptic sterilization processes by means of a multi-sensor set-up". PhD thesis. Hasselt, Belgium: Hasselt University, 2014.

[73] P. Kirchner, J. Oberländer, H.-P. Suso, G. Rysstad, M. Keusgen, and M. J. Schöning. "Monitoring the microbicidal effectiveness of gaseous hydrogen peroxide in sterilization processes by means of a calorimetric gas sensor". *Food Control* 31 (2013), 530–538.

[74] S. Reisert, H. Geissler, C. Weiler, P. H. Wagner, and M. J. Schöning. "Multiple sensor-type system for monitoring the microbicidal effectiveness of aseptic sterilization processes". *Food Control* 47 (2015), 615–622.

[75] SY-Lab Geräte GmbH. *BacTrac 4300: Mikrobiologisches Multi-Monitoring-System*. Neupurkersdorf, Austria. 2017. URL: `http://www.sylab.at`.

[76] P. Silley and S. Forsythe. "Impedance microbiology - a rapid change for microbiologists". *Journal of Applied Bacteriology* 80 (1996), 233–243.

[77] J. D. Owens, D. S. Thomas, P. S. Thompson, and W. Timmerman. "Indirect conductimetry: a novel approach to the conductimetric enumeration of microbial populations". *Letters in Applied Microbiology* 9 (1989), 245–249.

[78] Deutsches Institut für Normung e.V. *Grundlagen des Nachweises und der Bestimmung von Mikroorganismen in Lebensmitteln mittels Impedanz-Verfahren*. Beuth Verlag GmbH. Berlin, Germany. DIN 10115. 1999.

[79] Deutsches Institut für Normung e.V. *Untersuchung von Lebensmitteln – Zählung von Mikroorganismen mittels Impedanzverfahren – Bestimmung der aeroben mesophilen Keimzahl*. Beuth Verlag GmbH. Berlin, Germany. DIN 10122. 2005.

[80] Y. C. Lu, Y. S. Chuang, Y. Y. Chen, A. C. Shu, H. Y. Hsu, H. Y. Chang, and T. R. Yew. "Bacteria detection utilizing electrical conductivity". *Biosensors and Bioelectronics* 23 (2008), 1856–1861.

[81] D. L. Rosen, C. Sharpless, and L. B. McGown. "Bacterial spore detection and determination by use of terbium dipicolinate photoluminescence". *Analytical Chemistry* 69 (1997), 1082–1085.

[82] G. H. Lee, J.-C. Pyun, and S. Cho. "Electrical impedance characterization of cell growth on interdigitated microelectrode array". *Journal of Nanoscience and Nanotechnology* 14 (2014), 8342–8346.

[83] R. T. Noble. "A review of technologies for rapid detection of bacteria in recreational waters". *Journal of Water and Health* 3 (2005), 381–392.

[84] P. Cady, S. W. Dufour, J. Shaw, and S. J. Kraeger. "Electrical impedance measurements: rapid method for detecting and monitoring microorganisms". *Journal of Clinical Microbiology* 7 (1978), 265–272.

[85] M. Brischwein, S. Herrmann, W. Vonau, F. Berthold, H. Grothe, E. R. Motrescu, and B. Wolf. "Electric cell-substrate impedance sensing with screen printed electrode structures". *Lab on a Chip* 6 (2006), 819–822.

[86] S. Aigner. "Mikrostrukturierte Interdigitalkondensatoren zur Typisierung und Charakterisierung von Erythrozyten mittels kapazitativer und resistiver Messprinzipien und massensensitiver Messungen". PhD thesis. Wien, Austria: Universität Wien, 2011.

[87] N. Couniot, D. Flandre, L. A. Francis, and A. Afzalian. "Bacteria detection with interdigitated microelectrodes: noise consideration and design optimization". *Procedia Engineering* 47 (2012), 188–191.

[88] M. A. Mansor and M. R. Ahmad. "Single cell electrical characterization techniques". *International Journal of Molecular Sciences* 16 (2015), 12686–12712.

[89] I. Giaever and C. R. Keese. "A morphological biosensor for mammalian cells". *Nature* 366 (1993), 591–592.

2 Theory of sensing principles

2.1 Calorimetric gas sensing

Calorimetric or thermometric gas sensing has been introduced in 1910s and 1920s. In these years, the first electrically driven devices to monitor combustible gas concentrations (e.g., methane) in air have been patented [1, 2]. The development of gas sensors have been driven by the mining and coal industries, as well as by the companies of oil shipping. In both industries, the air quality requires monitoring due to safety issues. In coal mines the technical gas sensors replaced the canary bird and the inaccurate safety lamp to monitor the air quality [3, 4].

In general, the principle of calorimetric gas sensing can be differentiated into three types: thermal conductivity, adsorbent and catalytic gas sensors [5]. All these sensor types rely on the detection of temperature changes, which correlate with the present gas molecules. The temperature change can arise due to different thermal conductivities of the gas constituents or the chemical reactions at the sensor surface. In order to capture these temperature changes it is necessary to embed a highly sensitive and precise temperature measurement. Mostly, a differential set-up is applied for all of these principles, which is based e.g., on two resistance temperature detectors (RTD). The differential set-up can be realized as follows, one RTD is used for sensing applied in the gas to be analyzed (R_{sens}), and the second RTD is used as reference (R_{ref}), either specially passivated or placed in a separate housing, shielded against the gas [6]. The differential set-up enables the subtraction of thermal changes caused by e.g., variation in gas velocity, gas temperature or humidity. To analyze a gas of interest, both RTDs are adapted to an arm of a Wheatstone bridge circuit, as depicted in Fig. 2.1.

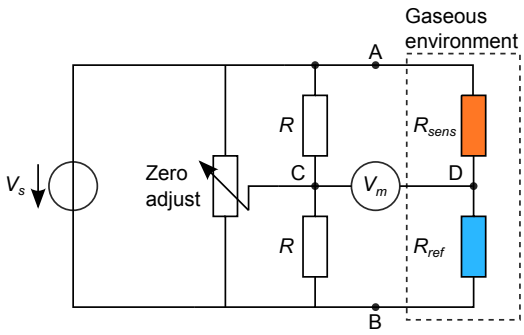

Fig. 2.1: Wheatstone bridge circuit depicting the supply voltage (V_s), the voltmeter (V_m), bridge resistors (R), zero adjustment potentiometer (Zero adjust) and the RTDs placed in the gaseous environment to be analyzed (modified from [7, 8]).

A supply voltage (V_s) is applied to heat the two RTDs to a desired temperature, e.g., for gas combustion, thermal conductivity measurements or adsorption/desorption analysis. During reference gas measurements or zero gas concentrations, the Wheatstone bridge is set to zero (by the zero adjustment potentiometer, s. Fig. 2.1), resulting in no voltage difference between point C and D ($V_m = 0\ V$). In case of an analyte present at the RTDs, the Wheatstone bridge becomes unbalanced, resulting in a measurable voltage difference. That is in correlation with the present gas concentration.

2.1.1 Thermal conductivity gas sensor

Gas analysis based on thermal conductivity is one of the longest known principles for determining gas concentrations [1, 6, 9]. In this principle, two passivated RTDs or coil wires are heated, a gas to be analyzed passing only one RTD (R_{sens}). Whereas, the second RTD (R_{ref}) is sealed or exposed to a reference gas, with same gas constituents and flow rate but lacking the analyte molecules. Due to the difference in gas constituents the Wheatstone bridge becomes unbalanced, as a result of individual heat transfer at the sensing element. Calibration to various gases can be performed, which is in relation with the thermal conductivity (λ) of the investigated gas.

The thermal conductivity of a gas is based on the kinetic gas theory, which gives the relation to the molar mass (M). For a monatomic gas the thermal conductivity can be described by Eq. (2.1), where the Chapman-Enskog theory is applied. In general, the smaller the gas molecules or atoms are, the better is the heat conduction due to molecular movement [10, 11].

$$\lambda = 0.0829 \frac{\sqrt{T/M}}{\sigma^2 \Omega_k} \tag{2.1}$$

Here, λ is in W m^{-1} K^{-1}, temperature (T) in K, M is the molar mass in g/mol, σ is the molecular collision diameter in Å, and Ω_k is the Lennard-Jones collision integral. The values of σ and Ω_k are both tabulated in Ref. [11].

The resulting power loss of a heated RTD or coil by heat conduction of the environmental gas can be described by Eq. (2.2).

$$P = k_{TC} \lambda \Delta T \tag{2.2}$$

Here P, is the power dissipation of the heater by thermal transport, k_{TC} is a constant for the given RTD geometry, and ΔT the temperature difference between heater and the surrounding gas [5].

Since, this type of gas sensor does not rely on flammability of the gas and the RTD temperature can be lower than the gas ignition temperature, it is applicable to analyze gas mixtures above the lower explosive limit (LEL). For example, this sensor type can be used to measure e.g., hydrogen, methane, carbon dioxide or helium in air between 0 and 100% v/v. Important fact to analyze gas concentrations with this sensor type is a significant difference in thermal conductivities of the two gases present [12].

2.1.2 Measurement of gas molecule adsorption/desorption enthalpies

Measurement of adsorption and desorption enthalpies is a further calorimetric principle to analyze gas samples. The gas molecules are adsorbed onto a selective adsorbent and the resulting release of heat of this exothermic reaction can be measured [13–15]. To capture this release of thermal energy, a precise and sensitive temperature measurement is required. For this purpose, thermopiles consisting of a series of thermocouples are used. On-top of this thermopiles the adsorbent is deposited. Common materials to serve as a selective adsorbent are made of e.g., polymers, aluminum oxide, zeolite or activated charcoal [16, 17]. Desorption of the gas molecules is achieved by a thermal treatment of the adsorbent. Both processes, adsorption and desorption, can be used to analyze the present gas [18, 19]. By this sensor type, for example, volatile organic compounds (VOCs) can be analyzed, such as octane, propane or toluene.

2.1.3 Catalytic gas sensors

A further gas-sensing principle is based on catalytic or combustible gas sensors, as in the examples before, where a differential set-up of two temperature-sensing elements is placed into the gas of interest. In first gas-sensing applications, platinum or tungsten coil wires have been applied as heating and temperature measurement element. Electrical current applied to the wire heats the coil to temperatures between 900 and 1000 °C. Reaction with e.g., methane on the heated platinum results in combustion of the gas accompanied with an increase of temperature. A differential set-up arranged in a Wheatstone measurement circuit can be used to identify the gas concentration. Main drawbacks of this sensor set-up can be found in the high temperature of the metal wire, which can ignite the present gas. This has been prevented by shielding the sensitive wires by a flame arrester, such as a diffusion mesh or sinter membrane. Moreover, at elevated temperatures of the wire, platinum starts to evaporate, which results in drift of the sensor signal and false reading of the present concentration [20].

In order to overcome these issues, the platinum coil structure has been embedded into a ceramic mass e.g., a bead of alumina (Al_2O_3). One ceramic bead is used to detect environmental changes of the gas to be analyzed, like temperature or flow variations. A second ceramic bead is activated by means of a catalytic material, usually noble metals (e.g., platinum, palladium, rhodium) or metal oxides (e.g., manganese oxide, tin dioxide), the so-called pellistor.

The first catalytic bead or pellistor has been patented by Baker [21, 22]. A schematic view of the sensor set-up is shown in Fig. 2.2. Both ceramic beads are arranged in a Wheatstone measurement bridge, as mentioned before (s. Fig. 2.1). The catalytic material lowers the activation energy (E_a) to initiate the combustion or decomposition reaction as shown in Fig. 2.3. Thereby, the temperature of the gas detector can be lowered (400-600 °C), which prevents the ignition of combustible gases and, moreover, the power to run the circuit can be reduced. This sensor principle is mostly applied to detect the exothermic reaction of combustible gases such as butane, methane or propane [5]. In order to detect these gases the combustion process needs oxygen in the environment.

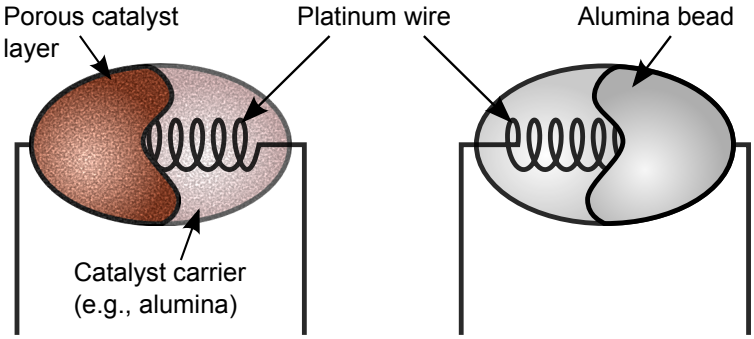

Fig. 2.2: Schematic view of calorimetric ceramic beads. Left side: activated ceramic bead or pellistor with catalyst, right side: passive alumina bead.

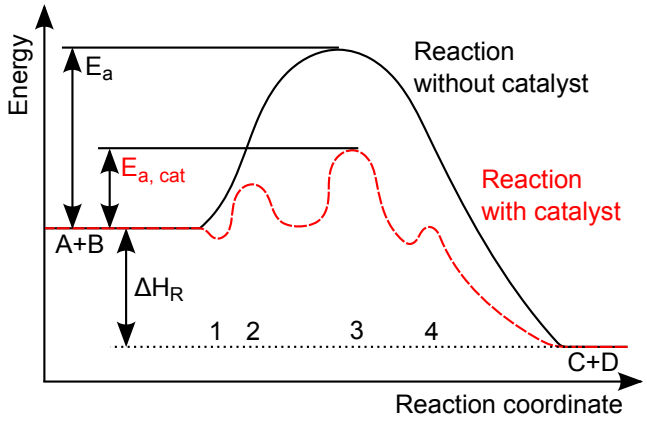

Fig. 2.3: Schematic view illustrating the reaction energies of a non-catalyzed (black, solid line) and a catalyzed reaction (red, dashed line) $A + B \rightleftharpoons C + D$. Intermediate steps of the catalyzed reaction are: adsorption (1), chemisorption (2), chemical reaction (3) and desorption (4); with E_a the activation energies and ΔH_R the reaction enthalpy (modified from [5, 29]).

Nowadays, different developments have been performed to miniaturize this sensing principle, which leads to additional improvements of the gas-sensing characteristics. For example, fabrication of thin-film temperature sensors on a silicon membrane reduces the thermal mass, which results in a faster sensor response [23, 24]. Flexible sensor substrates such as polyimide have been applied to increase the application of calorimetric gas sensors and also improves their sensitivity [25]. Active sensors have been developed by using thermopiles as temperature transducers, which can facilitate wireless applications [23, 26, 27].

Still remaining drawbacks of this sensor type are the low selectivity of the catalytic reaction and the catalyst poisoning by sulfur or chloride molecules. The first can be circumvented using different sensor temperatures. The latter can be avoided by diffusion membranes, separating the molecules to be analyzed. Additionally, burning steps at elevated sensor temperatures can be applied to remove substances from the catalyst [5, 28].

In recent works, the catalytic sensing principle has been adapted to monitor the relatively high concentrations (1–8% v/v) of hydrogen peroxide vapor during the sterilization of aseptic food packages [30–33]. Compared to conventional gases detected (e.g., methane) by this sensor type, the detection of H_2O_2 can be performed without environmental oxygen. H_2O_2 itself serves as an oxygen source during the reaction with a catalyst, thus a detection of H_2O_2 under vacuum conditions is possible [34]. The exothermic decomposition of H_2O_2 can be summarized in the following chemical reaction, with a release of ΔH_r=–105.3 kJ/mol:

$$2H_2O_2 \longrightarrow O_2 + 2H_2O + \Delta H_r \tag{2.3}$$

2.2 Impedance spectroscopy

Impedance spectroscopy is a powerful, electrochemical tool to analyze a variety of systems, for example: fuel cells, detection of particles in air samples, performing material analysis of solids and liquids or analysis of complex biological systems, such as in biosensor applications [35–39]. Within these applications, impedance spectroscopy is able to reveal electrical information about mass transfer, rates of chemical reactions and dielectric properties of a material [40]. In biosensor applications, impedance spectroscopy is applied to detect interactions between molecules or binding effects on transducer surfaces, for example, to detect the hybridization between two complementary DNA strands [41]. Further applications are the detection and analysis of whole microbiological cells, e.g., in cell growth studies or to reveal morphological deviations of cells [42–48].

2.2.1 Impedance

The electrical impedance is comparable to the electrical resistance in a direct current (DC) circuit, which is the ability of a circuit element to restrict the flow of electrical current. In an alternating current (AC) circuit, the impedance can be a result of a pure resistive element, as before, or an energy storage element such as an inductor or a capacitor. For electrochemical impedance analysis, usually a sinusoidal excitation voltage is applied with a small amplitude V_A and a frequency f, which can be expressed as a function of time.

$$V(t) = V_A \sin(2\pi f t + \varphi_V) = V_A \sin(\omega t + \varphi_V) \tag{2.4}$$

Here, ω is the angular frequency of the applied signal.

The resulting current of a linear or pseudo-linear system (linearity in a small region of excitation voltage) possesses the same frequency, with a decreased current amplitude (I_A) and a phase shift φ in dependency of the investigated circuit element, for example, $\varphi_I > 0$ for a capacitance and $\varphi_I < 0$ for an inductance. The resultant phase shift between voltage and current is used to further characterize a system in detail. The current of a system ($I(t)$) can be expressed by Eq (2.5).

$$I(t) = I_A \sin(2\pi f t + \varphi_I) = I_A \sin(\omega t + \varphi_I) \tag{2.5}$$

A schematic signal representation of voltage and current is shown in Fig. 2.4. The left side the same signals are given in the complex plane, the right side depicts the signals in the time domain. Based on the signal representation in the complex plane (Fig. 2.4, left side), the voltage and current signals can be expressed as complex functions ($\underline{V}(t)$), $\underline{I}(t)$) using Euler's relationship (s. Eq. (2.6) and Eq. (2.7)), with j representing the imaginary number.

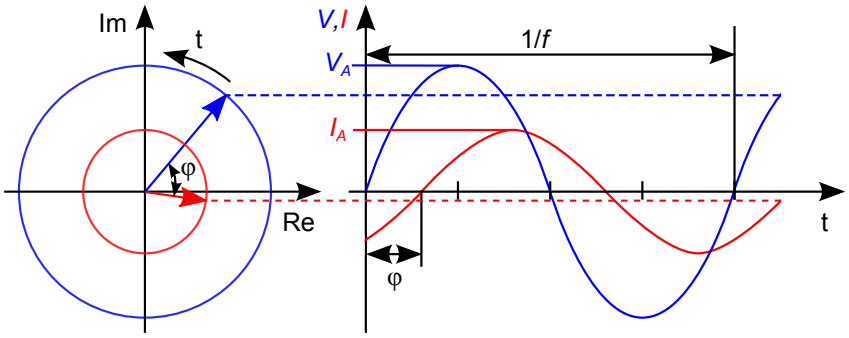

Fig. 2.4: Signal representation of a sinusoidal excitation voltage at a frequency f and a resulting current, showing the phase shift φ; left side: representation in the complex plane with real (Re) and imaginary (Im) axis; right side: representation in the time domain (V, I) and t axis. Modified from [40].

$$\underline{V}(t) = V_A \left(\cos(\omega t + \varphi_V) + j \sin(\omega t + \varphi_V)\right) = V_A \, e^{j(\omega t + \varphi_V)} \tag{2.6}$$

$$\underline{I}(t) = I_A \left(\cos(\omega t + \varphi_I) + j \sin(\omega t + \varphi_I)\right) = I_A \, e^{j(\omega t + \varphi_I)} \tag{2.7}$$

Using the complex signal representation, the electrical impedance can be determined by the ratio between the excitation voltage and the resulting current of the system, as by Ohm's law in a DC circuit.

$$\begin{aligned} \underline{Z} &= \frac{V_A \, e^{j(\omega t + \varphi_V)}}{I_A \, e^{j(\omega t + \varphi_I)}} && (2.8)\\ &= Z \, e^{j\varphi_Z} && (2.9)\\ &= Z \left(\cos(\varphi_Z) + j \sin(\varphi_Z)\right) && (2.10)\\ &= Z_{Re} + j \, Z_{Im} && (2.11) \end{aligned}$$

Here, $\underline{Z}$ and Z represent the complex and absolute impedance value, respectively. Z_{Re} and Z_{Im} are the real and imaginary part of the complex impedance. The resulting phase of the impedance is the phase difference between voltage and current ($\varphi_Z = \varphi_V - \varphi_I$), which is used for interpretation of the system behavior.

Analysis of an ideal resistive element response is a phase difference of 0°. For ideal capacitive and inductive elements a phase difference of -90° and 90° is measured, respectively. Real systems usually consist of a combination of non-ideal elements, whereby a phase difference between these values can be observed. Moreover, the system response

can vary with respect to the excitation frequency. This fact is used in impedance spectroscopy, whereby a set of impedance and phase values at different excitation frequencies are measured.

For data representation and analysis of materials or to characterize sensor behaviors, the Nyquist and Bode plots are used. The Nyquist plot is a parametric plot of the real and imaginary part in the complex plane. The Bode plot depicts the phase angle and the logarithmic magnitude of the impedance as a function of the investigated logarithmic frequency.

In a practical approach, the excitation voltage is applied to an electrochemical characterization set-up, like an electrolyte-insulator-semiconductor (EIS) structure or an interdigitated metal electrode (IDE) (see Sec. 2.2.2). The measured impedance and phase angle reveals information of the system, which can be an aqueous solution, a solid or even a gas. In dependence of the studied material and set-up, the response behavior can be capacitive ($\varphi_Z = -90°$); by analyzing a conductive substance a resistive characteristic can be observed ($\varphi_Z = 0°$), or the response can indicate a combinatorial system with a phase angle between 0° and −90°.

Moreover, impedance spectroscopy of EIS structures is applied to study the double-layer capacitance formed between an electrode and a liquid, or transport phenomena within the electrolyte, both in dependence of the applied frequency [40]. Additionally, at a fixed frequency the impedance analysis can be used to analyze substance concentrations within a solution [36].

2.2.2 Interdigitated electrodes

In this work, interdigitated electrodes (IDE) have been designed, fabricated and applied to detect interactions of immobilized microorganisms with a gaseous H_2O_2 sterilization process to measure its efficacy. Characteristic parameters for IDE structures are depicted in Fig. 2.5, which are the length of the electrode fingers (L), the finger width (w), the interspacing between each finger (s), the number of fingers (N) and the thickness of the electrodes (t).

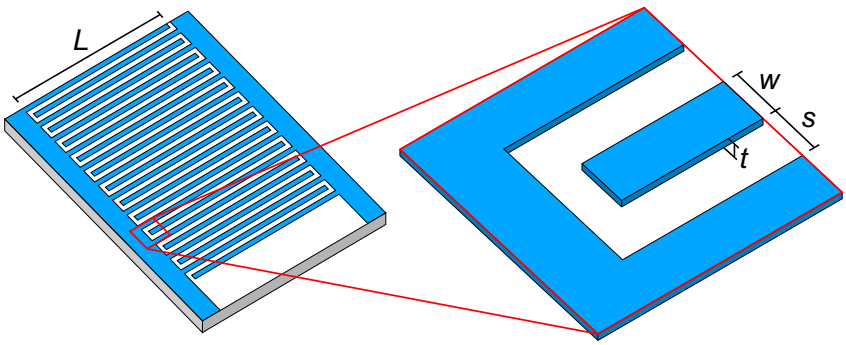

Fig. 2.5: Schematic view of interdigitated electrodes representing characteristic parameters.

An additional parameter is the substrate material on which the electrodes are fabricated. Usually, a non-conductive material such as glass, silicon/silicon oxide, or in case of high-temperature gas sensors, alumina (Al_2O_3) is chosen [49–51]. The substrate

material and the environment (e.g., air, vacuum) during analysis define the initial IDE impedance. Thereby, non-conductive materials result in a capacitive behavior of the IDE structure in dependence of the material's relative permittivity ε_r. Analytically, the theoretical capacitance of IDE structures can be expressed by applying the elliptical integral (s. Eq. (2.12)) [40, 52–55].

$$C = L(N-1)\left(\frac{\varepsilon_0 \varepsilon_{r,t}}{2}\frac{K\left((1-k^2)^{1/2}\right)}{K(k)} + 2\varepsilon_0 \varepsilon_{r,m}\frac{t}{s}\right) \tag{2.12}$$

$$K(k) = \int_{x=0}^{1} \frac{1}{[(1-x^2)(1-k^2x^2)]^{1/2}}\,\mathrm{d}x \tag{2.13}$$

$$k = \cos\left(\frac{\pi}{2}\frac{w}{s+w}\right) \tag{2.14}$$

Here, C is the calculated capacitance of the IDE structure in Farad (F), ε_0 represents the permittivity of vacuum with $8.851 \cdot 10^{-12}\,\mathrm{As\,V^{-1}\,m^{-1}}$ and $K(k)$ is the first order elliptical integral (Eq. (2.13)) to calculate the impact of the fringing field. The modulus k defined in Eq. (2.14) is determined by the periodic structure of the electrode geometry. $\varepsilon_{r,t}$ is the total permittivity surrounding the electrodes (substrate and medium). Finally, $\varepsilon_{r,m}$ describes the relative permittivity of the medium to represent the capacitance formed due to the homogeneous electric field between the electrodes.

Fig 2.6 depicts a schematic of the electric field lines between the electrodes. The sensitivity of IDE electrodes to variations of the material under test depends on the penetration depth of the electric field. The electric field distribution on IDEs has been theoretically described by van Gerwen et al. and den Otter [56, 57]. Thereby, the resultant penetration depth of the electric field into the substrate or medium on top can be approximated be one half of the spatial period of the electrodes $\lambda/2 = (w + s)/2$. Within this distance 80% of the electric field and current flow is concentrated. During the design procedure of IDE this needs to be considered in order to develop IDE structures related to the substances of interest.

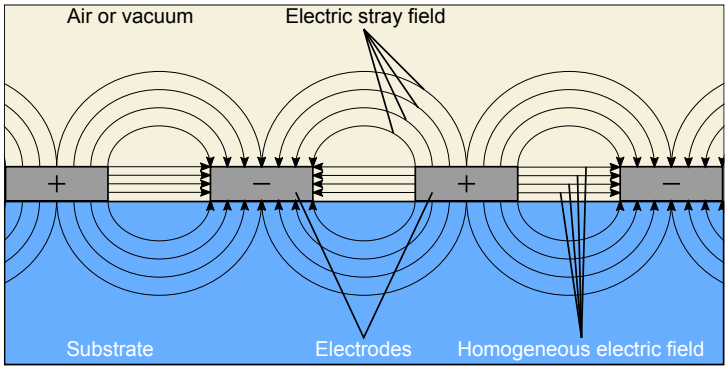

Fig. 2.6: Schematic cross-sectional view of IDEs representing the different, instantaneous electric field lines developed between the electrode structure.

Since substances between and on top of the electrodes interfere with the electric field, IDEs are applied in various applications to analyze substances or to monitor analyte

concentrations. Examples are the detection of particles in air [38, 50, 58–60], or as transducer structure for electrochemical gas sensors modified with a reception layer, to enable selective gas monitoring [61–65]. The reaction or adsorption of the analyte with the reception layer forms conductive paths, which result in an increasing conductivity. By deposition of a hygroscopic material, e.g., polymers or ceramics onto the IDE, humidity sensors can be realized [66, 67]. In biosensor applications this electrode structure is well known to monitor e.g., antigen-antibody reactions, interactions of DNA strands or DNA detection, biological cell morphology or biological cell responses to environmental changes [36, 56, 68–72]. Furthermore, IDE-based sensors have been developed to analyze food samples, for example, to detect *Salmonella typhimurium* or *Escherichia coli* in milk [73, 74].

References

[1] Siemens und Halske AG. "Verfahren und Einrichtung zum Anzeigen von Gasbeimengungen in der Luft, insbesondere Grubengas". DE 283677. 1915.

[2] C. M. Means. "Methane detector". US 1,231,045. 1917.

[3] P. T. Walsh and T. A. Jones. "Calorimetric chemical sensors". In: *Sensors: A Comprehensive Survey*. Ed. by W. Göpel, T. A. Jones, M. Kleitz, I. Lundström, and T. Seiyama. Vol. 2. Weinheim, Germany: VCH Verlagsgesellschaft mbH, 1991, 529–572.

[4] P. N. Bartlett and S. Guerin. "A micromachined calorimetric gas sensor: an application of electrodeposited nanostructured palladium for the detection of combustible gases". *Analytical Chemistry* 75 (2003), 126–132.

[5] I. Bársony, C. Dücso, and P. Fürjes. "Thermometric gas sensing". In: *Solid State Gas Sensing*. Ed. by E. Comini, G. Faglia, and G. Sberveglieri. Boston, MA: Springer Science and Business Media, 2009, 237–260.

[6] G. Wiegleb. *Gasmesstechnik in Theorie und Praxis*. Wiesbaden: Springer Vieweg, 2016.

[7] International Sensor Technology. *Catalytic combustible gas sensors*. 2015. URL: `http://www.intlsensor.com`.

[8] International Association for Hydrogen Safety. *Hydrogen safety barriers and safety measures*. 2006. URL: `http://www.hysafe.org`.

[9] B. Miller. "Gas analysis method and apparatus". US 2,219,540. 1940.

[10] R. B. Bird, W. E. Stewart, and E. N. Lightfoot. *Transport Phenomena*. 2nd ed. New York: John Wiley & Sons, Inc., 2002.

[11] J. R. Welty, C. E. Wicks, R. E. Wilson, and G. L. Rorrer. *Fundamentals of Momentum, Heat, and Mass Transfer*. 5th ed. Vol. 13. New York, NY, USA: John Wiley & Sons, Inc., 2008.

[12] SGX Sensortech Ltd. *Introduction to thermal conductivity sensors*. 2014. URL: `https://www.azosensors.com/article.aspx?ArticleID=538`.

[13] N. Kerness, A. Koll, A. Schaufelbuhl, C. Hagleitner, A. Hierlemann, O. Brand, and H. Baltes. "N-well based CMOS calorimetric chemical sensors". In: *IEEE The Thirteenth Annual International Conference on Micro Electro Mechanical Systems*. 2000, 96–101.

[14] D. Caspary, M. Schröpfer, J. Lerchner, and G. Wolf. "A high resolution IC-calorimeter for the determination of heats of absorption onto thin coatings". *Thermochimica Acta* 337 (1999), 19–26.

[15] S. M. Sarge, G. W. H. Höhne, and W. Hemminger. *Calorimetry: Fundamentals, Instrumentation and Applications*. Weinheim, Germany: Wiley-VCH Verlag, 2014.

[16] G. Korotcenkov. *Handbook of Gas Sensor Materials: Properties, Advantages and Shortcomings for Applications: Vol. 1: Conventional Approaches*. New York, NY: Springer, 2013.

[17] J. Lerchner, D. Caspary, and G. Wolf. "Calorimetric detection of volatile organic compounds". *Sensors and Actuators B: Chemical* 70 (2000), 57–66.

[18] C. Hagleitner, A. Hierlemann, D. Lange, A. Kummer, N. Kerness, O. Brand, and H. Baltes. "Smart single-chip gas sensor microsystem". *Nature* 414 (2001), 293–296.

[19] C. Hagleitner, D. Lange, A. Hierlemann, O. Brand, and H. Baltes. "CMOS single-chip gas detection system comprising capacitive, calorimetric and mass-sensitive microsensors". *IEEE Journal of Solid-State Circuits* 37 (2002), 1867–1878.

[20] R. E. Cavicchi. *Calorimetric Sensors*. Highland Park, NJ, USA: Momentum Press, 2011.

[21] R. A. Baker. "Improvements in or relating to electrically heatable filaments". GB 892,530. 1962.

[22] R. A. Baker. "Apparatus fo detecting combustible gases having an electrically conductive member enveloped in a refractory material". US 3,092,799. 1963.

[23] N. H. Park, T. Akamatsu, T. Itoh, N. Izu, and W. Shin. "Calorimetric thermoelectric gas sensor for the detection of hydrogen, methane and mixed gases". *Sensors (MDPI)* 14 (2014), 8350–8362.

[24] E. Vereshchagina, R. M. Tiggelaar, R. Sanders, R. Wolters, and J. Gardeniers. "Low power micro-calorimetric sensors for analysis of gaseous samples". *Sensors and Actuators B: Chemical* 206 (2015), 772–787.

[25] P. Kirchner, J. Oberländer, P. Friedrich, J. Berger, G. Rysstad, M. Keusgen, and M. J. Schöning. "Realization of a calorimetric gas sensor on polyimide foil for applications in aseptic food industry". *Sensors and Actuators B: Chemical* 170 (2012), 60–66.

[26] V. Casey, J. Cleary, G. D'Arcy, and J. B. McMonagle. "Calorimetric combustible gas sensor based on a planar thermopile array: fabrication, characterization, and gas response". *Sensors and Actuators B: Chemical* 96 (2003), 114–123.

[27] P. Kirchner, Y. A. Ng, H. Spelthahn, A. Schneider, H. Henkel, P. Friedrich, J. Kolstad, J. Berger, M. Keusgen, and M. J. Schöning. "Gas sensor investigation based on a catalytically activated thin-film thermopile for H_2O_2 detection". *Physica Status Solidi A* 207 (2010), 787–792.

[28] W. Moritz, S. Krause, U. Roth, D. Klimm, and A. Lippitz. "Re-activation of an all solid state oxygen sensor". *Analytica Chimica Acta* 437 (2001), 183–190.

[29] S. J. Gentry and T. A. Jones. "The role of catalysis in solid-state gas sensors". *Sensors and Actuators* 10 (1986), 141–163.

[30] N. Näther, L. M. Juárez, R. Emmerich, J. Berger, P. Friedrich, and M. J. Schöning. "Detection of hydrogen peroxide (H_2O_2) at exposed temperatures for industrial processes". *Sensors (MDPI)* 6 (2006), 308–317.

[31] P. Kirchner, J. Oberländer, H.-P. Suso, G. Rysstad, M. Keusgen, and M. J. Schöning. "Monitoring the microbicidal effectiveness of gaseous hydrogen peroxide in sterilization processes by means of a calorimetric gas sensor". *Food Control* 31 (2013), 530–538.

[32] N. Näther. "Entwicklung eines H_2O_2-Messverfahrens für die Überwachung der mikrobioziden Wirksamkeit bei der Sterilisation aseptischer Verpackungen". PhD thesis. Marburg, Germany: Philipps-Universität Marburg, 2009.

[33] P. Kirchner. "Thin-film calorimetric gas sensors for hydrogen peroxide monitoring in aseptic food processes". PhD thesis. Marburg, Germany: Philipps-Universität Marburg, 2013.

[34] P. Kirchner, S. Reisert, and M. J. Schöning. "Calorimetric gas sensors for hydrogen peroxide monitoring in aseptic food processes". In: *Gas Sensing Fundamentals*. Ed. by C.-D. Kohl and T. Wagner. Springer Series on Chemical Sensors and Biosensors. Heidelberg, Germany: Springer-Verlag GmbH, 2014, 279–310.

[35] N. J. Kidner, A. Meier, Z. J. Homrighaus, B. W. Wessels, T. O. Mason, and E. J. Garboczi. "Complex electrical (impedance/dielectric) properties of electroceramic thin films by impedance spectroscopy with interdigital electrodes". *Thin Solid Films* 515 (2007), 4588–4595.

[36] F. Lisdat and D. Schäfer. "The use of electrochemical impedance spectroscopy for biosensing". *Analytical and Bioanalytical Chemistry* 391 (2008), 1555–1567.

[37] J. S. Daniels and N. Pourmand. "Label-free impedance biosensors: opportunities and challenges". *Electroanalysis* 19 (2007), 1239–1257.

[38] M. Carminati, L. Pedalà, E. Bianchi, F. Nason, G. Dubini, L. Cortelezzi, G. Ferrari, and M. Sampietro. "Capacitive detection of micrometric airborne particulate matter for solid-state personal air quality monitors". *Sensors and Actuators A: Physical* 219 (2014), 80–87.

[39] A. J. Bard and L. R. Faulkner. *Electrochemical Methods: Fundamentals and Applications*. 2nd ed. New York, NY, USA: John Wiley & Sons, Inc., 2001.

[40] V. F. Lvovich. *Impedance Spectroscopy: Applications to Electrochemical and Dielectric Phenomena*. Hoboken, NJ, USA: John Wiley & Sons, Inc., 2012.

[41] M. Riedel, J. Kartchemnik, M. J. Schöning, and F. Lisdat. "Impedimetric DNA detection–steps forward to sensorial application". *Analytical Chemistry* 86 (2014), 7867–7874.

[42] C. R. Keese and I. Giaever. "A biosensor that monitors cell morphology with electrical fields". *IEEE Engineering in Medicine and Biology Magazine* 13 (1994), 402–408.

[43] S. Brosel-Oliu, N. Uria, N. Abramova, and A. Bratov. "Impedimetric sensors for bacteria detection". In: *Biosensors - Micro and Nanoscale Applications*. Ed. by T. Rinken. Rijeka, Croatia: InTech, 2015, 257–288.

[44] S. G. Dastider, S. Barizuddin, M. Dweik, and M. Almasri. "A micromachined impedance biosensor for accurate and rapid detection of *E. coli* O157:H7". *RSC Advances* 3 (2013), 26297–26306.

[45] B.-W. Chang, C.-H. Chen, S.-J. Ding, D. C.-H. Chen, and H.-C. Chang. "Impedimetric monitoring of cell attachment on interdigitated microelectrodes". *Sensors and Actuators B: Chemical* 105 (2005), 159–163.

[46] K. Heileman, J. Daoud, and M. Tabrizian. "Dielectric spectroscopy as a viable biosensing tool for cell and tissue characterization and analysis". *Biosensors and Bioelectronics* 49 (2013), 348–359.

[47] Y.-S. Liu, T. M. Walter, W.-J. Chang, K.-S. Lim, L. Yang, S. W. Lee, A. Aronson, and R. Bashir. "Electrical detection of germination of viable model *Bacillus anthracis* spores in microfluidic biochips". *Lab on a Chip* 7 (2007), 603–610.

[48] Q. Liu, J. Yu, L. Xiao, J. C. O. Tang, Y. Zhang, P. Wang, and M. Yang. "Impedance studies of bio-behavior and chemosensitivity of cancer cells by microelectrode arrays". *Biosensors and Bioelectronics* 24 (2009), 1305–1310.

[49] H.-E. Endres and S. Drost. "Optimization of the geometry of gas-sensitive interdigital capacitors". *Sensors and Actuators B: Chemical* 4 (1991), 95–98.

[50] M. Fleischer, R. Pohle, K. Wiesner, and H. Meixner. "Soot sensor for exhaust gases". In: *Proceedings of the Eurosensors XIX*. 2005.

[51] A. Fischerauer, C. Schwarzmüller, and G. Fischerauer. "Substrate influence on the characteristics of interdigital-electrode gas sensors". In: *6th International Multi-Conference on Systems, Signals and Devices (SSD)*. 2009, 1–5.

[52] W. Olthuis, W. Streekstra, and P. Bergveld. "Theoretical and experimental determination of cell constants of planar-interdigitated electrolyte conductivity sensors". *Sensors and Actuators B: Chemical* 24 (1995), 252–256.

[53] S. S. Gevorgian, T. Martinsson, P. Linner, and E. L. Kollberg. "CAD models for multilayered substrate interdigital capacitors". *IEEE Transactions on Microwave Theory and Techniques* 44 (1996), 896–904.

[54] B. Timmer, W. Sparreboom, W. Olthuis, P. Bergveld, and A. van den Berg. "Optimization of an electrolyte conductivity detector for measuring low ion concentrations". *Lab on a Chip* 2 (2002), 121–124.

[55] A. S. Abu-Abed and R. G. Lindquist. "Capacitive interdigital sensor with inhomogeneous nematic liquid crystal film". *Progress in Electromagnetics Research B* 7 (2008), 75–87.

[56] P. van Gerwen, W. Laureyn, W. Laureys, G. Huyberechts, M. op de Beeck, K. Baert, J. Suls, W. Sansen, P. Jacobs, L. Hermans, and R. Mertens. "Nanoscaled interdigitated electrode arrays for biochemical sensors". *Sensors and Actuators B: Chemical* 49 (1998), 73–80.

[57] M. W. den Otter. "Approximate expressions for the capacitance and electrostatic potential of interdigitated electrodes". *Sensors and Actuators A: Physical* 96 (2002), 140–144.

[58] T. A. York, I. G. Evans, Z. Pokusevski, and T. Dyakowski. "Particle detection using an integrated capacitance sensor". *Sensors and Actuators A: Physical* 92 (2001), 74–79.

[59] T. Ochs, H. Schittenhelm, A. Genssle, and B. Kamp. "Particulate matter sensor for on board diagnostics (OBD) of diesel particulate filters (DPF)". *SAE International Journal of Fuels and Lubricants* 3 (2010), 61–69.

[60] A. Weiss, M. Bauer, S. Eichenauer, E. A. Stadlbauer, and C.-D. Kohl. "Impedance spectroscopy characterization of an interdigital structure for continuous particle measurements in wood-driven heating systems". *Journal of Sensors and Sensor Systems* 4 (2015), 37–44.

[61] H.-E. Endres, S. Drost, and F. Hutter. "Impedance spectroscopy on dielectric gas sensors". *Sensors and Actuators B: Chemical* 22 (1994), 7–11.

[62] T. H. Tran, J.-W. Lee, K. Lee, Y. D. Lee, and B.-K. Ju. "The gas sensing properties of single-walled carbon nanotubes deposited on an aminosilane monolayer". *Sensors and Actuators B: Chemical* 129 (2008), 67–71.

[63] J. Hennemann, T. Sauerwald, C.-D. Kohl, T. Wagner, M. Bognitzki, and A. Greiner. "Electrospun copper oxide nanofibers for H_2S dosimetry". *Physica Status Solidi A* 209 (2012), 911–916.

[64] J. Hennemann, C.-D. Kohl, S. Reisert, P. Kirchner, and M. J. Schöning. "Copper oxide nanofibres for detection of hydrogen peroxide vapour at high concentrations". *Physica Status Solidi A* 210 (2013), 859–863.

[65] R. Blue and D. Uttamchandani. "Chemicapacitors as a versatile platform for miniature gas and vapor sensors". *Measurement Science and Technology* 28 (2017), 22001–22024.

[66] B. M. Kulwicki. "Humidity sensors". *Journal of the American Ceramic Society* 74 (1991), 697–708.

[67] H. Farahani, R. Wagiran, and M. N. Hamidon. "Humidity sensors principle, mechanism, and fabrication technologies: a comprehensive review". *Sensors (MDPI)* 14 (2014), 7881–7939.

[68] R. de la Rica, C. Fernández-Sánchez, C. Jiménez, and A. Baldi. "Suitability of polysilicon interdigitated electrodes for the fabrication of both impedimetric sensors and biosensors". In: *Ibersensor - 5th Ibero-American Congress in Sensors*. 2006, 1–5.

[69] N. Yu, J. M. Atienza, J. Bernard, S. Blanc, J. Zhu, X. Wang, X. Xu, and Y. A. Abassi. "Real-time monitoring of morphological changes in living cells by electronic cell sensor arrays: an approach to study G protein-coupled receptors". *Analytical Chemistry* 78 (2006), 35–43.

[70] M. Varshney and Y. Li. "Interdigitated array microelectrodes based impedance biosensors for detection of bacterial cells". *Biosensors and Bioelectronics* 24 (2009), 2951–2960.

[71] X. Tang, D. Flandre, J.-P. Raskin, Y. Nizet, L. Moreno-Hagelsieb, R. Pampin, and L. A. Francis. "A new interdigitated array microelectrode-oxide-silicon sensor with label-free, high sensitivity and specificity for fast bacteria detection". *Sensors and Actuators B: Chemical* 156 (2011), 578–587.

[72] U. Bohrn, E. Stutz, M. Fleischer, M. J. Schöning, and P. H. Wagner. "Using a cell-based gas biosensor for investigation of adverse effects of acetone vapors in vitro". *Biosensors and Bioelectronics* 40 (2013), 393–400.

[73] L. Yang, Y. Li, C. L. Griffis, and M. G. Johnson. "Interdigitated microelectrode (IME) impedance sensor for the detection of viable *Salmonella typhimurium*". *Biosensors and Bioelectronics* 19 (2004), 1139–1147.

[74] J.-T. Liu, K. Settu, J.-Z. Tsai, and C.-J. Chen. "Impedance sensor for rapid enumeration of *E. coli* in milk samples". *Electrochimica Acta* 182 (2015), 89–95.

3 Detection of hydrogen peroxide vapor by use of manganese(IV) oxide as catalyst for calorimetric gas sensors (*Physica Status Solidi A*, 211, 6 (2014), 1372–1376)

J. Oberländer, P. Kirchner, H.-G. Boyen, and M. J. Schöning

Published in: *Physica Status Solidi A: Applications and Materials Science,* Vol. 211, 6 (2014), 1372–1376.

Submitted: 2013-10-15; Accepted: 2014-02-24; Published: 2014-03-26

3.1 Abstract

In this work, the catalyst manganese(IV) oxide (MnO_2) for calorimetric gas sensors (to monitor the sterilization agent vaporized hydrogen peroxide) has been investigated in more detail. Chemical analyzes by means of X-ray-induced photoelectron spectroscopy have been performed to unravel the surface chemistry prior and after exposure to hydrogen peroxide vapor at elevated temperature, as applied in the sterilization processes of beverage cartons. The surface characterization reveals a change in oxidation states of the metal oxide catalyst after exposure to hydrogen peroxide. Additionally, a cleaning effect of the catalyst, which itself is attached to the sensor surface by means of a polymer interlayer, could be observed.

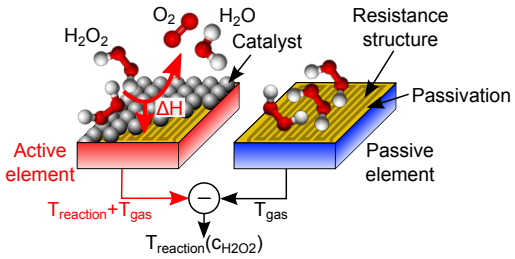

Fig. 3.1: Schematic demonstrating the principle of the calorimetric hydrogen peroxide gas sensor; right side: reference element passivated by an inert polymer, left side: temperature-sensitive element additionally activated with MnO_2.

3.2 Introduction

Sensitive food products such as milk or juice with an extended shelf life are delivered in composite packages. In order to avoid a recontamination of the sterilized food products, a separate sterilization of the packaging material is mandatory. For this packaging sterilization process, hydrogen peroxide (H_2O_2) in the gas phase has been established as sterilization agent on aseptic filling machines [1, 2]. In the packaging sterilization process, hydrogen peroxide is frequently utilized at elevated temperatures up to 300 °C, and concentrations in the range of 2–8% v/v. Due to the strong oxidizing properties of hydrogen peroxide and furthermore, the ability of radical formation at elevated gas temperatures, a high microbicidal efficacy in a short exposure time can be achieved [3]. Moreover, hydrogen peroxide decomposes finally into water vapor and oxygen, thus avoiding toxic residues on the sterilized surfaces. This is an advantage compared to other chemical gas sterilization methods, like ethylene oxide or formaldehyde. In order to monitor and validate the sterilization processes, nowadays time-consuming and costly microbiological tests are necessary. In those approaches, the sterilization efficiency depends mainly on the H_2O_2 concentration, the gas temperature and the sterilization time. To solve these problems and especially to directly monitor the H_2O_2 concentration, different types of calorimetric gas sensors have been developed recently [4–6]. The robustness of the developed sensor set-ups facilitates a possibility to monitor the gaseous hydrogen peroxide concentration under these harsh conditions [4, 6]. The calorimetric gas sensors are based upon a differential set-up of two temperature-sensitive elements as shown schematically in Fig. 3.2. One of these temperature-sensitive elements is specially passivated by an inert polymer layer, in order to capture the temperature of the gas stream, the second temperature-sensitive element is additionally covered by a layer of porous manganese(IV) oxide (MnO_2), which catalyzes the exothermic decomposition of hydrogen peroxide vapor. The resulting temperature difference between both temperature-sensitive elements correlates with the present hydrogen peroxide concentration in the gas stream. Recently, the linear sensor characteristic and signal stability at various influencing parameters, such as the variation in gas flow and gas temperature, have been demonstrated [6, 7].

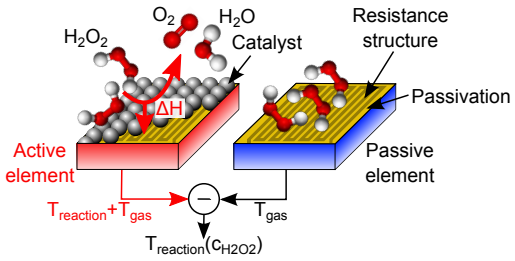

Fig. 3.2: Schematic demonstrating the principle of the calorimetric hydrogen peroxide gas sensor; right side: reference element passivated by an inert polymer, left side: temperature-sensitive element additionally activated with MnO_2.

In previous studies, the heterogeneous reaction of hydrogen peroxide vapors on metal oxides and inert surfaces has been studied [8–10]. In the present work, the catalyst

manganese(IV) oxide (MnO_2), which is described in literature [11–13] as catalyst for the decomposition of hydrogen peroxide, will be investigated in more detail with respect to the application as catalyst for calorimetric H_2O_2 gas sensors. The scope is to study the surface decomposition mechanisms of H_2O_2 vapor in particular.

3.3 Materials and methods

3.3.1 Materials

The applied catalyst manganese(IV) oxide powder (Merck KGaA) of the calorimetric H_2O_2 gas sensors will be investigated in more detail. For the characterization, catalyst powder was attached to a layer of SU-8 photoresist (MicroChem Inc.) following a procedure as described for sensor preparation in Ref. [5]. Furthermore, reference samples of pure MnO_2 have been analyzed as well. Additionally, the samples were exposed to a hydrogen peroxide vapor, evaporated from a water-based solution (liquid concentration 35% w/w) at 240 °C. An air stream of 10 m^3h^{-1} was applied to achieve an intensified H_2O_2 flow at the sample position. The H_2O_2 concentration within this gas stream has been adjusted to 7.5% v/v. The samples were exposed in a sterilization test rig, as described previously in [5, 14], for more than 4 h. The MnO_2 samples were treated similarly within the sterilization test rig as applied for sensor measurements, with a distance of 5.5 cm to the gas nozzle.

3.3.2 Material characterization

For the surface characterization X-ray-induced photoelectron spectroscopy (XPS) has been performed. All samples were analyzed by means of a 5600 LS electron spectrometer (Physical Electronics, Inc.) equipped with a small-spot X-ray source providing monochromatic Al Kα photons (spot size $\approx$ 1 mm, photon energy 1486.6 eV). The photoemission measurements were performed at a base pressure of $p \approx 6 \cdot 10^{-10}$ mbar. Since the information depth of the emitted photoelectrons is about 5 nm, this technique allows to investigate surface mechanisms/effects with high precision. The scope of this material study is therefore to reveal the surface chemistry of the transition metal oxide catalyst and to identify, especially possible catalyst poisoning induced by the exposure to H_2O_2 vapor.

3.4 Results and discussions

3.4.1 Characterization of MnO_2

In a first set of experiments, survey scans of the MnO_2 samples were investigated to observe an influence of the hydrogen peroxide vapor compared to pure MnO_2 (Fig. 3.3). In both survey scans, distinct peaks can be observed at binding energies of 652.8 and 641.2 eV, which can be assigned to photoelectrons emitted from the Mn 2p core doublet. An additional line is visible in both spectra at a binding energy of 528.8 eV corresponding to the O 1s core level. In both spectra a small amount of carbon can be detected at a binding energy of 284 eV (C 1s) as well, arising from the exposure of the samples

to ambient conditions. The comparison of these two survey scans thus underlines, that there are no major changes in the elemental distribution induced by the exposure to hydrogen peroxide vapor that can be identified.

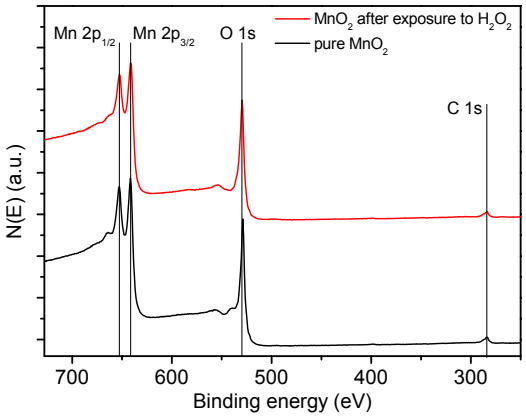

Fig. 3.3: XPS survey scans of pure MnO_2 and MnO_2 after exposure to hydrogen peroxide vapor (same scale).

In order to extract more details about the sensor surface, especially to characterize the manganese oxide with respect to its oxidation states, high-resolution XPS scans were performed in the binding energy region of the Mn $2p_{3/2}$ core line (638–645 eV). Fig. 3.4 presents the corresponding core level spectra acquired before and after H_2O_2 treatment. In case of the pure transition metal oxide, the photoelectron distribution is dominated by an intensity maximum centered at a binding energy of 641.9 eV, which corresponds to manganese with the oxidation state 4+, as expected for manganese(IV) oxide (MnO_2) [15, 16]. After treating the sample with H_2O_2 vapor, an increase in spectral weight at about 641.2 eV can be detected resulting in a well-pronounced additional shoulder. Using literature data as reference (summarized in Tab. 3.1 and added as vertical lines in Fig. 3.4), the new component observed at reduced binding energy can be assigned to manganese oxide with lower oxidation states. This indicates that, when exposing manganese(IV) oxide to H_2O_2 vapor, a chemical reduction into either MnO (oxidation state: 2+) or Mn_3O_4 (2+/3+) or a mixture hereof takes place at the sensor surface. Since the original MnO_2-related spectral component is still present after the peroxide treatment, a layer thickness of the (partially) reduced oxide of about 1–2 nm can be estimated residing on top of the (now buried) MnO_2. The difference of both spectra given in Fig. 3.4, points out the existence of a reduced layer on top of the transition metal oxide.

Tab. 3.1: Binding energies and corresponding oxidation states of different types of manganese oxides (Mn $2p_{3/2}$ peak); validated references from [17].

Manganese oxide	Oxidation state	Binding energy (eV)	Ref.
MnO	2+	640.9	[18]
Mn_3O_4	2+/3+	641.3	[19]
Mn_2O_3	3+	641.7	[20]
MnO_2	4+	641.9	[15, 16]

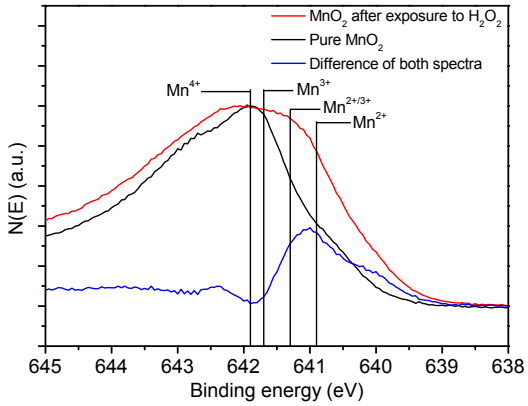

Fig. 3.4: XPS high-resolution scans of pure MnO_2 and MnO_2 after exposure to hydrogen peroxide vapor; the difference of both spectra emphasizes the reduction of MnO_2. The different oxidation states of manganese are indicated.

3.4.2 Decomposition mechanisms

The decomposition mechanism of hydrogen peroxide vapor by means of manganese oxides has been investigated and discussed in different references [6, 8–13, 21–23]. Mainly two different pathways for the reaction mechanism are proposed: on the one hand, the decomposition is believed to be initiated by an electron exchange reaction between the catalyst surface and H_2O_2 molecules, whereby a reduction of MnO_2 (Mn ox. state 4+) to Mn with lower oxidation states takes place, resulting in the formation of radicals ($HO^\bullet$, $HO_2^\bullet$). On the other hand, the decomposition at elevated temperature can also be initiated by a fission of the O–O bond, accompanied by the formation of hydroxyl radicals ($HO^\bullet$) as well [10]. Hereby, the O–O binding of H_2O_2 possesses a lower binding energy than the present O–H bonds [9, 10]. It might be speculated that these radicals undergo a chain reaction involving further H_2O_2 molecules as given in Eqs. (3.2) and (3.3) [6, 22, 23]. Especially, at elevated gas temperatures, where the thermal decomposition of hydrogen peroxide needs to be taken into account, a chain reaction is very probable, as described by Refs. [9, 10].

The initial reaction on the catalyst surface with electron transfer could be the following:

$$H_2O_2 + Mn^{4+} \longrightarrow H^+ + Mn^{3+} + HO_2^\bullet. \tag{3.1}$$

The evolved hydroperoxyl radical reacts either with a further H_2O_2 molecule and starts the chain reaction [10]:

$$HO_2^\bullet + H_2O_2 \longrightarrow H_2O + O_2 + HO^\bullet, \tag{3.2}$$

$$HO^\bullet + H_2O_2 \longrightarrow H_2O + HO_2^\bullet. \tag{3.3}$$

Or the hydroperoxyl radical re-oxidizes manganese, whereby the chain reaction will be terminated.

$$HO^\bullet + Mn^{3+} \longrightarrow Mn^{4+} + OH^-. \tag{3.4}$$

It is likely, that the hydroxide ion resulting from reaction (3.4) combines with the proton resulting from reaction (3.1) to form water:

$$H^+ + HO^- \longrightarrow H_2O. \tag{3.5}$$

Further pathways for the decomposition of H_2O_2 on MnO_2 catalyst surfaces were proposed thereby considering the formation of radicals without an ongoing chain reaction between the radicals and H_2O_2 molecules. By this non-chain decomposition mechanism, the starting chain will immediately be blocked following Eqs. (3.4) or (3.7) [22]. In both decomposition mechanisms, by use of the catalyst MnO_2, a reduction/oxidation cycle is proposed, where the manganese compound will be present with a lower oxidation state. Especially, the mechanism proposed in reference [22] emphasizes that, for the heterogeneous decomposition process, different oxidation states of manganese have to be taken into account. Additionally, in Ref. [22] a general decomposition mechanism has been introduced, where different manganese oxide species (Mn^{n+}; with $n = 2$ or 3) are involved in the decomposition process:

$$H_2O_2 + Mn^{(n+1)+} \longrightarrow H^+ + Mn^{n+} + HO_2^{\bullet}, \tag{3.6}$$

$$HO^{\bullet} + Mn^{n+} \longrightarrow Mn^{(n+1)+} + HO^-. \tag{3.7}$$

This general reaction scheme thus indicates the reduction of manganese towards an oxidation state 2+, which could be evidenced by the XPS results presented above. Regarding the application of MnO_2 as active component of the H_2O_2 gas sensors, the presence of Mn in lower oxidation states might be a reason for a decrease in sensitivity after extensive sensor operation. It is important to note, that a thermal reduction of MnO_2 to MnO can be excluded in our experiments, since the maximum temperature observed during sensor operation was below 300 °C [4]. In contrast, the thermal reduction of MnO_2 in reactive atmospheres has been observed to occur at temperatures above 500 °C only [24].

The decomposition mechanisms discussed before can be summarized by means of an overall cleavage of H_2O_2 into water and oxygen as shown in Eq. (3.8). In case of the hydrogen peroxide vaporized at 240 °C, the exothermal decomposition is accompanied by releasing the reaction heat $\Delta H_r = 105.3\ \mathrm{kJ\,mol^{-1}}$ as determined by Hess' law and thermodynamic data [25]. This release of energy results in a temperature increase of the calorimetric gas sensor, which is linearly correlated with the actual hydrogen peroxide concentration [4–7].

$$2H_2O_2 \longrightarrow 2H_2O + O_2 + \Delta H_r. \tag{3.8}$$

3.4.3 Characterization of catalyst dispersion

In a second part of this study, the influence of SU-8 photoresist exploited as an adhesion promoter between the catalyst powder and the sensor surface has been investigated. In Fig. 3.5, the XPS spectra of MnO_2 powder attached to the calorimetric sensor via

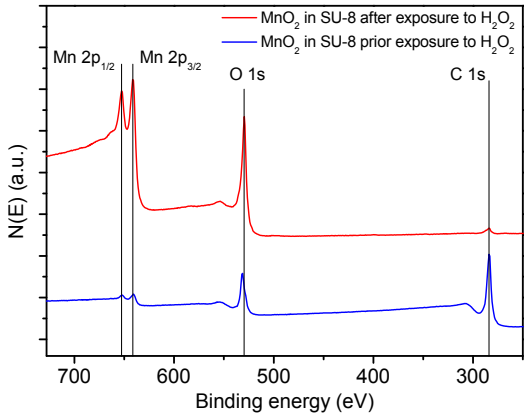

Fig. 3.5: XPS survey spectra of MnO_2 powder attached to the sensor surface by means of SU-8 photoresist before (bottom curve) and after (top curve) exposure to hydrogen peroxide vapor (same scale).

SU-8 photoresist is shown before (bottom curve) and after (top curve) its exposure to hydrogen peroxide.

Clearly, before the H_2O_2 treatment (bottom curve), the survey spectrum is dominated by photoemission from the C 1s core level (284 eV), thus indicating the presence of a thin polymer layer on top of the metal oxide powder (thickness 4–5 nm). Consequently, the emission of Mn 2p photoelectrons from the buried metal oxide is strongly suppressed by this polymer overlayer, resulting in a weak spectral contribution of the Mn 2p doublet to the survey spectrum, as can indeed be recognized in Fig. 3.5. The presence of a polymer overlayer can also be concluded from the observed O 1s binding energy position (532.0 eV), which can be assigned to oxygen atoms present in the SU-8 polymer [26]. After an initial H_2O_2 treatment intended to pre-condition the active sensor surface (upper curve), the carbon signal is found to be strongly reduced, thus evidencing the successful removal of the SU-8 layer by the hydrogen peroxide (the small remaining C 1s peak again arises from exposing the sample to ambient conditions before the XPS measurements). Now, a strong emission from the Mn 2p core doublet can be observed since Mn 2p photoelectrons are no longer damped by the polymer overlayer in contrast to before. Additionally, evidence for the successful removal of the polymer layer also arises from the O 1s binding energy (532.0 eV), which now corresponds to the value observed for the pure metal oxide. It is worth to mention, that this H_2O_2-induced surface cleaning of the active sensor material is similar to what has been reported when using an oxygen plasma to remove unintentional SU-8 overlayers [26]. Finally, a clean metal oxide surface is available after the pre-conditioning step thus allowing to reliably determining H_2O_2 concentrations in subsequent measurements.

A characteristic response curve of the H_2O_2 gas sensor, while offering different hydrogen peroxide concentrations is shown in Fig. 3.6. In the upper part, the temperatures of both temperature-sensitive elements are depicted. Here, in the lower part, the actual hydrogen peroxide concentration ($c(H_2O_2)$, right scale) and the temperature difference (dT, left scale) are presented. The resulting differential signal demonstrates the dura-

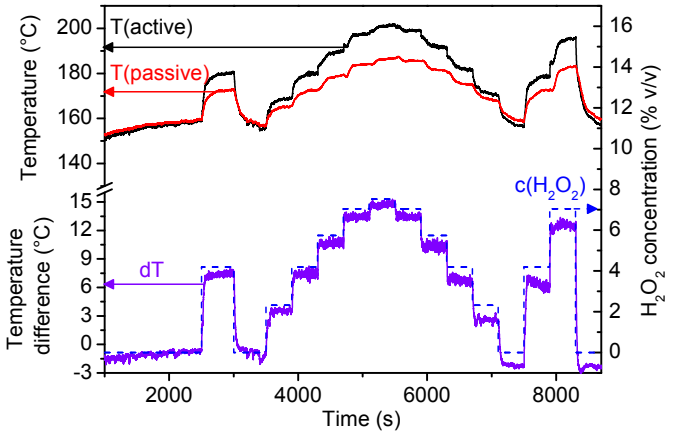

Fig. 3.6: Response curve of a H_2O_2 gas sensor. Upper part: temperatures of both temperature-sensitive elements as function of time; lower part: the actual hydrogen peroxide concentration ($c(H_2O_2)$) is indicated and the temperature difference (dT) as sensor output signal is given.

bility and chemical reactivity of the MnO_2 dispersion attached by SU-8 photoresist to one of the temperature-sensitive elements.

3.5 Conclusions

XPS as surface-sensitive tool has been used to characterize the catalytically active, H_2O_2-sensitive layer manganese(IV) oxide (MnO_2) of calorimetric gas sensors. Based on a chemical analysis, the catalyst surface is found to be partially reduced (with respect to the starting material, MnO_2) after sensor operation, as evidenced by the presence of lower oxidation states of the manganese. Our results indicate that the catalyst surface is involved into the decomposition process of hydrogen peroxide vapor, as thermal decomposition of the MnO_2 layer can be excluded in our experiments. Before reaching operational conditions within the chosen sensor design, the attachment of the catalyst material (the transition metal oxide) to the calorimetric sensor platform by means of SU-8 photoresist (acting as glue) is accompanied by the formation of a thin polymer overlayer on top of the metal oxide powder. This contamination layer, however, can easily be removed by means of an initial pre-conditioning step thereby exposing the catalyst surface to H_2O_2 vapor. Simultaneously, the thick SU-8 layer (2 mm), serving as passivation layer on top of the second temperature-sensitive element, remains unaffected. This simple treatment thus allows to efficiently produce clean metal oxide surfaces which are suitable for the subsequent detection of varying H_2O_2 concentrations in a reliable and reproducible manner.

References

[1] N. A. Klapes and D. Vesley. “Vapor-phase hydrogen peroxide as a surface decontaminant and sterilant”. *Applied and Environmental Microbiology* 56 (1990), 503–506.

[2] I. A. Ansari and A. K. Datta. "An overview of sterilization methods for packaging materials used in aseptic packaging systems". *Food and Bioproducts Processing* 81 (2003), 57–65.

[3] J. Wang and R. T. Toledo. "Sporicidal properties of mixtures of hydrogen peroxide vapor and hot air". *Food Technology* 40 (1986), 60–67.

[4] N. Näther, L. M. Juárez, R. Emmerich, J. Berger, P. Friedrich, and M. J. Schöning. "Detection of hydrogen peroxide (H_2O_2) at exposed temperatures for industrial processes". *Sensors (MDPI)* 6 (2006), 308–317.

[5] P. Kirchner, Y. A. Ng, H. Spelthahn, A. Schneider, H. Henkel, P. Friedrich, J. Kolstad, J. Berger, M. Keusgen, and M. J. Schöning. "Gas sensor investigation based on a catalytically activated thin-film thermopile for H_2O_2 detection". *Physica Status Solidi A* 207 (2010), 787–792.

[6] P. Kirchner, J. Oberländer, P. Friedrich, J. Berger, H.-P. Suso, A. Kupyna, M. Keusgen, and M. J. Schöning. "Optimization and fabrication of a calorimetric gas sensor built up on a polyimide substrate for H_2O_2 monitoring". *Physica Status Solidi A* 208 (2011), 1235–1240.

[7] P. Kirchner, J. Oberländer, P. Friedrich, J. Berger, G. Rysstad, M. Keusgen, and M. J. Schöning. "Realization of a calorimetric gas sensor on polyimide foil for applications in aseptic food industry". *Sensors and Actuators B: Chemical* 170 (2012), 60–66.

[8] C. N. Satterfield and T. Stein. "Decomposition of hydrogen peroxide vapor on relatively inert surfaces". *Industrial and Engineering Chemistry* 49 (1957), 1173–1180.

[9] A. B. Hart, J. McFadyen, and R. A. Ross. "Solid-oxide-catalyzed decomposition of hydrogen peroxide vapor". *Transactions of the Faraday Society* 59 (1963), 1458–1469.

[10] P. A. Giguère and I. D. Liu. "Kinetics of the thermal decomposition of hydrogen peroxide vapor". *Canadian Journal of Chemistry* 35 (1957), 283–293.

[11] D. B. Broughton and R. L. Wentworth. "Mechanism of decomposition of hydrogen peroxide solutions with manganese dioxide. I". *Journal of the American Chemical Society* 69 (1947), 741–744.

[12] M. A. Hasan, M. I. Zaki, L. Pasupulety, and K. Kumari. "Promotion of the hydrogen peroxide decomposition activity of manganese oxide catalysts". *Applied Catalysis A: General* 181 (1999), 171–179.

[13] S. H. Do, B. Batchelor, H. K. Lee, and S. H. Kong. "Hydrogen peroxide decomposition on manganese oxide (pyrolusite): kinetics, intermediates, and mechanism". *Chemosphere* 75 (2009), 8–12.

[14] N. Näther, H. Henkel, A. Schneider, and M. J. Schöning. "Investigation of different catalytically active and passive materials for realizing a hydrogen peroxide gas sensor". *Physica Status Solidi A* 206 (2009), 449–454.

[15] C. N. R. Rao, D. D. Sarma, S. Vasudevan, and M. S. Hegde. "Study of transition metal oxides by photoelectron spectroscopy". *Proceedings of the Royal Society A: Mathematical, Physical and Engineering Sciences* 367 (1979), 239–252.

[16] J. F. Moulder. *Handbook of X-Ray Photoelectron Spectroscopy: A Reference Book of Standard Spectra for Identification and Interpretation of XPS Data*. Update. Eden Prairie, Minnesota: Physical Electronics Division, Perkin-Elmer Corporation, 1992.

[17] NIST. *X-ray Photoelectron Spectroscopy Database, Version 4.1*. 2012. URL: `http://srdata.nist.gov/xps/`.

[18] J. S. Foord, R. B. Jackman, and G. C. Allen. "A X-ray photoelectron spectroscopic investigation of the oxidation of manganese". *Philosophical Magazine A* 49 (1984), 657–663.

[19] V. DiCastro and G. Polzonetti. "XPS study of MnO oxidation". *Journal of Electron Spectroscopy and Related Phenomena* 48 (1989), 117–123.

[20] M. Oku, K. Hirokawa, and S. Ikeda. "X-ray photoelectron spectroscopy of manganese-oxygen systems". *Journal of Electron Spectroscopy and Related Phenomena* 7 (1975), 465–473.

[21] Y. Zhao, Z. Chen, X. Shen, and X. Zhang. "Kinetics and mechanisms of heterogeneous reaction of gaseous hydrogen peroxide on mineral oxide particles". *Environmental Science and Technology* 45 (2011), 3317–3324.

[22] L. Micoli, G. Bagnasco, M. Turco, M. Trifuoggi, A. Russo Sorge, E. Fanelli, P. Pernice, and A. Aronne. "Vapor phase H_2O_2 decomposition on Mn based monolithic catalysts synthesized by innovative procedures". *Applied Catalysis B: Environmental* 140-141 (2013), 516–522.

[23] A. R. Sorge, M. Turco, G. Pilone, and G. Bagnasco. "Decomposition of hydrogen peroxide on MnO_2/TiO_2 catalysts". *Journal of Propulsion and Power* 20 (2004), 1069–1075.

[24] M. I. Zaki, M. A. Hasan, L. Pasupulety, and K. Kumari. "Thermochemistry of manganese oxides in reactive gas atmospheres: probing redox compositions in the decomposition course $MnO_2 \rightarrow MnO$". *Thermochimica Acta* 303 (1997), 171–181.

[25] Glenn Research Center, NASA. *Database of thermodynamic properties*. 2012. URL: `http://www.grc.nasa.gov/www/CEAWeb/ceaThermoBuild.htm`.

[26] F. Walther, P. Davydovskaya, S. Zürcher, M. Kaiser, H. Herberg, A. M. Gigler, and R. W. Stark. "Stability of the hydrophilic behavior of oxygen plasma activated SU-8". *Journal of Micromechanics and Microengineering* 17 (2007), 524–531.

4 Strategies in developing thin-film sensors for monitoring aseptic food processes: theoretical considerations and investigations of passivation materials (*Electrochimica Acta*, 183 (2015), 130–136)

J. Oberländer, P. Kirchner, M. Keusgen, and M. J. Schöning

Published in: *Electrochimica Acta,* Vol. 183 (2015), 130–136.

Submitted: 2015-02-22; Accepted: 2015-06-27; Published: 2015-07-02

4.1 Abstract

The sterilization of packages in aseptic food processes is highly significant to maintain a consumer-safe product with extended shelf-life. Today, the sterilization of food packages is predominantly accomplished by gaseous hydrogen peroxide (H_2O_2) in combination with heat. In order to monitor this sterilization process, calorimetric gas sensors as differential set-up of two platinum temperature sensors representing a catalytically active (additionally deposition of MnO_2) and a passive segment have been recently developed. The temperature rise of the exothermic decomposition serves as an indicator of the present H_2O_2 concentration. In the present work, a theoretical approach considering the sensor's thermochemistry and physical transport phenomena was formulated to evaluate the temperature rise based on the energy content of gaseous H_2O_2. In a further part of this work, three polymers have been analyzed with respect to their application as passivation materials. The examined polymers are photoresist SU-8, perfluoroalkoxy (PFA) and fluorinated ethylene propylene (FEP). Thermal analyses by means of differential scanning calorimetry (DSC) and thermogravimetric analysis (TGA) have been conducted to determine the operation limits of the polymers. The overall chemical resistance and stability of the polymers against the harsh environmental conditions during the sterilization process have been examined by attenuated total reflection Fourier transform infrared spectroscopy (ATR-FTIR).

4.2 Introduction

Packaging of sensitive liquid food products (e.g., milk, juice) requires a high grade of sterility in terms of absence of any microbiological contamination to maintain extended shelf-life of products and to guarantee consumer safety. These requirements are fulfilled by aseptic food processes, which is defined as the filling of commercially sterile products into separate sterilized packages, which are finally hermetically sealed [1]. These steps are performed in a sterile environment to prevent recontaminations. Major criteria during aseptic packaging are the two independent sterilization processes: i) the product to be filled is typically sterilized by a thermal treatment (pasteurization); ii) the packaging material, notably the food contact surfaces, is sterilized by a combination of heat and a chemical treatment. For semi-rigid composite packages, hydrogen peroxide (H_2O_2) has become the preferred sterilization medium [2, 3]. Main advantage of H_2O_2 in comparison to other sterilization media is its high microbicidal and sporicidal activity in particular at elevated temperatures. Furthermore, H_2O_2 finally decomposes to environmental-friendly end-products (water, oxygen) [4]. Depending on the filling machine, different application forms of the sterilization medium are applied: i) spraying; ii) roller systems; iii) immersion bath (all liquid H_2O_2) or iv) gaseous H_2O_2 [2, 3, 5].

In this work, only the gas-phase sterilization in aseptic food processes will be regarded. This sterilization process is mainly applied for pre-formed packages. In the first step of the sterilization process, the packaging materials are pre-heated by a stream of hot, sterile air, to maintain the gaseous phase of sterilization medium during the whole process. The sterilization medium comprises of a mixture of sterile air, as carrier gas, and liquid H_2O_2. This mixture is thermally vaporized at temperatures up to 300 °C. The H_2O_2 concentration within the gaseous mixture is typically between 2–7.5% v/v. This hot mixture will be guided into the pre-formed packages. Subsequently, a further hot, sterile air stream is applied into the packages to remove the sterilization agent prior product filling. To avoid product contamination the chemical (residual) concentration must be less than 0.5 ppm [6]. Monitoring of the sterilization process is essential towards aseptically packaged food. Nowadays, process control and periodical validations are performed by means of time- and lab-consuming microbiological methods (e.g., challenge tests such as end-point or count-reduction test) [6, 7]. Beside these microbiologic methods, monitoring of the sterilization process is only possible by monitoring machine parameters, like H_2O_2 dosage, gas temperature and exposure time. However, the parametric process monitoring is not able to capture systematic failures such as reduced H_2O_2 concentrations at the surfaces to be sterilized. An enhancement of process reliability can be achieved by implementing H_2O_2 gas sensors into the process. To enable in-line process monitoring specially designed calorimetric gas sensors have been discussed, recently [8–12]. Since, commercially available gas sensors are not able to withstand the harsh process conditions.

The calorimetric gas sensors are based on a differential set-up of two platinum temperature sensors. A schematic view of the calorimetric H_2O_2 gas sensor is depicted in Fig. 4.1. One of these temperature sensors is covered with a passivation layer to capture the environmental gas temperature. In the harsh environment of the sterilization process, the passivation layer possesses a crucial role in terms of sensor long-term stability.

The passivation materials have to fulfill special requirements: thermal stability, chemically resistant, no catalytic activity towards H_2O_2 and thin-film processability. For this purpose, different polymeric layers have been investigated. Suitable material candidates are the epoxy-based photoresist SU-8 and the two Teflon derivatives: perfluoroalkoxy (PFA) and fluorinated ethylene propylene (FEP). On the second temperature sensor, a catalytically active material is deposited to force the exothermal decomposition of H_2O_2. The following catalytic materials have been recently successfully implemented as sensor catalysts: manganese(IV) oxide (MnO_2), platinum (Pt) and palladium (Pd). The different catalytic materials have already been characterized with respect to their suitability for this sensor approach and to the resulting reaction mechanism [8, 13].

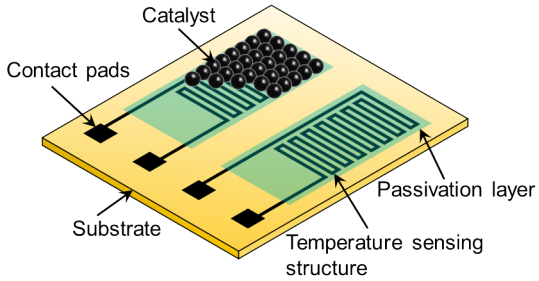

Fig. 4.1: Schematic representation of a thin-film calorimetric H_2O_2.

The latest generation of calorimetric H_2O_2 gas sensors is based on a flexible polyimide film [10, 14]. This substrate enhances the intrinsic sensor properties of the calorimetric gas sensors. On the one hand, the implementation of the sensor into the packages is enhanced by means of the flexible substrate. On the other hand, the low thermal conductivity of the polyimide film improves the sensor features. Notably, the sensor sensitivity and the response time of the sensor are improved. These benefits are resulting from the low thermal conductivity of polyimide ($0.16 \cdot 10^{-2}$ W cm^{-1} K^{-1}) compared to conventional thin-film substrates such as silicon (1.3 W cm^{-1} K^{-1}). The sensor response time has been reduced from $t_{90\%} = 6.7$ s for a Si-substrate to $t_{90\%} = 3.8$ s of polyimide [15]. The online characterization of the sterilization process has been facilitated by these thin-film sensors for the first time [15, 16].

The present work will focus on theoretical considerations of the calorimetric H_2O_2 gas sensor. Approaches of physical transport phenomena as well as of the thermochemistry are introduced. The theoretical analyses are discussed in context with related sensor measurements. A further aspect within this work is the characterization of the polymeric passivation layers (SU-8, PFA, FEP) with regard to their durability as sensor passivation material in the harsh conditions of the sterilization process. The materials under test will be examined by means of thermal analyses, in particular, differential scanning calorimetry (DSC) and thermogravimetric analysis (TGA). The overall chemical stability against the H_2O_2 sterilization in aseptic food processes will be analyzed by attenuated total reflection Fourier transform infrared spectroscopy (ATR-FTIR).

4.3 Experimental

4.3.1 Theoretical considerations of the decomposition process

The following theoretical considerations are based on the work of McBride et al. [17]. Three different operation modes of the calorimetric H_2O_2 gas sensors are of interest. The initial concept considers the steady-state condition of the chemical reaction. The calculation is based on the enthalpies of the involved reaction partners. Hereby, the upper limit of the released energy in terms of the temperature rise is derived [17, 18]. Subsequently, transport mechanisms such as diffusion and convection are introduced to the calculation model. Unless otherwise stated, all calculations are performed for a typical process temperature of the gaseous sterilization process of 240 °C.

Decomposition temperature of a steady-state process

The theoretical enthalpy of chemical reactions can be derived by use of the formation enthalpies of the involved reaction partners combined by Hess's law and the stoichiometric relation. The stoichiometric relation of the H_2O_2 decomposition is expanded by the reaction enthalpy ΔH_r:

$$2H_2O_2 \longrightarrow O_2 + 2H_2O + \Delta H_r \tag{4.1}$$

At a gaseous temperature of 240 °C the reaction enthalpy ΔH_r is determined to be -105.3 kJ mol^{-1} (exothermic), by application of data listed in literature [19], and assuming that the reaction takes place at a constant pressure and all H_2O_2 molecules are completely consumed by this reaction. The energy balance leads to a proportional relation between the reaction heat (ΔQ) and the resulting change in temperature (ΔT_{max}):

$$\Delta Q = (-\Delta H_r)n = \rho c_p \Delta T_{max} \tag{4.2}$$

Here, n depicts the number density of reactant molecules representing the concentration. The further proportional factors are: ρ and c_p, the density and specific heat of the gas mixture, respectively. In contrast to a former calculation model established by McBride et al. [17], the specific heat of the H_2O_2 gas mixture is calculated by Eq. (4.3) and the molar fractions x_i of the substances, because in the present consideration the specific heat is significantly changed by the different gas composition.

$$c_{p-mix} = \sum x_i c_{p-i} \tag{4.3}$$

This first relation constitutes the maximum achievable temperature increase by the gas-phase decomposition of H_2O_2. The temperature increase is proportional to the energy content of H_2O_2. In this upper limit of temperature rise the effects of thermal transportation phenomena as well as sensor dimensions are neglected [17, 18].

Decomposition temperature with respect to diffusion processes

In the second modeling approach, diffusion effects (namely for heat and mass) will be taken into account. This results in a temperature rise for systems with none or low

gas-flow rate: the temperature rise is then expanded by the thermal conductivity (λ) and the diffusion coefficient ($D_{H_2O_2-air}$) of H_2O_2 in a system comprising of air.

$$\Delta T_d = \frac{D_{H_2O_2-air}(-\Delta H_r)n}{\lambda_p c_p} \tag{4.4}$$

The determination of the temperature-dependent diffusion coefficient is presented in Eq. (4.5). The calculation of the diffusion coefficient is based on the Chapman-Enskog theory as described in [20, 21].

$$D_{H_2O_2-air} = \frac{1.858 \cdot 10^{-3}\sqrt{T^3}(M_{H_2O_2}^{-1} + M_{air}^{-1})}{p\sigma_{H_2O_2}^2 \Omega} \tag{4.5}$$

The diffusion coefficient of H_2O_2 in air depends on the absolute temperature T, the molecular mass of the corresponding substances M_x, the absolute pressure p, the collision diameter $\sigma_{H_2O_2}$ and the collision integral Ω, both given in [20, 22].

Decomposition temperature comprising gas diffusion and convection processes

In order to establish a more precise calculation of the temperature rise, the impact of a forced gas flow will be included to the calculations. The energy balance (Eq. (4.2)) is extended by transfer coefficients for mass (h_{mass}) and heat (h_{heat}):

$$\Delta Q = h_{mass}(-\Delta H_r)n = h_{heat}\Delta T_c \tag{4.6}$$

The transfer coefficients comprise the transport phenomena of gas diffusion and forced convection, as well as the sensor's geometry. The geometrical factors are related to heat and mass transfer, respectively, of a body employed in a flow system. Similar to the design considerations in [17], the sensor geometry is simplified to a sphere (radius r_s) situated in the gas stream. In accordance to [17, 20, 21] the coefficients for this case can be expressed as:

$$h_{mass} = \frac{D_{H_2O_2-air}}{r_s}(1 + 0.3N_{Re}^{1/2}N_{Sc}^{1/3}) \tag{4.7}$$

$$h_{mass} = \frac{\lambda}{r_s}(1 + 0.3N_{Re}^{1/2}N_{Pr}^{1/3}) \tag{4.8}$$

Here, N_{Re}, N_{Sc} and N_{Pr} represent the Reynolds, Schmidt and Prandtl number of thermodynamics, respectively:

$$N_{Re} = \frac{2r_s\rho u}{\mu};\ N_{Sc} = \frac{\mu}{\rho D_{H_2O_2-air}};\ N_{Pr} = \frac{\mu c_p}{\lambda}$$

By means of the thermodynamic numbers, the theoretical temperature rise becomes dependent on the flow velocity u and the dynamic viscosity μ of the carrier gas. The theoretical temperature rise comprising convection and gas diffusion processes (ΔT_c) can be expressed as:

$$h_{mass} = \frac{D_{H_2O_2-air}(-\Delta H_r)n}{\lambda} \cdot \frac{1 + 0.3N_{Re}^{1/2}N_{Sc}^{1/3}}{1 + 0.3N_{Re}^{1/2}N_{Pr}^{1/3}} \tag{4.9}$$

The applied literature coefficients of the above stated calculations are summarized in Tab. 4.1.

Tab. 4.1: Thermal transport coefficients applied for the theoretical considerations of H_2O_2 gas sensors at a gas temperature of 240 °C and a carrier gas stream of 10 $m^3\,h^{-1}$ (adapted from [20, 21, 23]).

ρ_{air} ($kg\,m^{-3}$)	λ ($W\,m^{-1}\,K^{-1}$)	u ($m\,s^{-1}$)	Ω (-)	$\sigma_{H_2O_2-air}$ (nm)
0.395	0.693	$40.4 \cdot 10^{-3}$	6.38	0.9186

c_{p-air} ($J\,mol^{-1}\,K^{-1}$)	c_{p-H_2O} ($J\,mol^{-1}\,K^{-1}$)	$c_{p-H_2O_2}$ ($J\,mol^{-1}\,K^{-1}$)
29.9	35.4	50.7

4.3.2 Characterization of passivation materials

The sensor response as well as the long-term stability of the calorimetric H_2O_2 gas sensors is obviously depending on the catalytic layer. An additional major key role possesses the passivation layer, which should not undergo degradation processes induced by the sterilization process to be monitored. Therefore, the three following passivation materials are subjected in material characterizations. The epoxy-based negative-tone photoresist SU-8 2 (Microchem Corp., USA) and two Teflon derivatives: perfluoroalkoxy (PFA) (PFA, 857-110, DuPont, USA) and fluorinated ethylene propylene (FEP) (FEP 6300GZ, 3M Dyneon, Germany). The monomeric chemical structures of these materials are depicted in Fig. 4.2, the chemical distinguishing features of PFA and FEP are highlighted. Thin-films of the polymeric layers were fabricated by spin-coating processes onto silicon wafers for the characterization. The sensor fabrication method is described in [24]. A resulting layer thickness of about 1.5 μm could be obtained for all materials.

Two thermal stress characterizations on these polymers were performed. Differential scanning calorimetry (DSC) of the materials was conducted to study the melting temperatures of the materials and to observe temperature-related deviations, such as cross-linking. These characterizations were performed with a DSC 200 PC (Netzsch GmbH, Germany) in a temperature range of 20–320 °C. The device measures the heat flow, which is required to increase the temperature of the material under test against a reference probe, as a function of temperature.

Thermogravimetric analyses (TGA) were conducted with the objective to determine the degradation temperature of the various materials. The TGA device TG 209 F1 Iris (Netzsch GmbH, Germany) was applied for all characterizations within the temperature range of 20–600 °C. The TGA device captures the change in mass as a function of temperature.

In both thermal analysis methods, polymer samples of about 8 mg were studied. To avoid oxidative reactions the sample chambers were continuously purged with nitrogen. A constant heating rate of 20 $K\,min^{-1}$ was maintained.

The overall sterilization process durability of the polymeric materials has been studied by use of attenuated total reflection Fourier transform infrared spectroscopy (ATR-FTIR). The material-specific infrared absorption bands, determined by this spec-

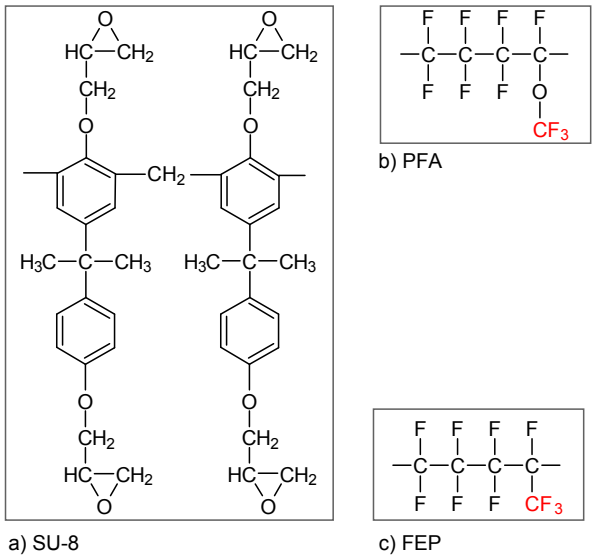

Fig. 4.2: Chemical structures of the examined polymers: a) photoresist SU-8, b) PFA and c) FEP (modified from [25, 26]).

troscopy method, facilitate the detection of chemical deviations. The polymer samples for this survey were analyzed prior and after a treatment in the sterilization process (gas temperature: 240 °C, H_2O_2 conc.: 7.5% v/v, about 3 h). The Tensor 24 (Bruker Corp., USA) ATR-FTIR device was applied for this study; the spectra are recorded within a wavenumber range of 750–2000 cm^{-1}.

4.4 Results and discussions

4.4.1 Results of the theoretical sensor considerations

The initial calculation represents the determination of the theoretical temperature rise based on the energy balance of the chemical decomposition of H_2O_2, which is also defined as the upper sensitivity limit of calorimetric gas-sensing devices [17, 18]. In terms of the gaseous H_2O_2 detection the upper sensitivity limit has been derived to $\Delta T_{max} = c(H_2O_2) \cdot 20.4$ °C/(% v/v), depending on the present H_2O_2 concentration $c(H_2O_2)$. The maximum temperature rise is neglecting all transport phenomena as well as geometrical factors.

The second consideration takes diffusion processes of heat and mass transfer into account. Hereby, the temperature rise is limited compared to the first observation of the upper sensitivity. The limitation arises by the fact that diffusion processes and heat loss into the gaseous system are introduced to the calculation. The diffusion coefficient of H_2O_2 in air for a gas temperature of 240 °C has been derived to $3.80 \cdot 10^{-5}$ $m^2\,s^{-1}$. The temperature rise for the diffusion-limited process is determined to $\Delta T_d = c(H_2O_2) \cdot 14.4$ °C/(% v/v). This calculation of the temperature rise with respect to the diffusion process is still independent of the sensor's geometry.

In the final theoretical consideration, diffusion processes and forced convection are regarded. A typically applied gas flow of 10 $m^3\,h^{-1}$ has been taken into account. The resulting theoretical temperature rise will become additionally dependent on the sensor's geometry. In the following considerations the sensor geometry has been simplified to a sphere with a diameter of 10 mm. This resulting temperature rise is determined to ΔT_c = c(H_2O_2) · 15.8 °C/(% v/v).

In previously performed sensor experiments, a maximum sensor temperature rise of ΔT_{signal} = c(H_2O_2) · 7.15 °C/(% v/v) has been achieved on a polyimide-based thin-film sensor [14]. The rise in sensor temperature is substantially lower than in the presented theoretical thermochemical considerations. Discrepancies between the theoretical calculations and the sensor sensitivity could result from different aspects: for the calculation, the assumption of a complete conversion of the present H_2O_2 molecules has been applied, whereby the possible decomposition caused during the evaporation process is neglected. In the applied calculations, factors for the catalyst's activity towards the H_2O_2 decomposition are missing. Currently, no models regarding the catalyst's activity are available and should be focused in further works. Additionally, the sensor design itself could result in reduced sensitivities; both temperature sensors are placed as close as possible to each other, whereby thermal transport due to the substrate or radiation can occur. The sensor housing, e.g., heat loss due to support structures, is a further reason for a decreased sensitivity. It should be noted that the aim of the calculations was to determine restrictions (upper limits) of the temperature rise for the H_2O_2 decomposition, based on thermochemistry and physical transport phenomena, with no regards to material properties.

Even though, the sensor response is substantially lower than the theoretically determined value. Fig. 4.3 shows exemplarily a sensor measurement plot of a calorimetric H_2O_2 gas sensor at different H_2O_2 concentrations (sensor fabrication of this set-up is found in, e.g., [27]). In the upper part of the measurement plot the temperatures of both temperature sensors (catalytically activated and passivated) are presented. As the resulting sensor signal the temperature difference is shown in the lower part (left y-axis). The varying H_2O_2 concentration is also depicted in the lower part (right y-axis). The gas flow has been varied between 8 $m^3\,h^{-1}$ and 12 $m^3\,h^{-1}$. In the measurement plot slight changes of the sensor signal due to the variations in the gas flow can be recognized.

In Fig. 4.4, the effect of different gas-flow rates onto the gas sensor is compared with the calculations for the forced convection. The theoretical consideration exhibits a variation in the temperature rise of 0.2 °C/(% v/v)/($m^3\,h^{-1}$). The sensor measurements exhibit a similar behavior between 8 $m^3\,h^{-1}$ and 10 $m^3\,h^{-1}$, for which the temperature rise was more pronounced than between 10 $m^3\,h^{-1}$ and 12 $m^3\,h^{-1}$ (s. Table 4.2). A reason for the reduced influence at elevated gas flow can be related to the involved diffusion processes. At higher flow rates the diffusion processes outside the catalyst (film diffusion) are no longer rate-determining, whereas the inner diffusion processes (pore diffusion) limit the catalytic decomposition, similar to the evaluations in [18].

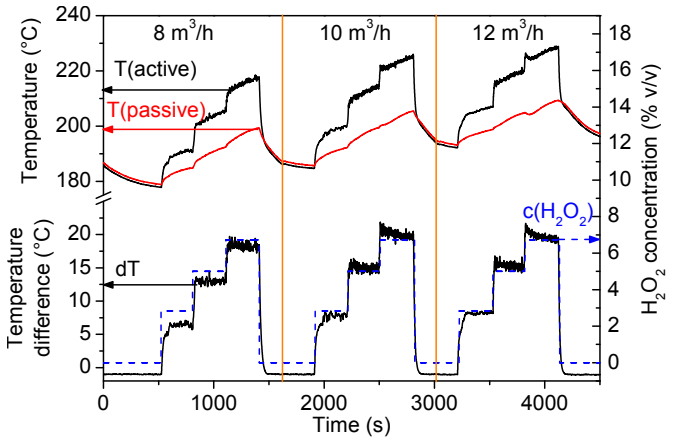

Fig. 4.3: Characteristic measurement plot of a calorimetric H_2O_2 gas sensor exposed to various H_2O_2 concentrations from 0–6.8% v/v. The calorimetric gas sensor consists of two platinum temperature sensors, passivation material: PFA, catalyst: MnO_2, set-up as described in [27]. The upper part depicts the temperatures of both temperature sensors (catalytically activated and passivated). The lower part shows the resulting temperature difference (left y-axis) and the adjusted H_2O_2 concentration (right y-axis). The carrier gas flow has been varied between 8 $m^3\,h^{-1}$ and 12 $m^3\,h^{-1}$.

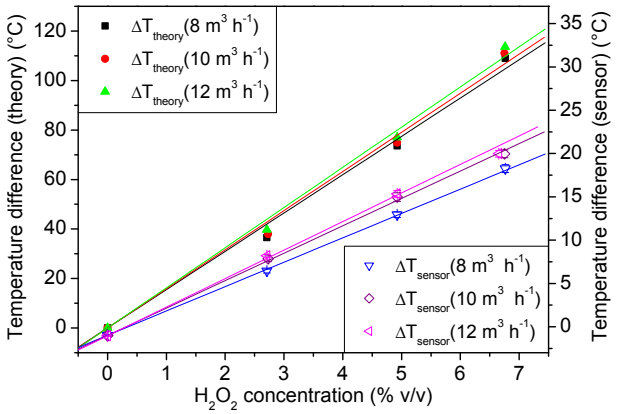

Fig. 4.4: Effect of the volume flow on the temperature rise; left-hand scale depicts the temperature difference for the theoretical calculation, right-hand scale for the performed sensor measurements of Fig. 4.3.

Tab. 4.2: Comparison of the theoretical and sensor slopes (S_x) of the temperature rise determined from the plots in Fig. 4.4.

Gas flow rate	8 $m^3\,h^{-1}$	10 $m^3\,h^{-1}$	12 $m^3\,h^{-1}$
S_{theory} (°C/(% v/v))	15.4	15.8	16.2
S_{sensor} (°C/(% v/v))	2.8	3.2	3.3

4.4.2 Characterization of polymeric passivation layers

The DSC analyses of the different spin-coated passivation materials are depicted in Fig. 4.5. In case of both Teflon derivatives (PFA and FEP) distinct melting temperatures can be ascertained at 309 °C and 268 °C, respectively. The photoresist SU-8 exhibits no melting point within the considered temperature range of up to 320 °C. The area below the melting peaks is defined as the heat of fusion ΔH_f of the material under test. For PFA and FEP, the heat of fusion can be determined to 20.7 J g^{-1} and 11.9 J g^{-1}, respectively, which is in good agreement with values found in literature [28].

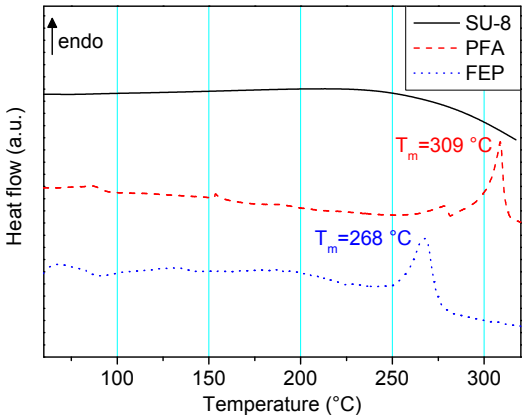

Fig. 4.5: DSC analysis of the three investigated passivation materials SU-8 photoresist, PFA and FEP. Distinct melting peaks for PFA and FEP can be observed, whereas no melting peak for SU-8 within the temperature range was found; endo: endothermic reaction corresponds to increasing peaks.

Thermogravimetric analyses of the passivation polymers were conducted to determine the mass fluctuation, induced by a thermal treatment, as a function of temperature. The resulting TGA profiles are presented in Fig. 4.6. The initial temperature-related change in mass (weight loss of about 5%) has been elected as the degradation temperature. This method is in contrast to literature [29], where the first derivative is usually applied for the determination of the degradation temperature, resulting in slightly higher temperatures. In case of the sensor passivation layer, a small deviation of the material composition is related to changes in thermal properties (e.g., heat capacity, heat conduction) that might influence the sensor signal. The photoresist SU-8 exhibits a degradation temperature of 393 °C. The initial degradation temperatures of the Teflon derivatives were achieved at 516 °C and 485 °C for PFA and FEP, respectively.

The thermal characterizations of the different polymers for sensor passivation demonstrated their thermal durability within the expected sensor operation temperature range (170–300 °C). Only the melting point of FEP might be critical to serve as a passivation material for monitoring the H_2O_2 concentration above 260 °C.

In order to examine the chemical durability of the polymer layers against the harsh sterilization process, i.e., the elevated H_2O_2 concentrations, the materials were subjected to chemical surface analysis by means of ATR-FTIR spectroscopy. The spectra of all materials were recorded before and after an exposure to the sterilization process (gas

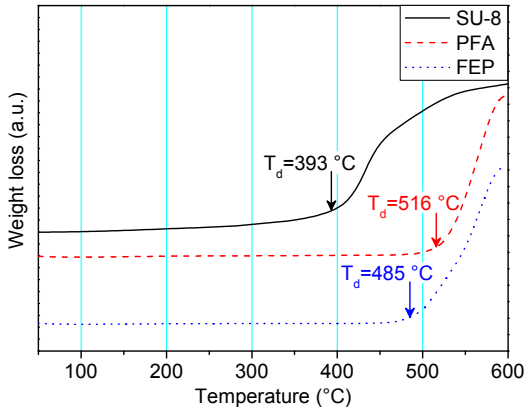

Fig. 4.6: TG analysis of the passivation materials SU-8, PFA and FEP. The starting degradation temperatures of the materials are indicated by arrows.

temperature: 240 °C, H_2O_2 conc.: 7.5% v/v, about 3 h), to observe process-related chemical deviations.

In Fig. 4.7, the observed spectra of the photoresist SU-8 are shown. With regard to the presented chemical composition (Fig. 4.2 a)), a high number of absorption bands can be observed. Characteristic absorption bands and especially, bands which undergo a change induced by the sterilization process will be considered in detail. The major absorption band at 1500 cm^{-1} can be assigned to the C=C stretching vibrations of the aromatic rings; both spectra have been normalized with respect to this major absorption band. A residual content of the solvent within the layer is represented by the absorption band at 1180 cm^{-1}. The degree of cross-linking can be estimated by the CH_2 vibration (1463 cm^{-1}), the band of the aliphatic ether (1032 cm^{-1}) and the minor absorption at 912 cm^{-1} corresponding to the epoxide rings [30, 31]. Especially, the disappearance of the minor band at 912 cm^{-1}, after exposure to the sterilization process, indicates a further curing of the polymer layer. Additionally, the carbonyl compound is related to the absorption at 1750 cm^{-1}, which is increased after the sterilization treatment. In an overall comparison, both spectra of SU-8 correspond mainly to each other (only a further curing can be observed), indicating that the SU-8 layer is not affected by H_2O_2 exposure.

The analyses of the Teflon derivatives exhibit similar spectra for both materials with two major absorption bands and one minor absorption band (s. Figs. 4.8 and 4.9). The two major absorption bands (1200 cm^{-1}, 1145 cm^{-1}) are characteristics of fluoropolymers and can be assigned to the CF_2 asymmetric and symmetric stretching vibrations [32]. The minor absorption bands can be used to distinguish the Teflon derivatives. The minor characteristic absorption band of PFA can be found at 993 cm^{-1}, whereas for FEP the absorption band is present at 981 cm^{-1}. These adsorption bands are related to the CF_3 stretching mode of the specific side groups, as highlighted in Fig. 4.2 b), c). In the chemical analyses, both Teflon derivatives exhibit excellent inertness against the sterilization agent at elevated temperature, because for both materials no degradation behavior exists when comparing the spectra before and after H_2O_2 exposure.

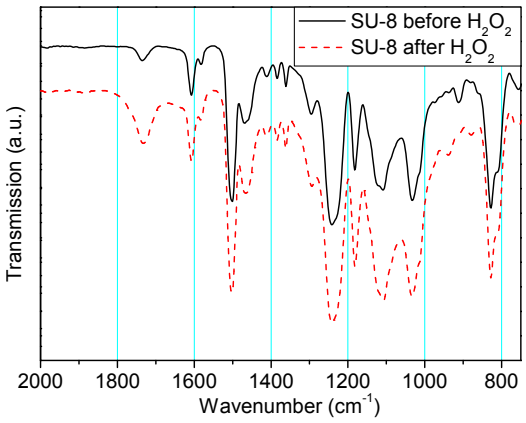

Fig. 4.7: ATR-FTIR spectra of SU-8 photoresist before and after exposure to the sterilization process (flow: 10 $m^3\,h^{-1}$; H_2O_2 concentration: 7.5% v/v; exposure time 3 h).

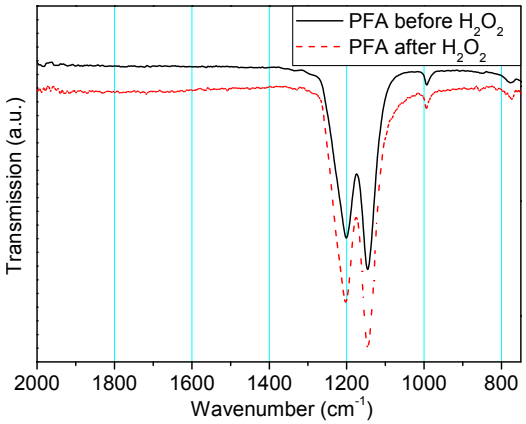

Fig. 4.8: ATR-FTIR spectra of PFA before and after exposure to the sterilization process (flow: 10 $m^3\,h^{-1}$; H_2O_2 concentration: 7.5% v/v; exposure time 3 h).

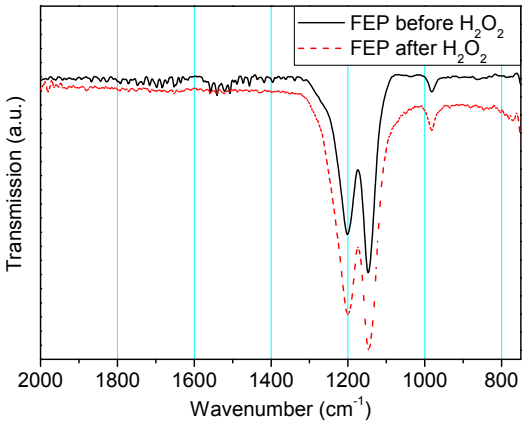

Fig. 4.9: ATR-FTIR spectra of FEP before and after exposure to the sterilization process (flow: 10 $m^3\,h^{-1}$; H_2O_2 concentration: 7.5% v/v; exposure time 3 h)

4.5 Conclusions

In the present work, approaches for the sensor's thermochemistry and physical transport phenomena have been introduced with the aim to evaluate the theoretical temperature rise of the H_2O_2 decomposition. Three different cases at a gaseous temperature of 240 °C and H_2O_2 gas concentrations between 0 and 7.5% v/v have been considered. First, steady state was assumed to calculate the maximum temperature rise based on the energy content of gaseous H_2O_2. Second, diffusion limitation was introduced. Third, forced convection processes at a volume flow of 10 $m^3\,h^{-1}$ have been considered. The calculated temperature rise amounts to be $\Delta T_c = c(H_2O_2) \cdot 15.8$ °C/(% v/v) and the actual sensor's temperature rise is $\Delta T_{sensor} = c(H_2O_2) \cdot 7.1$ °C/(% v/v). Discrepancies between the theoretical temperature rise and the determined temperature rise of calorimetric H_2O_2 gas sensors have been discussed. Finally, a comparison between the theoretical calculations and sensor measurements at different gas-flow rates was drawn.

Three different polymer passivation layers, namely SU-8 photoresist, PFA and FEP, were investigated by two thermal analysis methods (DSC, TGA) to determine their melting and degradation temperatures. The thermal characterization revealed that all examined materials are suitable candidates for sensor passivation with respect to the operation temperature for package sterilization in aseptic food processes.

By means of ATR-FTIR the overall durability of the passivation layers against the sterilization process (H_2O_2 agent) was studied. In this analysis, both Teflon derivatives exhibit their thermal and chemical resistance. The SU-8 photoresist showed slight changes due to the exposure to the sterilization medium. The effects could be related to a further cross-linking of the material. In conclusion, the chemical analyses of the polymers have revealed the suitability as passivation materials for hydrogen peroxide gas sensors. In particular, the durability against the extreme process conditions (elevated temperature and H_2O_2 concentrations up to 7.5% v/v), has been demonstrated. In terms of fabrication steps of thin-film sensors the photoresist SU-8 possesses the advantage to enable a direct patterning by means of photolithography.

Acknowledgments

The project has been financially supported by the Federal Ministry of Education and Research (BMBF: Project: "ImpediPack"), Germany. The authors gratefully thank M. Raue from the Institute of Applied Polymer Chemistry (Jülich) for technical support of the material analysis.

References

[1] B. A. H. von Bockelmann and I. L. I. von Bockelmann. "Aseptic packaging of liquid food products: a literature review". *Journal of Agricultural and Food Chemistry* 34 (1986), 384–392.

[2] B. A. H. von Bockelmann and I. L. I. von Bockelmann. *Long-Life Products: Heat-Treated, Aseptically Packed: A Guide to Quality*. Åkarp, Sweden: B. von Bockelmann, 1998.

[3] R. T. Toledo. "Overview of sterilization methods for aseptic packaging materials". In: *Food and Packaging Interactions: Developed from a Symposium Sponsored by the Division of Agricultural and Food Chemistry at the 193rd Meeting of the American Chemical Society, Denver, Colorado, April 5-10, 1987*. Ed. by J. H. Hotchkiss. Vol. 365. ACS symposium series. Washington, DC, USA: American Chemical Society, 1988, 94–105.

[4] R. T. Toledo, F. E. Escher, and J. C. Ayres. "Sporicidal properties of hydrogen peroxide against food spoilage organisms". *Applied Microbiology* 26 (1973), 592–597.

[5] I. A. Ansari and A. K. Datta. "An overview of sterilization methods for packaging materials used in aseptic packaging systems". *Food and Bioproducts Processing* 81 (2003), 57–65.

[6] Food and Drug Administration. *Code of federal registrations: food and drugs: indirect food additives: adjuvants, production aids, and sanitizers*. Code of Federal Regulations (CFR). 2011. URL: `http://www.fda.gov`.

[7] Verband Deutscher Maschinen- und Anlagenbau e.V. "Code of practice: filling machines of VDMA hygiene class V: testing the effectiveness of packaging sterilization devices". *VDMA-Fachverbandsschriften* 6 (2008), 1–16.

[8] P. Kirchner, B. Li, H. Spelthahn, H. Henkel, A. Schneider, P. Friedrich, J. Kolstad, M. Keusgen, and M. J. Schöning. "Thin-film calorimetric H_2O_2 gas sensor for the validation of germicidal effectivity in aseptic filling processes". *Sensors and Actuators B: Chemical* 154 (2011), 257–263.

[9] P. Kirchner, Y. A. Ng, H. Spelthahn, A. Schneider, H. Henkel, P. Friedrich, J. Kolstad, J. Berger, M. Keusgen, and M. J. Schöning. "Gas sensor investigation based on a catalytically activated thin-film thermopile for H_2O_2 detection". *Physica Status Solidi A* 207 (2010), 787–792.

[10] P. Kirchner, J. Oberländer, P. Friedrich, J. Berger, G. Rysstad, M. Keusgen, and M. J. Schöning. "Realization of a calorimetric gas sensor on polyimide foil for applications in aseptic food industry". *Sensors and Actuators B: Chemical* 170 (2012), 60–66.

[11] P. Kirchner, S. Reisert, and M. J. Schöning. "Calorimetric gas sensors for hydrogen peroxide monitoring in aseptic food processes". In: *Gas Sensing Fundamentals*. Ed. by C.-D. Kohl and T. Wagner. Springer Series on Chemical Sensors and Biosensors. Heidelberg, Germany: Springer-Verlag GmbH, 2014, 279–310.

[12] N. Näther, L. M. Juárez, R. Emmerich, J. Berger, P. Friedrich, and M. J. Schöning. "Detection of hydrogen peroxide (H_2O_2) at exposed temperatures for industrial processes". *Sensors (MDPI)* 6 (2006), 308–317.

[13] J. Oberländer, P. Kirchner, H.-G. Boyen, and M. J. Schöning. "Detection of hydrogen peroxide vapor by use of manganese(IV) oxide as catalyst for calorimetric gas sensors". *Physica Status Solidi A* 211 (2014), 1372–1376.

[14] P. Kirchner, J. Oberländer, P. Friedrich, J. Berger, H.-P. Suso, A. Kupyna, M. Keusgen, and M. J. Schöning. "Optimization and fabrication of a calorimetric gas sensor built up on a polyimide substrate for H_2O_2 monitoring". *Physica Status Solidi A* 208 (2011), 1235–1240.

[15] P. Kirchner, J. Oberländer, H.-P. Suso, G. Rysstad, M. Keusgen, and M. J. Schöning. "Towards a wireless sensor system for real-time H_2O_2 monitoring in aseptic food processes". *Physica Status Solidi A* 210 (2013), 877–883.

[16] P. Kirchner, J. Oberländer, H.-P. Suso, G. Rysstad, M. Keusgen, and M. J. Schöning. "Monitoring the microbicidal effectiveness of gaseous hydrogen peroxide in sterilization processes by means of a calorimetric gas sensor". *Food Control* 31 (2013), 530–538.

[17] J. R. McBride, K. E. Nietering, and K. R. Ellwood. "Design considerations for optimizing the sensitivity of catalytic calorimetric gas sensors: modeling and experimental results". *Sensors and Actuators B: Chemical* 73 (2001), 163–173.

[18] V. Casey, J. Cleary, G. D'Arcy, and J. B. McMonagle. "Calorimetric combustible gas sensor based on a planar thermopile array: fabrication, characterization, and gas response". *Sensors and Actuators B: Chemical* 96 (2003), 114–123.

[19] B. J. McBride, M. J. Zehe, and S. Gordon. *Coefficients for calculating thermodynamic properties of individual species*. 2002. URL: `http://gltrs.grc.nasa.gov/GLTRS`.

[20] R. B. Bird, W. E. Stewart, and E. N. Lightfoot. *Transport Phenomena*. 2nd ed. New York: John Wiley & Sons, Inc., 2002.

[21] J. R. Welty, C. E. Wicks, R. E. Wilson, and G. L. Rorrer. *Fundamentals of Momentum, Heat, and Mass Transfer*. 5th ed. Vol. 13. New York, NY, USA: John Wiley & Sons, Inc., 2008.

[22] R. C. Reid, J. M. Prausnitz, and B. E. Poling. *The Properties of Gases and Liquids*. 4. Ed. McGraw-Hill Books in Chemical Engineering. New York: McGraw-Hill, 1987.

[23] Glenn Research Center, NASA. *Database of thermodynamic properties*. 2012. URL: `http://www.grc.nasa.gov/www/CEAWeb/ceaThermoBuild.htm`.

[24] P. Kirchner, S. Reisert, P. Pütz, M. Keusgen, and M. J. Schöning. "Characterization of polymeric materials as passivation layer for calorimetric H_2O_2 gas sensors". *Physica Status Solidi A* 209 (2012), 859–863.

[25] T. Katoh and Y. Zhang. "Deposition of Teflon-polymer thin films by synchrotron radiation photodecomposition". *Applied Surface Science* 138-139 (1999), 165–168.

[26] Y. Wang, J.-H. Pai, H.-H. Lai, C. E. Sims, M. Bachman, G. P. Li, and N. L. Allbritton. "Surface graft polymerization of SU-8 for bio-MEMS applications". *Journal of Micromechanics and Microengineering* 17 (2007), 1371–1380.

[27] N. Näther, H. Henkel, A. Schneider, and M. J. Schöning. "Investigation of different catalytically active and passive materials for realizing a hydrogen peroxide gas sensor". *Physica Status Solidi A* 206 (2009), 449–454.

[28] J.-C. Lee, S. Namura, S. Kondo, and A. Abe. "Miscibility and cocrystallization behavior of two melt-processable random copolymers of tetrafluoroethylene and perfluoroalkylvinylether". *Polymer* 42 (2001), 5453–5461.

[29] J. Schawe, R. Riesen, G. Widmann, M. Schubnell, and U. Jörimann. "Interpreting TGA curves". *UserCom* 13 (2001), 1–20.

[30] S. Keller, G. Blagoi, M. Lillemose, D. Haefliger, and A. Boisen. "Processing of thin SU-8 films". *Journal of Micromechanics and Microengineering* 18 (2008), 125020–125030.

[31] T. L. Tan, D. Wong, P. Lee, R. S. Rawat, S. Springham, and A. Patran. "Characterization of chemically amplified resist for X-ray lithography by Fourier transform infrared spectroscopy". *Thin Solid Films* 504 (2006), 113–116.

[32] H. Lobo and J. V. Bonilla. *Handbook of Plastics Analysis*. Vol. 68. Plastics Engineering. New York, NY, USA: Marcel Dekker, Inc., 2003.

5 Study of interdigitated electrode arrays using experiments and finite element models for the evaluation of sterilization processes (*Sensors (MDPI)*, 15, 10 (2015), 26115–26127)

J. Oberländer*, Z. B. Jildeh*, P. Kirchner, L. Wendeler, A. Bromm, H. Iken, P. H. Wagner, M. Keusgen and M. J. Schöning

Published in: *Sensors (MDPI)*, Vol. 15, 10 (2015), 26115–26127.

Submitted: 2015-08-31; Accepted: 2015-10-09; Published: 2015-10-14

* Both authors contributed equally to this work.

5.1 Abstract

In this work, a sensor to evaluate sterilization processes with hydrogen peroxide vapor has been characterized. Experimental, analytical and numerical methods were applied to evaluate and study the sensor behavior. The sensor set-up is based on planar interdigitated electrodes. The interdigitated electrode structure consists of 614 electrode fingers spanning over a total sensing area of 20 mm^2. Sensor measurements were conducted with and without microbiological spores as well as after an industrial sterilization protocol. The measurements were verified using an analytical expression based on a first-order elliptical integral. A model based on the finite element method with periodic boundary conditions in two dimensions was developed and utilized to validate the experimental findings.

5.2 Introduction

Sterilization processes are important in various industrial fields such as pharmaceutics, medicine and food packaging. The processes have to ensure the inactivation of all microorganisms even of highly resistant bacterial spores to achieve an extended shelf-life of products and to improve consumer safety. In food packaging industry various sterilization processes are used and the applied method depends on the object to be sterilized. For the sterilization of multi-layered composite food packages, which will contain the pre-sterilized and sensitive food product (e.g., milk and juice), hydrogen peroxide (H_2O_2) vapor has become the preferred choice among other chemical sterilizations [1].

H_2O_2 possesses strong oxidizing properties and is able to form radicals as reaction intermediates, in particular at elevated temperature. The formed radicals are chemically instable, yet they impart the microbicidal and sporicidal characteristics of H_2O_2. Finally, H_2O_2 dissociates to the environmentally friendly end-products oxygen and water vapor [2–4].

Prior to product filling, pre-formed food packages are guided through the sterilization chamber of the aseptic filling machine. An evaporator unit is used to form the sterilization medium at temperatures up to 300 °C from a mixture of an aqueous H_2O_2 solution (35% w/w) and air. The vapor mixture is then injected into the packages interacting and destroying the microorganisms present on their surface. The standard methods to evaluate the sterilization process effectiveness are microbiological challenge tests (end-point or count-reduction tests) [5, 6]. For these methods the surfaces of multiple test packages are inoculated with a refined sample of a resilient microorganism. Typically, spores of *Bacillus atrophaeus* (*B. atrophaeus*) are applied as an indicator microorganism to evaluate H_2O_2 vapor sterilization processes. However, the mentioned testing methods require fitted laboratories, trained staff and sample preparation; therefore, these methods are expensive and time-consuming.

In this article, a faster technique to evaluate sterilization processes with H_2O_2 vapor is introduced. The monitoring method is based on an impedimetric analysis of *B. atrophaeus* spores before and after the sterilization process. A sensor based on an interdigitated electrode (IDE) array has been developed to enable such analysis [7]. Instead of inoculating the surface of test packages, the indicator microorganisms are immobilized directly on the sensor surface. An alternating voltage applied to the sensor terminals induces a current depending on the intrinsic properties of the sensor and the spores on its surface. By measuring and noting the relation between voltage and current, the impedance of the sensor can be calculated. Moreover, the capacitance of the sensor can also be derived using an equivalent circuit approach.

To verify and validate the sensor results, analytical expressions and numerical models were applied. For the verification of interdigitated electrode structures, an analytical expression described in earlier literature was used [8–10]. The sensor validation was achieved by developing a representative numerical model based on the finite element method finite element method (FEM).

5.3 Experimental section

5.3.1 Sensor design and fabrication

The IDEs are designed to record transformations of the indicator microorganisms (spores of *B. atrophaeus*, DSMZ 675) induced by the sterilization process. The IDEs (as stated in [7]) consist of 614 electrodes with a thickness of 110 nm, and 5 μm width and interspacing. This geometry is imposed by the resolution limit of the applied in-house lithography process. The length of the electrodes is 3.25 mm, providing a total sensing area of about 20 mm^2. A wall structure with a height of 400 μm was designed around the IDEs to hold a liquid sample of an ethanol-based spore suspension with a volume of 10 μl. This volume corresponds to the volume of the above mentioned challenge tests [6].

A schematic representation of the sensor fabrication is shown in Fig. 5.1. The sensor fabrication starts with a glass wafer (Borofloat® 33, Schott GmbH, Jena, Germany), which serves as a non-conductive substrate to reduce the total parasitic capacitance [11].

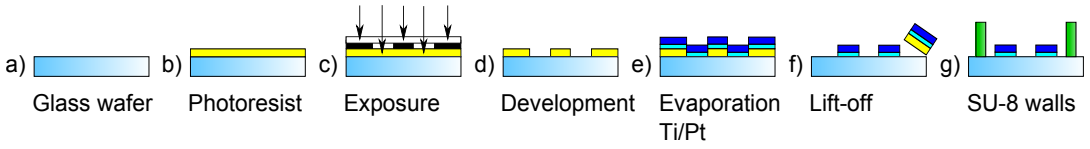

Fig. 5.1: Schematic representation demonstrating the individual sensor fabrication steps.

The first fabrication step is wafer cleaning with acetone, isopropyl and deionized (DI) water. As adhesion promoter for the photoresist layer TI-Prime (Microchemicals GmbH, Ulm, Germany) is deposited by spin-coating at 4000 rpm. Subsequently, the photoresist AZ 5214-E (AZ Electronic Materials GmbH, Wiesbaden, Germany), required for the later lift-off process, is deposited by an additional spin-coating step, resulting in a final thickness of 1.4 μm. The parameters are described in detail in [7]. Hence, the electrode and meander structures are patterned by a lithography step that is performed on a mask aligner (Süss Microtec AG, Garching, Germany) using a custom-made glass mask. The meander structures were introduced at this initial stage of sensor development to set up a platform for temperature sensing. Development of the photoresist is performed in developer AZ 326 MIF obtaining the patterned surface. On top of the resulting surface two layers of titanium and platinum are deposited by electron-beam evaporation (Univex, Leybold GmbH, Cologne, Germany). The titanium layer with a thickness of 10 nm serves as an adhesion promoter between the glass substrate and the platinum electrode structure with 100 nm thickness. The final electrode structure was obtained after a lift-off process in dimethyl sulfoxide (DMSO), supported by an ultrasonic bath. For the fabrication of the wall structure a high-viscose negative-tone photoresist (SU-8 2150, Microchem, Inc., Newton, MA, USA) is deposited. A consecutive two-step prebake (7 min at 65 °C and 120 min at 95 °C) is performed to release the thermal stress of the photoresist. The resulting photoresist layer is then patterned lithographically. Prior to development, a consecutive two-step post-exposure bake (5 min at 60 °C and 30 min at

95 °C) is conducted. The developer mr-DEV 600 is applied for photoresist development and the hard bake of the wall structures was conducted at 150 °C for 15 min. The final wafer is diced into single chips of 5×10 mm^2. An image of the sensor is depicted in Fig. 5.2.

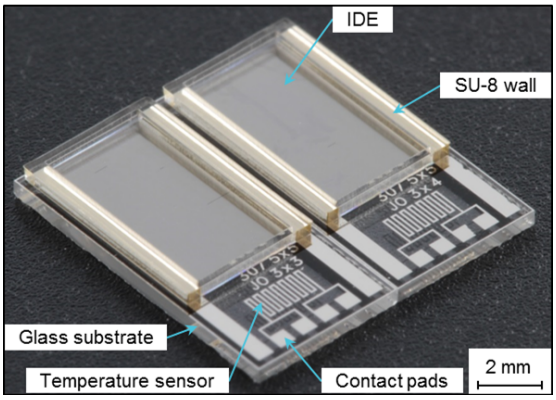

Fig. 5.2: Micrograph of the sensor based on a glass substrate, depicting the IDE structure surrounded by SU-8 walls; the lower part shows the temperature sensors and contact pads.

5.3.2 Impedimetric analysis

The data acquisition was performed with an E4980A impedance analyzer (Agilent Technologies Inc., Santa Clara, CA, USA). A four terminal point-probe station is used to connect the IDEs, thus eliminating the influence of connection lines' impedance on the measurement. An alternating voltage source of 20 mV with 0 V bias is used to excite the IDEs. While the IDEs are exposed to air, the impedance spectra are recorded in the frequency range of 500 Hz to 1 MHz with a logarithmic-scaled step size. A minimum set of two different IDEs is used to evaluate the impact of the sterilization process. One IDE serves as a reference to monitor the impact of the sterilization process on the material and the sensor structure itself. On the second IDE, spores of the indicator microorganisms (*B. atrophaeus*) are immobilized. The spore immobilization is adapted from sterility tests of aseptic packaging machines in food industry [6]. The sensing structure is drop-coated with 10 μl of an ethanol (70% v/v)-based spore suspension, which contains 10^8 colony forming units per milliliter (cfu ml^{-1}). This results in a spore load count of 10^6 cfu on the sensing surface. The impedance spectrum of the IDE with immobilized spores is recorded after the complete evaporation of the ethanol solution. Measurements with the IDEs are performed at different states (blank IDE, after spore immobilization and after the sterilization process) to track changes in the impedance value.

5.3.3 Sterilization process

The sterilization of the IDEs (reference and sensing part) is conducted in a specially designed sterilization test rig as described in [12]. This test rig is a replica of the sterilization units found in industrial aseptic food packaging machines. A defined mixture

of air and an aqueous solution of H_2O_2 (35% w/w) is vaporized to achieve a vapor concentration of 7.5% v/v with a temperature of 240 °C at the outlet of the evaporator. The IDEs are placed for an exposure time of 0.3 s with a distance of 5.5 cm below the outlet nozzle, which provides a directed stream of H_2O_2 vapor. The parameters for the chosen sterilization process guarantee full sterility as shown in previous work in which microbiological sterility tests were performed in parallel to sensor-based experiments [13].

5.4 Sensor verification and validation

5.4.1 Sensor verification

In addition to sensor measurements, a tool was required to verify the functionality of the sensor. It should give a quantitative and qualitative representation of the expected results. Therefore, an analytical expression was selected, which was proposed by Olthuis *et al.* [14] and successfully applied by several other authors [8, 9]. Abu-Abed and Lindquist extended the original analytical expression to include also the capacitance contribution due to the transverse field in the narrow region between the electrode fingers [15]. Based on this prior work, the final analytical expression used to derive the capacitance of a periodic IDE sensor structure is given in Eq. (5.1).

$$C = L(N-1)\left(\frac{\varepsilon_0\varepsilon_{r,t}}{2}\frac{K\left((1-k^2)^{1/2}\right)}{K(k)} + 2\varepsilon_0\varepsilon_{r,m}\frac{t}{s}\right) \tag{5.1}$$

where C is the calculated capacitance of the IDE structure. L is the length of the electrode fingers and N the number of unit cells. ε_0 represents the permittivity of vacuum $8.851 \cdot 10^{-12}\,\mathrm{A\,s\,V^{-1}\,m^{-1}}$ and $\varepsilon_{r,t}$ is the total relative permittivity surrounding the electrodes (empty sensor: air and glass; sensor with spores: porous spore layer and glass). $K(k)$ represents the elliptical integral of first order to calculate the impact of the fringing field. The modulus k defined in Eq. (5.2) is determined by the periodic structure of the electrode geometry. $\varepsilon_{r,m}$ describes the relative permittivity present between the electrodes to represent the capacitance formed due to the transverse field (empty sensor: air; sensor with spores: porous spore layer). The geometrical parameters t, s, and w are the electrode thickness, interspacing between electrodes and the width of electrode fingers, respectively (see Fig. 5.3).

$$k = \cos\left(\frac{\pi}{2}\frac{w}{s+w}\right) \tag{5.2}$$

5.4.2 Sensor validation

The initial idea was to model and simulate the full 3D geometry of the sensor and its surroundings (air and sensor substrate) as shown in Fig. 5.4. The geometrical ratio between the thickness of a single electrode finger and its length is in the order of 1:29,500 while the ratio between the electrode width and length is approximately 1:650. Hence, the final FEM-based numerical model, built with COMSOL® Multiphysics (Stockholm,

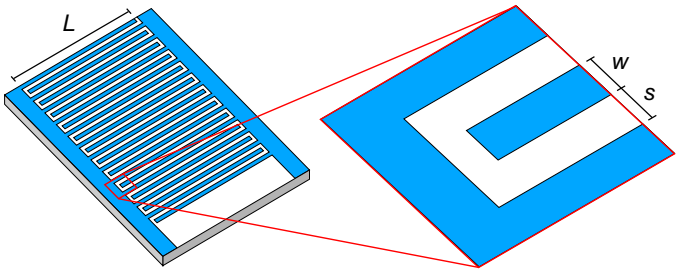

Fig. 5.3: Simplified view: defining the geometric parameters of the IDE structure.

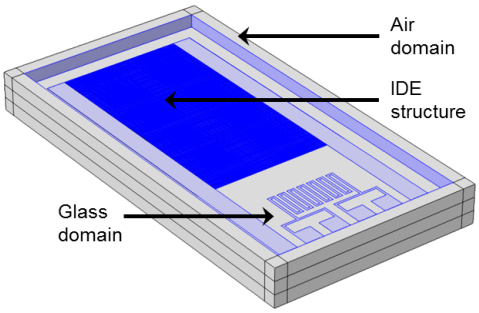

Fig. 5.4: FEM-generated 3D sensor model including the IDE structure surrounded by air and glass domains.

Sweden) tools, is expected to require a huge number of elements in order to achieve accurate results. This causes long pre-processing, solving and post-processing periods in addition to the need for advanced computer hardware. To develop nevertheless a representative model that can be used for fast acquisition of results and multi-parametric simulations, various simplifications for the FEM model were considered.

As stated previously, the IDE design consists of 307 electrode pairs. Each set is connected to a sensor terminal representing the ground and voltage source, respectively. The terminal extends beyond the IDE structure to provide contact pads for the sensor reading device.

The design of the IDE sensors shows a clear redundancy in layout, hence a periodicity in the design is present that can be exploited. Consequently, simulation time and model complexity are reduced by modeling only one electrode pair, instead of simulating all 307 pairs. This simplification was carried out by applying periodic conditions to the external boundaries. Finally, the electrode length can be seen as an extension parameter of a 2D model to approximate the 3D case.

The 2D model used to simulate a blank IDE sensor is depicted in Fig. 5.5. The model includes an electrode finger pair situated on top of a glass substrate, which is exposed to air. The FEM-based numerical model solves Gauss's law for the electric field using the defined value of the electric potential as the independent variable. Therefore, the capacitance of the design can be calculated in the FEM model by two methods:

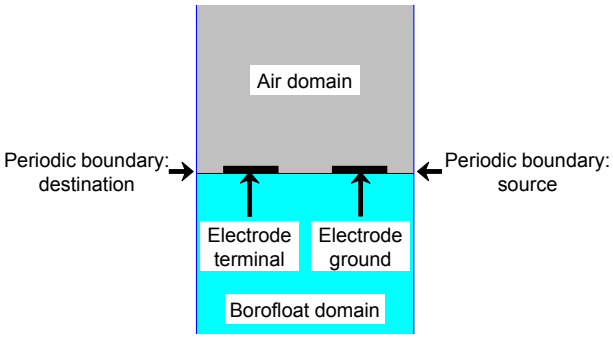

Fig. 5.5: Simplified representative model of a blank sensor in 2D, showing an electrode finger pair surrounded by air and glass domains.

calculation based on the terminal charge (Eq. (5.3)), or calculation based on the surface integral of the stored electric energy W_e (Eq. (5.4)).

$$C = \frac{NQ}{2U_0} \tag{5.3}$$

$$C = N\frac{2}{U_0^2}\int_\Omega W_e \, d\Omega \tag{5.4}$$

Here, C represents the capacitance of the system, N is the number of electrode fingers, Q is the total charge and U_0 is the applied potential difference between terminal and ground electrode. Ω is the enclosed 2D model surface (domain).

The stored electric energy (W_e) is calculated by Eq. (5.5).

$$W_e = \frac{1}{2}\varepsilon_0(\underline{\varepsilon}_r \cdot \boldsymbol{E})^T \cdot \mathbf{E} \tag{5.5}$$

where $\underline{\boldsymbol{\varepsilon}}_{\boldsymbol{r}}$represents the relative permittivity tensor of the material under test and $\boldsymbol{E}$ the electric field vector. The sensor base materials used in this model are isotropic, which means that the relative permittivity is constant.

In the experimental work, an impedance analysis was performed to find the capacitive response of the IDE structure at different frequency values. Using the numerical model, a frequency analysis is also possible by applying parametric sweeps over a pre-defined frequency range in a frequency domain analysis. In principle, the frequency dependence of the material properties should be known in order to model the capacitance changes of the IDEs in a broader frequency range. The major contribution to the capacitance is related to the substrate material, which has the highest electric permittivity value. Unfortunately, information on the frequency-dependent electric permittivity of Borofloat glass is not provided by the manufacturer. Nevertheless, a constant value of $\underline{\varepsilon}_{r,glass} = 4.6$ at a frequency of 1 MHz was assumed and also used in the frequency analysis of the 2D model.

5.5 Results and discussions

5.5.1 Impedimetric characterization

In the following section, the acquired impedance and phase spectra plots (Bode plots) before and after the immobilization of spores and sterilization are presented and discussed. All measurements are carried out with air as surrounding sensor medium.

As stated in Sec. 5.3.1, a reference IDE is used to examine the impact of the sterilization process on the sensor set-up itself and to provide further information on the long-term behavior of the sensor output. The impedance of the sensor is derived from the ratio between the excitation voltage and the induced current, thus consisting of the impedance modulus (Z) and the phase shift (φ) between voltage and current. In Fig. 5.6 a), the Bode plots of the reference IDE before and after sterilization are depicted. As demonstrated in the figure, no changes of the impedance and phase are visible, which proves the stability and inertness of the sensor. In addition, the constant phase angle of about –90° indicates a capacitive behavior. This can be directly related to the non-conductive properties of the media surrounding the IDE.

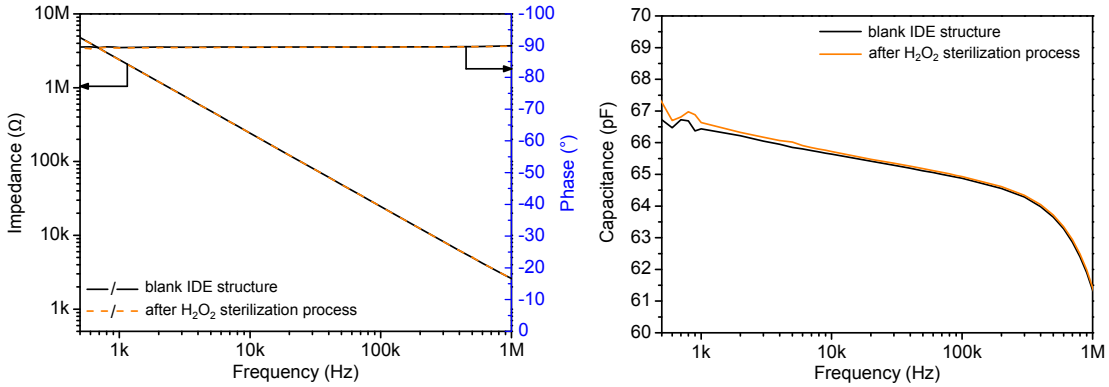

a) b)

Fig. 5.6: Analysis of a blank sensor exposed to the H_2O_2 sterilization process: a) Bode plot before and after sterilization; b) plot of the corresponding capacitance spectra.

A detailed analysis of the IDE structure is then performed by applying Eq. (5.6) to calculate the capacitance of the sensor.

$$C = \frac{-\sin(\varphi)}{2\pi f \cdot Z} \tag{5.6}$$

This equation was developed using an equivalent circuit model consisting of resistive (R) and capacitive (C) elements, where C is the resulting capacitance, φ is the phase angle, Z the impedance taken from the Bode plot and f the respective frequency.

Fig. 5.6 b) shows the plot of the calculated capacitance values derived from Fig. 5.6 a) for a blank IDE structure prior and after sterilization. Both curves exhibit a frequency dependence of the capacitance in the range from 500 Hz to 1 MHz, which can be related to the properties of the sensor material (glass substrate, electrode structure and SU-8 walls). Furthermore, the capacitance plot shows minor deviations within the frequency

range between 500 Hz and 5 kHz that can be related to the sterilization process. This implies the necessity of testing a differential sensor set-up for each experiment.

Further analyses of the blank IDEs were conducted to determine the base capacitance at a fixed frequency of 3 kHz, which shows minor fluctuation of ±0.9 pF around an average value of 66.1 pF. These small deviations might be explained by fluctuations in sensor production.

Fig. 5.7 a) depicts the average impedance and phase spectra of four different IDE structures. In the first step, the blank structures were analyzed (black solid and dashed lines). The second analysis was conducted after the immobilization of spores onto the IDE (solid and dashed blue lines). The final analysis was performed after the H_2O_2 sterilization process (orange solid and dashed lines). The resulting Bode plots exhibit the impact of different test conditions on the IDEs. For example, the immobilization of microbiological spores results in a reduced impedance response in comparison to the empty IDE structure, which is related to the conductive properties of the microorganisms [16]. After the sterilization process, the impedance modulus further decreases as compared to the recorded spectrum of immobilized spores. The impedance change is related to the collapse and/or rupture of the spores, which was observed in previously published work [13]. The spore rupture is accompanied by a leakage of internal conductive substances [16, 17]. Additional microbiological tests (count-reduction test) in parallel to IDE analyses have shown sample sterility. Since the capacitive behavior is still dominant, further analyses were performed using the capacitance spectra given in Fig. 5.7 b).

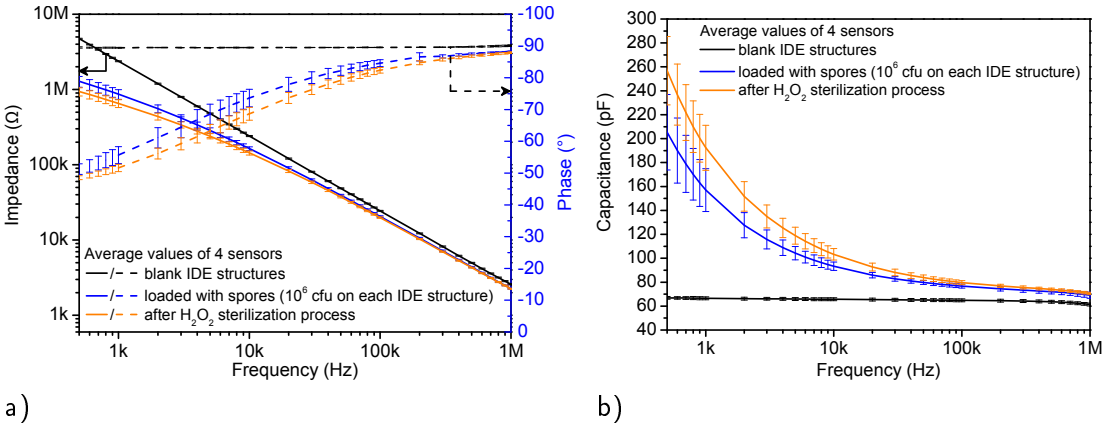

Fig. 5.7: a) Bode plots recorded with a blank IDE structure, after immobilization of *B. atrophaeus* spores (10^6 cfu on IDE structure) and after the H_2O_2 sterilization process. The impedance analyses were performed while the sensors were exposed to air; b) plot of the derived capacitance spectra.

The study of the capacitance plot highlights that the sensor sensitivity is highest in the frequency range from 500 Hz to 10 kHz while it is reduced at frequencies higher than 10 kHz. However, as observed in Fig. 5.6 b), the frequency region to analyze the sensor response has to be restricted due to measurement instabilities between 500 Hz and 1 kHz. Therefore, the current and future sensor analyses are performed at a fixed frequency of 3 kHz. The resultant average capacitance of four tested sensors at this

predetermined frequency and under different test conditions is noted in Tab. 5.1. The results demonstrate a distinguishable capacitance change of about 20 pF between the situation before and after the H_2O_2 sterilization. Finally, the one-point frequency analysis provides an extra advantage when e.g., designing a low-cost handheld read-out device.

Tab. 5.1: Summary of the one-point capacitance analyses of the three sensor states (average of 4 sensors) at a fixed frequency of 3 kHz.

Sensor state	C (f = 3 kHz)(pF)	Relative error
Blank sensors	66.1	2.6
Loaded with spores	115.7	7.2
After sterilization	135.0	4.3

5.5.2 Verification and validation of the IDE sensor

In parallel to the experiments in Sec. 5.5.1, analytical and numerical analyses of the blank IDEs were carried out. Tab. 5.2 summarizes the resultant capacitance values, where the results of the analytical expression and numerical simulations are in good agreement with each other. Therefore, Tab. 5.2 proves that the analytical expression defined in Eq. (5.1) matches the values obtained by the numerical model. However, the relative error between experimental measurement and the numerical result of ideal electrodes amounts to about 12.4% (deviation between C_{exp} and C_{ideal} of Tab. 5.2).

Analysis of the IDE structure with atomic force microscopy (AFM) depicts uneven electrode edges, which are related to the lift-off process and the mechanical stability of the thin structures (Fig. 5.8).

Tab. 5.2: Summary of the capacitance values derived from the experiments and derived by analytical and numerical analyses.

IDE geometry			Results			
			Experimental	Analytical (Eq. (5.1))	FEM model	
w (μm)	s (μm)	t (nm)	C_{exp} (pF)	C_{anal} (pF)	C_{ideal} (pF)	C_{AFM} (pF)
5	5	110	–	50.09	50.07	–
6	4	110	66.1	57.98	57.91	60.05
6	4	220	–	58.95	58.57	–

w: finger width; s: finger interspacing; t: finger thickness; C_{ideal}: geometry as given in Fig. 5.5; C_{AFM}: IDE geometry based on AFM data.

Hence, the model shown in Fig. 5.5 was adapted with the AFM profile (as shown in Fig. 5.9) and simulated. The result was an increase of the capacitance value in comparison to the previous value and thus, a decrease of the relative error to 9.15%. In addition to the error due to geometric uncertainty, air humidity, temperature and material purity have an effect on the capacitance measurements in contrast to the ideal conditions of the numerical model.

Furthermore, Tab. 5.2 shows that the height (thickness t) of the electrodes has a minor effect on the capacitance value as in the case of the blank sensor. The direct

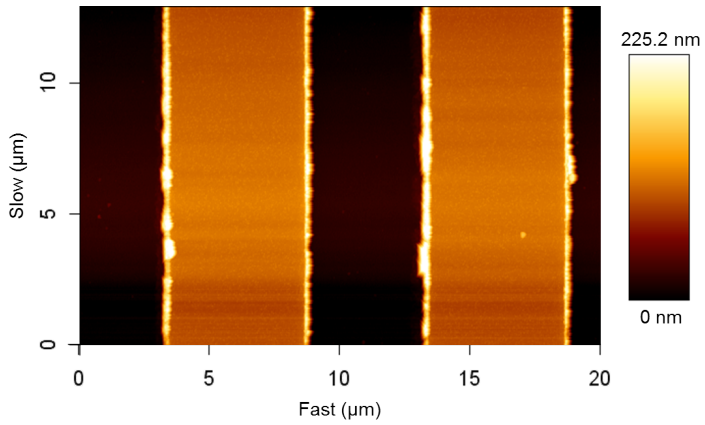

Fig. 5.8: AFM characterization of the IDE structure depicting the uneven electrode edges due to the lift-off process. Scan directions of the AFM tip are given in fast (x-axis) and slow (y-axis).

reason is related to the fact that, unlike parallel plate capacitors, the transverse fields have a smaller value (and hence effect) than fringing fields. This effect can be well perceived in Fig. 5.9.

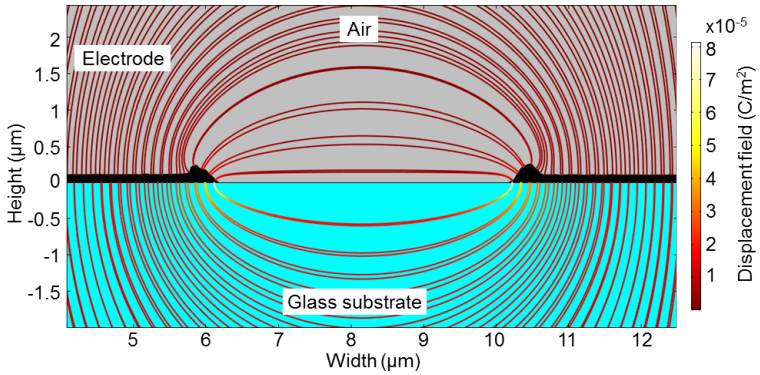

Fig. 5.9: Distribution of the electric displacement field presented as streamlines between two electrode fingers. The electrode geometry determined by AFM characterization demonstrates a wide distribution of the fringing field and a reduced transverse field.

5.6 Conclusions and outlook

In this work, a sensor consisting of interdigitated electrodes deposited on an insulating glass substrate was successfully introduced. A blank reference IDE structure was used to demonstrate the inertness and stability against the sterilization process using H_2O_2 vapor. Nonetheless, a reference electrode structure defined in a differential sensor set-up is still essential to capture possible variations such as process-induced changes of the sensor materials (electrode structure or SU-8-layer).

Resilient microorganisms (*B. atrophaeus* spores), commonly applied for sterility tests in food industry, were immobilized on the sensing structure. A significant change in

the impedance of the sensor was observed after spore immobilization. Whereby, after exposure to the sterilization process the spore morphology changed resulting in an impedance shift recorded by an impedance analyzer. Further evaluation of the data was performed calculating the capacitance of the IDEs using a simplified RC equivalent circuit.

From the output measurements an optimal fixed frequency of 3 kHz was determined for a latter impedance handheld device. As a result of the sterilization process, a capacitance change of about 20 pF was recorded at that fixed frequency. In addition, by means of analytical and numerical methods, a verification and validation of the IDE structure was performed. Analytical expressions provided in literature were analyzed and modified. For numerical validation a FEM-based simulation model of the IDEs was designed. Systematic simplification approaches of the model enabled the simulation of the complex geometry. Hence, further improvements and multiple tests can be achieved in short time and with the available hardware at hand. In future work, this IDE model will be applied to acquire further information about the electrical properties of the spores, such as electric permittivity and conductivity. Moreover, the validated FEM model can be applied to study different sensor modifications towards sensor optimization with regard to geometrical variations or spore deposition.

Acknowledgments

This work has been financially supported by the Bundesministerium für Bildung und Forschung (BMBF), Germany, project "ImpediPack".

Author contributions

Jan Oberländer designed the IDE device and the experimental concept and he performed the sensor experiments together with the data analysis. Zaid B. Jildeh was responsible for the FEM simulations and contributed to the data analysis. Both (Jan Oberländer and Zaid B. Jildeh) contributed equally to write this article. Patrick Kirchner supported the FEM simulations. Luisa Wendeler and Alexander Bromm performed sensor measurements. Heiko Iken was responsible for the thin-film fabrication of the IDE. Patrick Wagner, Michael Keusgen and Michael J. Schöning have been supervising, discussing the experiments and edited the presented work.

Conflicts of interest

The authors declare no conflict of interest.

References

[1] E. Linley, S. P. Denyer, G. McDonnell, C. Simons, and J. Y. Maillard. "Use of hydrogen peroxide as a biocide: new consideration of its mechanisms of biocidal action". *The Journal of Antimicrobial Chemotherapy* 67 (2012), 1589–1596.

[2] P. A. Giguère and I. D. Liu. "Kinetics of the thermal decomposition of hydrogen peroxide vapor". *Canadian Journal of Chemistry* 35 (1957), 283–293.

[3] P. Kirchner, J. Oberländer, P. Friedrich, J. Berger, H.-P. Suso, A. Kupyna, M. Keusgen, and M. J. Schöning. "Optimization and fabrication of a calorimetric gas sensor built up on a polyimide substrate for H_2O_2 monitoring". *Physica Status Solidi A* 208 (2011), 1235–1240.

[4] J. Oberländer, P. Kirchner, H.-G. Boyen, and M. J. Schöning. "Detection of hydrogen peroxide vapor by use of manganese(IV) oxide as catalyst for calorimetric gas sensors". *Physica Status Solidi A* 211 (2014), 1372–1376.

[5] Food and Drug Administration. *Code of federal registrations: food and drugs: indirect food additives: adjuvants, production aids, and sanitizers.* Code of Federal Regulations (CFR). 2011. URL: `http://www.fda.gov`.

[6] Verband Deutscher Maschinen- und Anlagenbau e.V. "Code of practice: filling machines of VDMA hygiene class V: testing the effectiveness of packaging sterilization devices". *VDMA-Fachverbandsschriften* 6 (2008), 1–16.

[7] J. Oberländer, A. Bromm, L. Wendeler, H. Iken, M. P. Durán, A. Greeff, P. Kirchner, M. Keusgen, and M. J. Schöning. "Towards a biosensor to monitor the sterilization efficiency of aseptic filling machines". *Physica Status Solidi A* 212 (2015), 1299–1305.

[8] V. F. Lvovich, C. C. Liu, and M. F. Smiechowski. "Optimization and fabrication of planar interdigitated impedance sensors for highly resistive non-aqueous industrial fluids". *Sensors and Actuators B: Chemical* 119 (2006), 490–496.

[9] B. Timmer, W. Sparreboom, W. Olthuis, P. Bergveld, and A. van den Berg. "Optimization of an electrolyte conductivity detector for measuring low ion concentrations". *Lab on a Chip* 2 (2002), 121–124.

[10] M. C. Zaretsky, L. Mouayad, and J. R. Melcher. "Continuum properties from interdigital electrode dielectrometry". *IEEE Transactions on Electrical Insulation* 23 (1988), 897–917.

[11] W. Olthuis, A. J. Sprenkels, J. G. Bomer, and P. Bergveld. "Planar interdigitated electrolyte-conductivity sensors on an insulating substrate covered with Ta_2O_5". *Sensors and Actuators B: Chemical* 43 (1997), 211–216.

[12] P. Kirchner, Y. A. Ng, H. Spelthahn, A. Schneider, H. Henkel, P. Friedrich, J. Kolstad, J. Berger, M. Keusgen, and M. J. Schöning. "Gas sensor investigation based on a catalytically activated thin-film thermopile for H_2O_2 detection". *Physica Status Solidi A* 207 (2010), 787–792.

[13] P. Kirchner, J. Oberländer, H.-P. Suso, G. Rysstad, M. Keusgen, and M. J. Schöning. "Monitoring the microbicidal effectiveness of gaseous hydrogen peroxide in sterilization processes by means of a calorimetric gas sensor". *Food Control* 31 (2013), 530–538.

[14] W. Olthuis, W. Streekstra, and P. Bergveld. "Theoretical and experimental determination of cell constants of planar-interdigitated electrolyte conductivity sensors". *Sensors and Actuators B: Chemical* 24 (1995), 252–256.

[15] A. S. Abu-Abed and R. G. Lindquist. "Capacitive interdigital sensor with inhomogeneous nematic liquid crystal film". *Progress in Electromagnetics Research B* 7 (2008), 75–87.

[16] E. L. Carstensen, R. E. Marquis, S. Z. Child, and G. R. Bender. "Dielectric properties of native and decoated spores of *Bacillus megaterium*". *Journal of Bacteriology* 140 (1979), 917–928.

[17] B. Setlow, C. A. Loshon, P. C. Genest, A. E. Cowan, C. A. Setlow, and P. Setlow. "Mechanisms of killing spores of *Bacillus subtilis* by acid, alkali and ethanol". *Journal of Applied Microbiology* 92 (2002), 362–375.

6 Experimental and numerical analyses of a sensor based on interdigitated electrodes for studying microbiological alterations (*Physica Status Solidi A*, (2018), 1700920 (1–9))

Z. B. Jildeh*, **J. Oberländer***, P. Kirchner, M. Keusgen, P. H. Wagner, and M. J. Schöning

Published in: *Physica Status Solidi A: Applications and Materials Science,* (2018), 1700920 (1–9).

Submitted: 2017-11-23; Accepted: 2018-04-06; Published: 2018-05-17
DOI: 10.1002/pssa.201700920

* Both authors contributed equally to this work.

6.1 Abstract

In this work, a cell-based biosensor to evaluate the sterilization efficacy of hydrogen peroxide vapor sterilization processes is characterized. The transducer of the biosensor is based on interdigitated gold electrodes fabricated on an inert glass substrate. Impedance spectroscopy is applied to evaluate the sensor behavior and the alteration of test microorganisms due to the sterilization process. These alterations are related to changes in relative permittivity and electrical conductivity of the bacterial spores. Sensor measurements are conducted with and without bacterial spores (*Bacillus atrophaeus*), as well as after an industrial sterilization protocol. Equivalent two-dimensional numerical models based on finite element method of the periodic finger structures of the interdigitated gold electrodes are designed and validated using COMSOL® Multiphysics software by the application of known dielectric properties. The validated models are used to compute the electrical properties at different sensor states (blank, loaded with spores and after sterilization). As a final result, we will derive and tabulate the frequency-dependent electrical parameters of the spore layer using a novel model that combines experimental data with numerical optimization techniques.

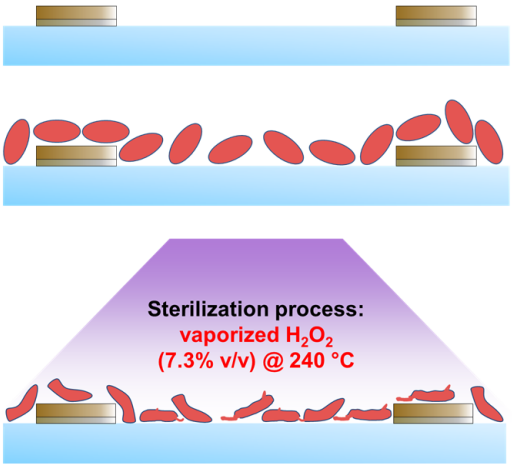

Fig. 6.1: Schematic demonstrating different sensor states of the developed and investigated biosensor: blank sensor, immobilized spores and after sterilization process with H_2O_2.

6.2 Introduction

A sterile product or surface is defined by the absence of viable microorganisms, including resilient spores [1]. In pharmaceutical, food and beverage industries it is crucial for the final packaging material to be free of microorganisms that lead to product spoilage [2]. Aseptic filling designates a process, in which package and product are separately sterilized and the filling process is executed under sterile conditions. The final aseptic product sustains a longer shelf-life without addition of preservatives or requirement of a cool chain for distribution [2, 3].

A common method to sterilize preformed packages is the application of a high-temperature gas mixture containing hydrogen peroxide (H_2O_2). The germicidal and sporicidal activity of H_2O_2 is assigned to its oxidative properties and the generation of reactive radical species (such as $O_2^{\bullet -}$, $HO^{\bullet}$, $HO_2^{\bullet}$, $O^{\bullet}$, $H^{\bullet}$), which lead to cell death [4, 5]. The strong sterilizing efficacy of hot H_2O_2 gas enables a fast sterilization process at gas concentrations up to 8% v/v [4, 6, 7].

The state-of-the-art methods to quantify the efficacy of package sterilization process are microbiological challenge tests (count reduction test or end point test) [8]. Drawbacks of these tests are the requirement of fitted laboratories and qualified personnel to handle test microorganisms. Additionally, the preparation of the microbiological samples such as the required incubation time (up to 7 days) and the evaluation entails a long downtime of the filling machine and a delay in product release [8]. To overcome these limitations and drawbacks, development of rapid quantification methods is required.

An impedimetric biosensor based on interdigitated electrode (IDE) structures has been developed by the authors in previous work [9–11]. A test microorganism (spores of *Bacillus atrophaeus* taken from a spore suspension based on deionized (DI)-water) has been immobilized on the IDE structure and characterized in respect to the H_2O_2 sterilization process. After drying the spore sample on the IDE structure (in a sterile flow hood at room temperature), the impedimetric measurements were conducted before and after performing the sterilization protocol.

The interpretation of the impedimetric sensor data depends on the electrical properties of the *B. atrophaeus* spores in air or under low-pressure conditions. Due to the lack of research on the electrical properties of the spores, analytical methods (e.g., capacitance calculation of IDE structures by applying the complete elliptical integral of first kind that has been described for the blank structure in our previous article [10]) cannot be applied for verification so far [12, 13].

In this work, a method is presented to evaluate the electrical properties (relative permittivity and electrical conductivity) of the applied test microorganisms at different sensor states (loaded with spores and after sterilization). In order to improve and facilitate the physical understanding of the impedimetric biosensor, numerical methods and optimization techniques are employed. To support the identification of the above stated material properties, a novel method that combines experimental impedimetric analysis data, validated numerical models based on finite element method (FEM) and optimization methods for parameter estimation based on weighted least square error (LSE) method will be presented.

6.3 Experimental methods and materials

6.3.1 Sterilization process

For the sterilization of the spore samples immobilized on the biosensors under study, an industrial sterilization test-rig has been utilized, which is described in a previous work [14]. In brief, a mixture of dry air and aqueous H_2O_2 solution (food-grade, 35% w/w) is evaporated and heated to a temperature of 240 °C, using a specialized evaporation unit. Dry air represents the carrier medium to dilute the hydrogen peroxide vapor (resulting H_2O_2 concentration: 7.3% v/v) and to convey the resultant vapor into the sterilization chamber. The sterilization protocol of the biosensors is performed with an exposure time of 0.3 s. The sensor chips are positioned 5.5 cm below the outlet of the evaporation unit. This sterilization protocol is adapted from industrial standards, which guarantees complete inactivation of all resilient spores.

6.3.2 Sensor design and fabrication

The impedimetric biosensor chip has been developed and characterized in previous works [9–11]. A planar IDE structure has been designed as follows: 307 electrode pairs each with a length of 3.25 mm; the width of one electrode finger is 4 μm with an interspacing of 6 μm (as depicted in Fig. 6.2 a)). The total IDE structure covers an area of 20 mm^2.

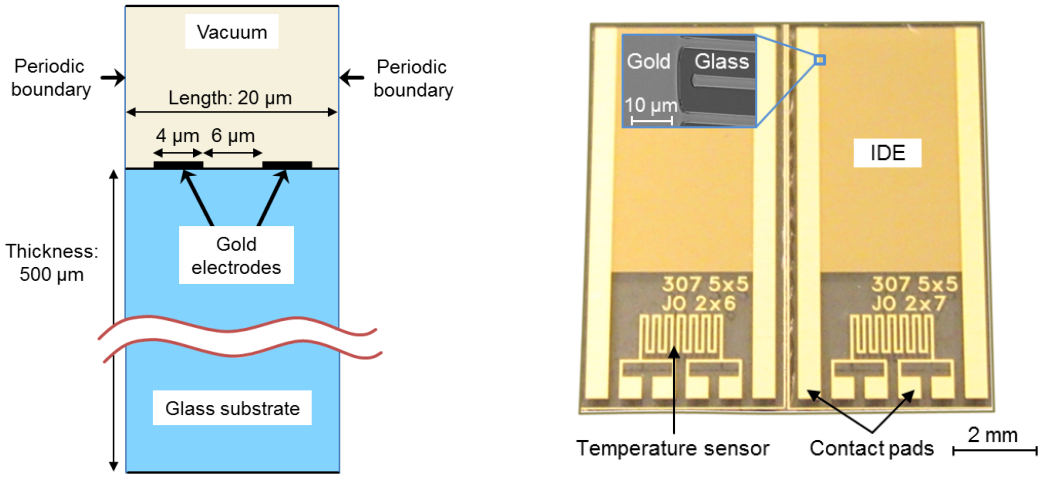

Fig. 6.2: a) Schematic cross-sectional view of one electrode pair on a glass substrate in a low-pressure environment. b) Picture of the biosensor differential set-up depicting the different sensor parts; inset shows the electrode structure captured by SEM characterization.

The sensors have been in-house fabricated on a 500 μm thick Borofloat 33® glass wafer (Schott AG, Germany) by means of standard photolithography and thin-film processing steps [9]. The thin-film electrode materials, 100 nm gold on top of 10 nm chromium were deposited in an e-beam evaporation device (Leybold GmbH, Germany). The chromium layer serves as an adhesion promoter between the gold and glass surfaces. A negative

photoresist masking-layer (AZ 2020 nLOF, Merck Performance Materials GmbH, Germany) is spin-coated on top of the gold layer. The sensor pattern was transferred from a customized chromium glass mask via photolithography. Subsequently, after photoresist development, reactive ion etching (RIE) was performed to pattern the non-masked metal layers (RIE: Plasmalab 100, Oxford Instruments plc, UK). Gold and chromium etching was performed by applying a gas mixture of argon 10 $cm^3\,min^{-1}$ and oxygen 15 $cm^3\,min^{-1}$ for 8.5 min. During the RIE process, oxygen plasma has been applied to remove the photoresist layer. To enable a precise immobilization of the test microorganisms, a 400 μm SU-8 wall has been fabricated surrounding the IDE structure. The prepared wafer was diced into single chips with a size of 5×10 mm^2. Cleaning of the biosensor chips was performed by applying acetone, isopropanol and deionized (DI) water prior to characterization and measurement.

A differential set-up of the developed biosensor chip is shown exemplarily in Fig. 6.2 b). One of the IDE structures serves as a reference and on the other IDE structure microbiological spores are immobilized for evaluation. Here, the IDE structure is depicted in the upper part and the meander-structured temperature resistor is shown in the lower part as well as the contact pads. The inset shows a magnified scanning electron microscopy (SEM) image of the IDE.

6.3.3 Biosensor characterization procedure

In this work, the impedimetric biosensor has been characterized by using an impedance analyzer (E4980A, Agilent Technologies Inc., USA). In order to minimize and eliminate the influence of the surrounding environment, such as variations in temperature or humidity level, a customized vacuum measurement chamber has been utilized [15]. A constant low-pressure condition of 100 hPa air within the chamber is achieved by a laboratory vacuum pump (Laboport N 86 KN.18, KNF Neuberger GmbH, Germany). The application of a low-pressure environment during impedimetric measurements assures similar conditions (unaffected by ambient humidity and temperature) for all measurements.

The excitation source of the biosensor is a sinusoidal voltage of 20 mV without DC (direct current) bias. Hereby, the biosensors were analyzed in a frequency range between 1 kHz to 100 kHz, with a logarithmic-scaled step size (ten steps per decade).

There are three different sensor states, at which the biosensors were characterized. The first state, schematically shown in Fig. 6.3 a), is defined as the blank sensor state. The second state is the loaded sensor with the spores of *B. atrophaeus* (Fig. 6.3 b)). These have been immobilized similar to test specimen for industrial challenge tests by drop-coating of 10 μl of a DI water-based spore suspension with a concentration of 10^9 colony forming units per milliliter (cfu ml^{-1}), left to dry [8]. The third state represents the sensor after the sterilization protocol (Fig. 6.3 c)). The presented schematic sensor states are based on the observation made by SEM characterization of a spore layer before and after the sterilization protocol (s. Fig. 6.4 a) and b)). For characterization purposes a differential set-up arrangement consisting of two sensors is selected. One of these represents state two (immobilized spores without sterilization) or state three (immobilized spores after sterilization) and the other one is left blank to serve as ref-

erence channel for the experiments. The reference channel measures the impedance of one IDE structure to serve as an indicator to possible changes to sensor materials by the applied chemical sterilization protocol. During data analysis, there has been no noted changes to the impedance value of the IDE reference structure as noted in our previous studies [9, 10]. All sensor states have been independently characterized by impedance spectroscopy to track changes in the impedance value. Consequently, to reduce the computation resources, a single frequency value is chosen (f=3 kHz) to assess the sterilization efficacy.

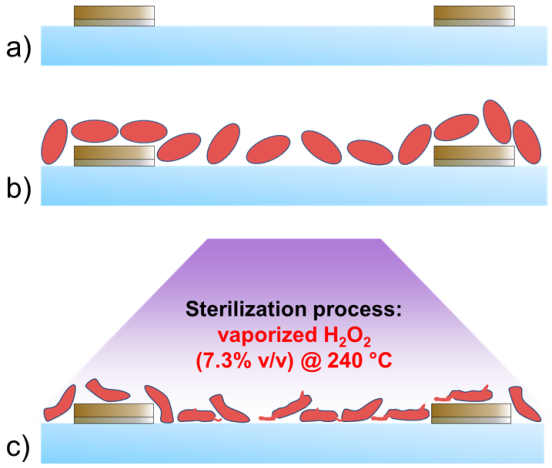

Fig. 6.3: Schematic view of the three different sensor states showing one electrode pair made of chromium and gold on a glass substrate; a) blank sensor state; b) spore-loaded sensor state; c) sensor state after sterilization process.

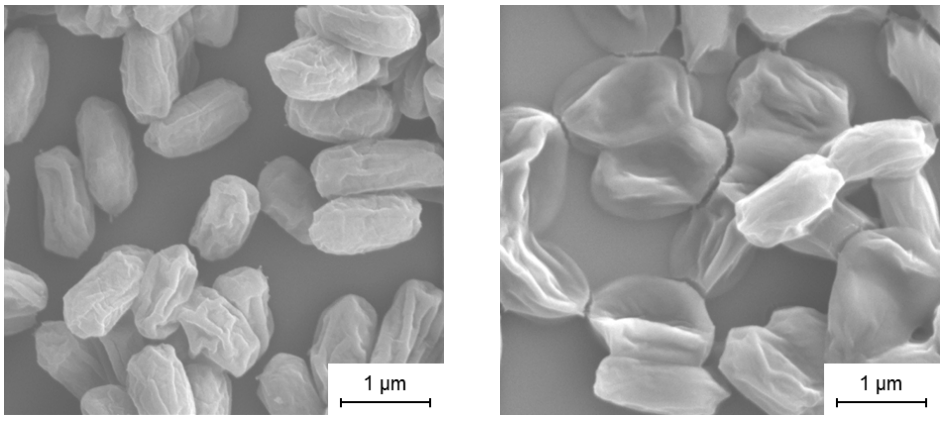

Fig. 6.4: SEM images of a) intact spores and b) spores subjugated to the sterilization process depicting their morphological alteration.

6.4 Design of numerical model

The numerical model applied in this work is based on FEM and designed with COMSOL® Multiphysics [10]. The full-fidelity IDE geometry involves a three-dimensional (3D) numerical model that requires a large number of elements and thereby computational resources. Accordingly, a simplified but still representative two-dimensional (2D) model has been designed to describe the IDE structure. As such, a decrease in the number of elements can be achieved, which results in a reduction of the computational requirements. Moreover, by incorporating the advantage of a periodic IDE structure a further decrease in the size of the numerical problem is achieved by modeling a single electrode pair instead of the 307 pairs. The continuity of electric field distribution at the IDE structure allows this model reduction by applying continuity conditions at the external boundaries of the model. This decrease in model size enables a thorough validation of experimental results and subsequent parametric investigation of electrical properties [16, 17]. Fig. 6.2 a) depicts a schematic view of the model geometry encompassing a single electrode pair (width: 4 μm, spacing: 6 μm), which is placed on a glass substrate (thickness: 500 μm) under low-pressure condition.

Two numerical models for studying the different sensor states were developed. The first model, depicted in Fig. 6.5 a), shows the electrodes (black) of a blank sensor state. The average geometry of the sensor structure was captured from various sections of an atomic force microscopy (AFM) characterization plot of the developed sensor (as shown in Fig. 6.6). The AFM characterization has been performed on a BioMat workstation (JPK Instruments, Germany) in non-contact, tapping mode, as described previously [9]. The AFM is used to verify the dimensions of the IDE structure and to include the real electrode geometry in the numerical simulations. The second model shown in Fig. 6.5 b) represents the loaded sensor state with the test microorganism layer. The height of the numerical model layer that represents the spores of *B. atrophaeus* is based on a simplification that the spores are perfectly ellipsoidal and are horizontally aligned on the sensor surface. The thickness and height of the spores is 500 nm with a length of 1.2 μm [7].

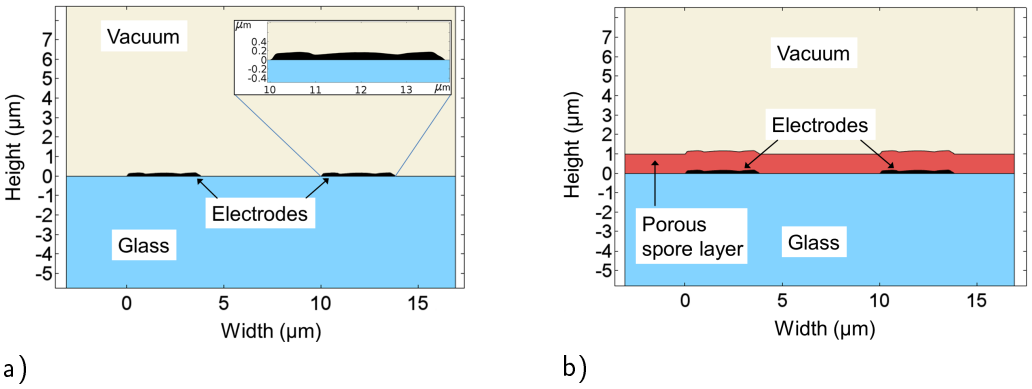

Fig. 6.5: Geometrical design of the numerical model showing: a) a blank sensor state depicting one electrode pair on a glass substrate, electrode geometry taken from AFM profilometry; b) a loaded sensor state depicting the geometry of the modeled porous spore layer.

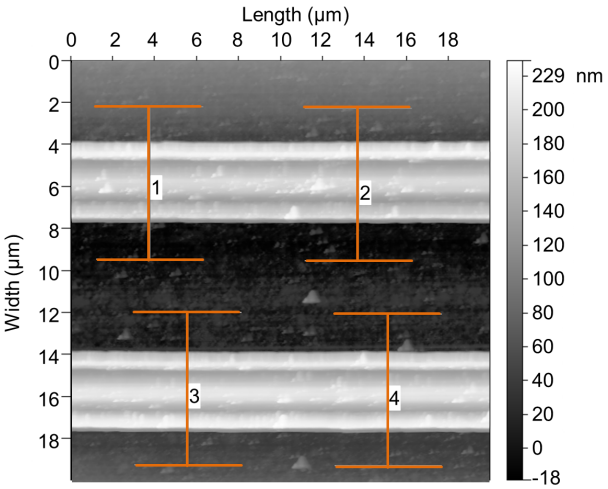

Fig. 6.6: AFM characterization of the IDE structures depicting four different cross-sectional regions used as mean value for the model geometry.

6.4.1 Governing equations

The simulation of the biosensor in a virtual environment requires knowledge of the physical effects, which have to be described in a mathematical way. As such, in the two-electrode arrangement, the electric potential (V) is defined as the potential difference between the electrode pair. An electric vector field ($\boldsymbol{E}$) is generated and can be derived as per Eq. (6.1).

$$\boldsymbol{E} = -\nabla V \tag{6.1}$$

This electric field results in a total current density ($\boldsymbol{J}_{\mathrm{tot}}$ in A m^{-2}). In the case of time-harmonic field analysis (in the frequency domain), $\boldsymbol{J}_{\mathrm{tot}}$ is defined in Eq. (6.2). The value of $\boldsymbol{J}_{\mathrm{tot}}$ is the sum of the induced current density ($\boldsymbol{J}_{\mathrm{i}}$, Ohm's law) and the displacement current density ($\boldsymbol{J}_{\mathrm{d}}$, Ampère's law).

$$\boldsymbol{J}_{tot} = \boldsymbol{J}_i + \boldsymbol{J}_d = \sigma \boldsymbol{E} + j\omega\varepsilon_0\varepsilon_r \boldsymbol{E} \tag{6.2}$$

Here, σ is the electric conductivity in S m^{-1}, j is the imaginary number (engineering application as i in a mathematical context), ω is the angular frequency in rad s^{-1}, ε_0 is the permittivity of vacuum $8.85 \cdot 10^{-12}$ As V^{-1} m^{-1} and ε_r is the relative permittivity of the material.

In the impedimetric measurements, a phase shift (φ_{meas}) is registered between the applied voltage and the measured current. In the numerical model, the phase shift (φ_{mod}) is derived as the argument of the complex vector $\boldsymbol{J}_{\mathrm{tot}}$. Here, φ_{mod} is independent from the electric field and intrinsically related to the equivalent material property of the model (σ_{mod} and $\varepsilon_{\mathrm{r,mod}}$).

The test microorganism layer was approximated as a porous layer (s. Fig. 6.5 b)). Assuming the porous layer has negligible dielectric loss, the effective electrical properties

are derived as volume average values as given in Eqs. (6.3) and (6.4) where, θ indicates the volume ratios.

$$\varepsilon_{\mathrm{r,layer}} = \theta_{\mathrm{vacuum}} \cdot \varepsilon_{\mathrm{r,vacuum}} + \theta_{\mathrm{spores}} \cdot \varepsilon_{\mathrm{r,spores}} \tag{6.3}$$

$$\sigma_{\mathrm{layer}} = \theta_{\mathrm{vacuum}} \cdot \sigma_{\mathrm{vacuum}} + \theta_{\mathrm{spores}} \cdot \sigma_{\mathrm{spores}} \tag{6.4}$$

With the approximated dimension of a single spore (approximated as an ellipsoid with average dimensions of 1.2 µm × 500 nm × 500 nm), the volume is about $1.6 \cdot 10^{-10}$ mm^3. For sensor-based evaluations, $1 \cdot 10^7$ *s*pores are immobilized on the IDE structure. Thereby, the total volume of spores (V_{spores}) is $1.6 \cdot 10^{-3}$ mm^3. Assuming a homogeneous distribution of the spores and the height of the model layer, the volume of the layer is $9.6 \cdot 10^{-3}$ mm^3. As such, the volume ratio of spores is θ_{spores}=16% and the volume ratio of vacuum (or 100 hPa) is θ_{vacuum}=84%.

6.4.2 Numerical optimization

Numerical optimization is defined as the process, by which unknown model parameters are varied to minimize the error between numerical results and experimental values. The numerical modeling and optimization steps are outlined in the flow chart shown in Fig. 6.7. The global objective is to decrease the LSE between the numerical results and the experimental data. For this purpose, the electrical parameters of the model are adjusted by an iterative process. The numerical model to estimate the relative permittivity and the electrical conductivity of the spore layer is divided into three successive optimization models (designated as scenarios).

During the first optimization scenario (Scenario 1) with LSE objective, the frequency-dependent impedance measurements were used to attain an equivalent relative permittivity value of the substrate material (blank sensor state). The derived relative permittivity of the substrate material at the frequency of f=3 kHz was used for the second optimization scenario (Scenario 2). In this scenario, an initial relative permittivity value of the spore layer at different sensor states (loaded sensor state, sterile sensor state) was obtained.

As mentioned in Sec. 6.4.1, φ_{mod} is dependent on the equivalent material properties of the model (σ_{mod} and $\varepsilon_{\mathrm{r,mod}}$). Therefore, a small change of the relative permittivity or electrical conductivity of spores has a large impact on the impedance value and the phase shift (s. Eq. (6.2)). In the third scenario (Scenario 3), a multi-parameter estimation study (similar to Scenario 1 and 2) is required to derive unknown values of relative permittivity and electrical conductivity. To save time and computational resources in this case, the parameters of spores at different sensor states were derived using a Monte Carlo simulation. During the Monte Carlo simulation, a sequence of random set of sample numbers is generated within a user-defined population size. Consequently, each of these random numbers is tested in the original equation and the LSE objective is recorded. At the end of the population size, the random number with the lowest LSE objective is determined in the numerical model as the local minimum (optimal solution) [18]. Since the set of random number differs from one simulation run to the

other, multiple Monte Carlo simulations are required to ascertain that the solution remains in the local minimum.

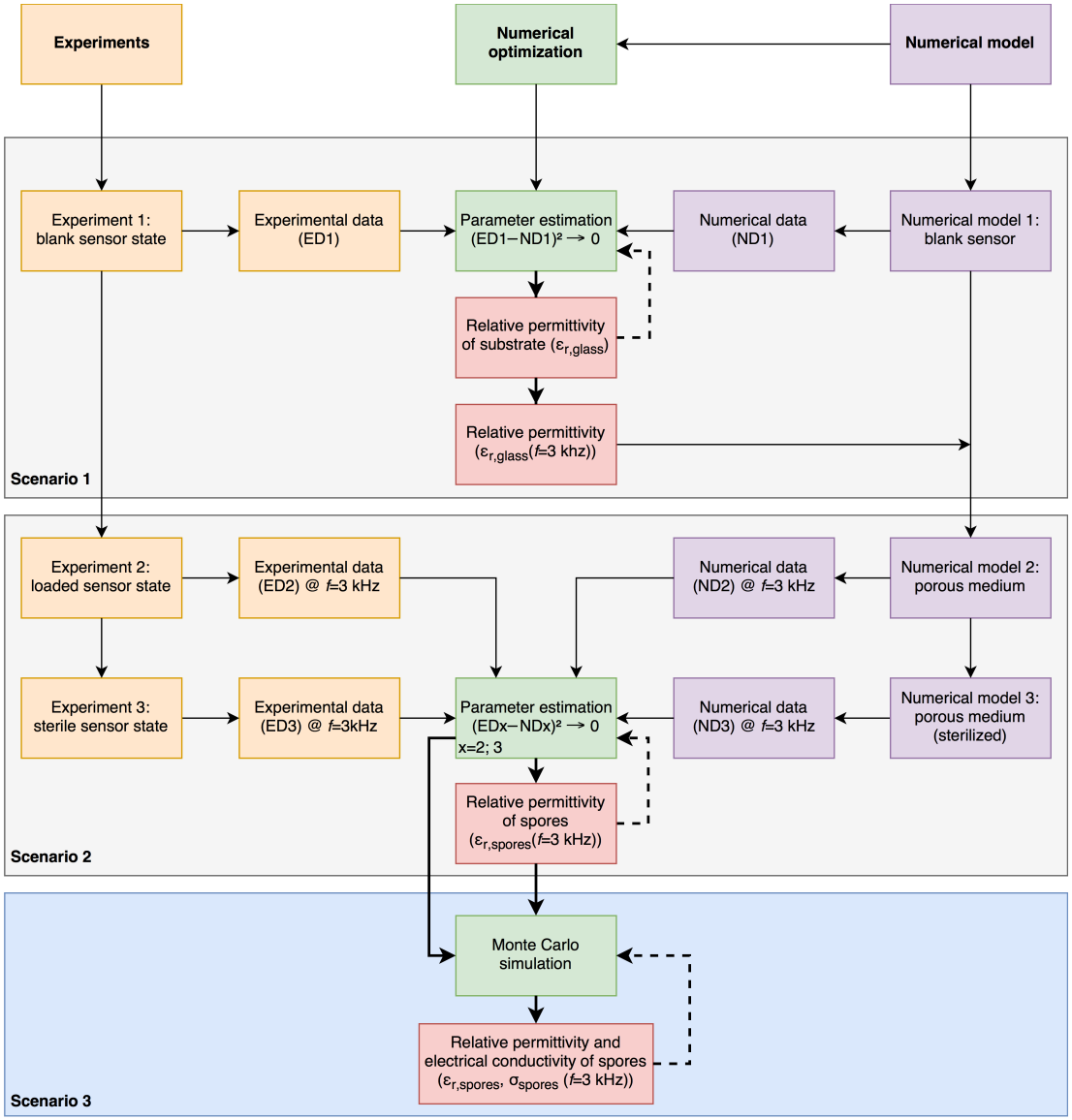

Fig. 6.7: Flow chart representing the numerical optimization scenarios, visualizing the procedure to combine impedimetric experiments and numerical method for deriving the relative permittivity and electrical conductivity (Scenario 1: glass substrate; Scenario 2 and 3: spore layer).

6.5 Results and discussions

The Bode plot in Fig. 6.8 a) depicts the average experimental data of four independent impedimetric biosensor chips. The experimental data include the different impedance and phase signals that are captured for the different sensor states (blank, loaded with

spores and after sterilization). Fig. 6.8 b) shows the average impedance and phase angle values at a fixed frequency of f=3 kHz. The blank sensor impedance has been recorded before and after sterilization, which shows no change and hence no reaction within the sensor material [10]. The blank sensors possess a purely capacitive behavior (phase of about –90°). After immobilization of *B. atrophaeus* spores, a decrease in impedance value by about 25% compared to the blank sensor is noted. This decrease is associated by the decrease in capacitive behavior (phase of about –87°, change of ≈ 2% compared to blank sensor). The impedance measurement after the sterilization protocol (s. Sec. 6.3.1) reveals a further decrease in the impedance value of ≈ 8% compared to the sensor signal after spores' immobilization. This is accompanied by a decrease in the capacitive behavior (phase of about –85°, change of ≈ 2% compared to the sensor signal after spores' immobilization). The latter change in impedance and phase is related to morphological alterations of the spores caused by the sterilization process (s. Fig. 6.4 b)) [7, 10, 11].

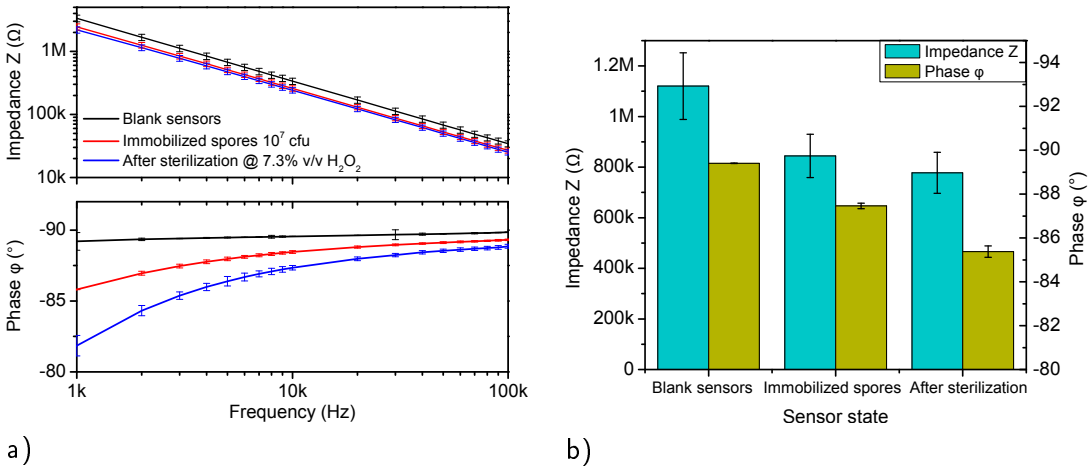

Fig. 6.8: a) Bode plot of the impedimetric biosensor at different sensor states, mean values and standard deviations from four different sensors: blank sensors (black lines); loaded sensors with immobilized *B. atrophaeus* spores 10^7 cfu (10 μl of 10^9 cfu ml^{-1}) on the IDE (red lines); after performed sterilization protocol at a gas temperature of 240 °C, H_2O_2 gas concentration 7.3% v/v (blue lines). b) Impedance and phase angle values at a fixed frequency of 3 kHz for the different sensor states.

The range of the error bars (s. Fig. 6.8 b)) indicate a fluctuation in the initial conditions of the sensors (blank, loaded and sterilized), which is related to small variations during fabrication of the measured chips. Moreover, the microbiological spores are drop-coated from suspension, which results in an uneven distribution over the IDEs. Nonetheless, the tendency of the results underlines a decrease in impedance signal.

Fig. 6.9 depicts the numerical results of the electric field lines of the three different sensor states. The first sensor state shown in Fig. 6.9 a) illustrates the field lines of a blank electrode pair interacting with vacuum and glass substrate. The electric field lines are concentrated at the electrode edges, which arise due to the sharp corners of the electrodes (s. Fig. 6.6). An equidistance distribution can be observed further away from the electrode plane. Furthermore, the first sensor state has been used to

perform a validation of the developed model by using the experimental impedance data of the biosensor at blank state. Thereby, the relative permittivity value of the glass substrate has been determined to be 4.7 (f=3 kHz). Compared to the value given by the producing company Schott (4.6 (f=3 kHz)), the numerically derived value of glass is in good agreement. At this stage the numerical model of the biosensor is validated.

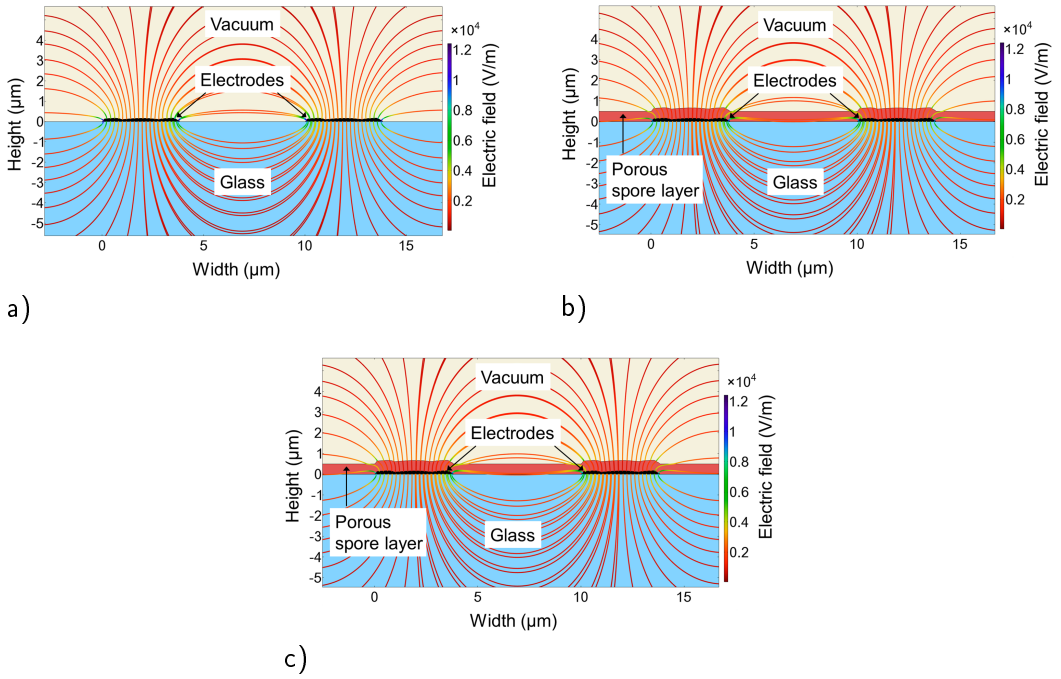

Fig. 6.9: Results of the numerical models showing the electric field distributions: a) of a blank electrode pair, situated on top of a glass substrate in a low-pressure environment; b) change in field lines due to the porous spore layer; c) minor change in the electric field lines affected by the material layer properties after the sterilization, especially between and on top of the electrodes.

In the following optimization steps described in the flow chart (Fig. 6.7), material data for the different sensor states are determined. Tab. 6.1 summarizes the derived numerical results of the electrical permittivity and the conductivity, as well as the error between the numerical results and the experiments. These errors can be either related to the standard deviation in the measurements and/or the idealized conditions of the numerical model (sensor and spore layer design). However, as shown in Tab. 6.1, the errors between the experiment and the numerical results are low for all three sensor states. This indicates a good model representation and validates the numerical method.

The resulting numerical value for the electrical permittivity that represents the intact spore layer can be compared with literature values. In the study performed by van der Hofstadt *et al.*, the permittivity of *B. cereus* spores was evaluated at different humidity levels to be in the range of 4-17 [19]. In the present article, we were able to derive the frequency-dependent electric properties of the spore layer at different states as finite values. For instance, the relative permittivity was estimated to be 13 with an error between the numerical to experimental data of less than 10% for the impedance and phase shift angle values.

Tab. 6.1: Results of the numerical investigations and error to experimental data summarized for the different sensor states.

Material	Glass[a)]		Spore layer[b)]		Error between numerical results and experiment	
Sensor state (f=3 kHz)	ε_r (dimensionless)	σ (S m^{-1})	ε_r[c)] (dimensionless)	σ[d)] (S m^{-1})	Impedance (%)	Phase angle (%)
Blank			–	–	2.8	2.3
Loaded	4.7	≈0	13.0	$4.0 \cdot 10^{-8}$	9.5	3.7
After sterilization			16.7	$6.3 \cdot 10^{-8}$	7.2	1.5

[a)] Parameters derived from LSE optimization (s. Fig. 6.7, Scenario 1); [b)] numerical determination for the porous layer assumption; [c)] parameters derived from the Monte Carlo optimization (s. Fig. 6.7, Scenario 2 and 3); [d)] within the limits of the optimization solver.

Fig. 6.9 b) presents the electric field deviation due to the insertion of the porous spore layer (second sensor state). It can be observed that the electric field distribution within the glass substrate, far away from the electrode and the porous layer, is similar to the first state. Nevertheless, the electric field lines between the two electrodes are affected by the change in electrical permittivity and conductivity.

Fig. 6.9 c) shows the third sensor state (sterile spore layer), where minor changes in the electric field distribution are detected in the layer between and above the electrodes. Compared to the loaded sensor state, these minor changes are related to variations in relative permittivity and electrical conductivity of the spore layer caused by the sterilization process.

As indicated by the results in Tab. 6.1 the permittivity and conductivity values of the spore layer give an insight to its state on the sensor surface. Initially, the non-sterile spore layer possesses a lower permittivity compared to the sterilized spore layer. The loaded, non-sterile sensor state holds intact spore structures (s. Fig. 6.3 b) and Fig. 6.4 a)), where water and ionic substances are enclosed. The higher relative permittivity of the sterilized spore layer can be related to the spore rupture that results in a geometrical deformation of the spores (s. Fig. 6.3 c) and Fig. 6.4 b) and Ref. [7]). The rupture of the spores is accompanied by the release of water and ionic substances (s. Fig. 6.4 b)), which fills the void between the spores. This might additionally explain the increase in relative permittivity after the sterilization. Nevertheless, the applied low-pressure in the measurement chamber is not sufficient for the removal of the water at ambient temperature. In this context, a decrease in impedance is observed that is reflected by the tabulated numerical results. Furthermore, the release of these ionic substances (e.g., proteins, DNA, salts) causes an increase in the electrical conductivity and consequently higher relative permittivity, which results in the formation of conductive paths between the electrode fingers in dry state.

6.6 Conclusion

Experimental characterizations of a biosensor based on interdigitated electrodes have been conducted applying impedance spectroscopy. Furthermore, a numerical model of the biosensor was designed using COMSOL® Multiphysics. In both cases, three

different sensor states were considered: blank, spore-loaded and sterilized sensor. The experimental data and the numerical model as well as the optimization methods have been combined to assess missing material properties (electrical conductivity and relative permittivity) of the different sensor states. The results of the numerical models have been compared with available literature data. By including the impedance measurement data of the blank sensor in the numerical model, an estimated numerical value for the relative permittivity of glass substrate was found to be 4.7. The estimated value is in good agreement with the reported value of 4.6 by the manufacturing company. The model can be further enhanced by including geometric deformation of the spores after the sterilization process. This can be achieved by introducing a direct representation of the spores instead of the porous layer approximation, for example by spore models. The current model can be applied to optimize the electrode geometry for different microorganisms in order to increase the sensitivity of the biosensor. The described combination of experimental and numerical techniques represents a method that can be used to characterize further organic and inorganic materials to acquire knowledge of their material properties and interaction with the environment.

Acknowledgments

Z. B. Jildeh and J. Oberländer contributed equally to this work. J. Arreola is acknowledged for performing the AFM characterization. This work has been financially supported by the Bundesministerium für Bildung und Forschung (BMBF), Germany, project "ImpediPack".

References

[1] T. von Woedtke and A. Kramer. "The limits of sterility assurance". *GMS Krankenhaushygiene Interdisziplinär* 3 (2008), Doc. 19, 1–10.

[2] B. A. H. von Bockelmann and I. L. I. von Bockelmann. *Long-Life Products: Heat-Treated, Aseptically Packed: A Guide to Quality*. Åkarp, Sweden: B. von Bockelmann, 1998.

[3] J. E. Akers and Y. Izumi. "Technological advancements in aseptic processing and the elimination of contamination risk". In: *Advanced Aseptic Processing Technology*. Ed. by J. Agalloco and J. E. Akers. Drugs and the Pharmaceutical Sciences. Boca Raton, FL, USA: CRC Press, 2010, 404–410.

[4] G. McDonnell. "The use of hydrogen peroxide for disinfection and sterilization applications". In: *PATAI'S Chemistry of Functional Groups*. Ed. by Z. Rappoport. Chichester, UK: John Wiley & Sons, Ltd, 2009, 1–34.

[5] P. Kačer, J. Švrček, K. Syslová, J. Václavík, D. Pavlík, J. Červený, and M. Kuzm. "Vapor phase hydrogen peroxide – method for decontamination of surfaces and working areas from organic pollutants". In: *Organic Pollutants Ten Years after the Stockholm Convention*. Ed. by T. Puzyn. Rijeka, Croatia: InTech, 2012.

[6] J. Oberländer, P. Kirchner, H.-G. Boyen, and M. J. Schöning. "Detection of hydrogen peroxide vapor by use of manganese(IV) oxide as catalyst for calorimetric gas sensors". *Physica Status Solidi A* 211 (2014), 1372–1376.

[7] P. Kirchner, J. Oberländer, H.-P. Suso, G. Rysstad, M. Keusgen, and M. J. Schöning. "Monitoring the microbicidal effectiveness of gaseous hydrogen peroxide in sterilization processes by means of a calorimetric gas sensor". *Food Control* 31 (2013), 530–538.

[8] Verband Deutscher Maschinen- und Anlagenbau e.V. "Code of practice: filling machines of VDMA hygiene class V: testing the effectiveness of packaging sterilization devices". *VDMA-Fachverbandsschriften* 6 (2008), 1–16.

[9] J. Arreola, J. Oberländer, M. Mätzkow, M. Keusgen, and M. J. Schöning. "Surface functionalization for spore-based biosensors with organosilanes". *Electrochimica Acta* 241 (2017), 237–243.

[10] J. Oberländer, Z. B. Jildeh, P. Kirchner, L. Wendeler, A. Bromm, H. Iken, P. H. Wagner, M. Keusgen, and M. J. Schöning. "Study of interdigitated electrode arrays using experiments and finite element models for the evaluation of sterilization processes". *Sensors (MDPI)* 15 (2015), 26115–26127.

[11] J. Oberländer, A. Bromm, L. Wendeler, H. Iken, M. P. Durán, A. Greeff, P. Kirchner, M. Keusgen, and M. J. Schöning. "Towards a biosensor to monitor the sterilization efficiency of aseptic filling machines". *Physica Status Solidi A* 212 (2015), 1299–1305.

[12] W. Olthuis, W. Streekstra, and P. Bergveld. "Theoretical and experimental determination of cell constants of planar-interdigitated electrolyte conductivity sensors". *Sensors and Actuators B: Chemical* 24 (1995), 252–256.

[13] R. Igreja and C. J. Dias. "Analytical evaluation of the interdigital electrodes capacitance for a multi-layered structure". *Sensors and Actuators A: Physical* 112 (2004), 291–301.

[14] N. Näther, L. M. Juárez, R. Emmerich, J. Berger, P. Friedrich, and M. J. Schöning. "Detection of hydrogen peroxide (H_2O_2) at exposed temperatures for industrial processes". *Sensors (MDPI)* 6 (2006), 308–317.

[15] J. Oberländer, M. Mayer, A. Greeff, M. Keusgen, and M. J. Schöning. "Spore-based biosensor to monitor the microbicidal efficacy of gaseous hydrogen peroxide sterilization processes". *Biosensors and Bioelectronics* 104 (2018), 87–94.

[16] M. C. Zaretsky, L. Mouayad, and J. R. Melcher. "Continuum properties from interdigital electrode dielectrometry". *IEEE Transactions on Electrical Insulation* 23 (1988), 897–917.

[17] V. F. Lvovich. *Impedance Spectroscopy: Applications to Electrochemical and Dielectric Phenomena*. Hoboken, NJ, USA: John Wiley & Sons, Inc., 2012.

[18] D. P. Landau and K. Binder. *A Guide to Monte Carlo Simulations in Statistical Physics*. 4. Ed. Cambridge, UK: Cambridge University Press, 2015.

[19] M. van der Hofstadt, R. Fabregas, R. Millan-Solsona, A. Juarez, L. Fumagalli, and G. Gomila. "Internal hydration properties of single bacterial endospores probed by electrostatic force microscopy". *ACS Nano* 10 (2016), 11327–11336.

7 Towards a biosensor to monitor the sterilization efficiency of aseptic filling machines (*Physica Status Solidi A*, 212, 6 (2015), 1299–1305)

J. Oberländer, A. Bromm, L. Wendeler, H. Iken, M. Palomar Durán, A. Greeff, P. Kirchner, M. Keusgen, and M. J. Schöning

Published in: *Physica Status Solidi A: Applications and Materials Science,* Vol. 212, 6 (2015), 1299–1305.

Submitted: 2015-02-22; Accepted: 2015-06-27; Published: 2015-07-02

7.1 Abstract

Sterilization processes are compulsory in medicine, pharmacy, and food industries to prevent infections of consumers and microbiological contaminations of products. Monitoring the sterilization by conventional microbiological methods is time- and lab-consuming. To overcome this problem, in this work a novel biosensor has been proposed. The sensor enables a fast method to evaluate sterilization processes. By means of thin-film technology the sensor's transducer structures in form of IDEs (interdigitated electrodes) have been fabricated on a silicon substrate. Physical characterization of the developed sensor was done by AFM, SEM, and profilometry. Impedance analyses were conducted for the electrical characterization. As microbiological layer spores of *B. atrophaeus* have been immobilized on the sensing structure; spores of this type are a well-known sterilization test organisms. Impedance measurements at a fixed frequency over time were performed to monitor the immobilization process. A sterilization process according to aseptic filling machines was applied to demonstrate the sensor functionality. After both, immobilization and sterilization, a change in impedance could successfully be detected.

7.2 Introduction

Aseptic filling of sensitive food products, such as milk and juice, in carton-based packages has been highly significant within the recent years. Aseptic packaging defines thereby the absence of any microbial contamination within the food in order to increase the shelf-life stability and especially, the consumer safety. To achieve a consumer-safe and sterile product two independent sterilization processes are performed: i) the product to be filled is in general sterilized by heat treatment, and ii) the food contact surfaces of the packages are sterilized by application of either heat, irradiation, chemical treatment, or combination thereof. The advantage of the separated sterilization compared to autoclaving is the preservation of nutrients and food freshness. Furthermore, the extended product shelf-life can be achieved without addition of preservatives. Hydrogen peroxide (H_2O_2) has become the sterilization medium of choice in food industry for the package material sterilization. Hereby, the sterilization process differs in the application form of H_2O_2. A common technique is the utilization of liquid H_2O_2, subsequently followed by a thermal treatment. The H_2O_2 sterilization effect can further be raised by UV light irradiation. Herein, the irradiation induces a decomposition of H_2O_2 molecules into water and oxygen. During the decomposition, reactive radicals occur. These radicals and the strong oxidative properties of H_2O_2 are mainly responsible for the microbicidal and sporicidal activity of H_2O_2 [1]. In recent years, the combination of chemical and thermal treatment has become very favorable: a mixture of air, as carrier gas, and vaporized H_2O_2 will be heated and flushed into the packages to be sterilized. The temperature of this gaseous mixture for package sterilization is up to 300 °C. The combination of heat and H_2O_2 forces also the decomposition with the related radical formation [2]. Prior guiding the gaseous H_2O_2 into the packages a preheating is conducted. For this step, sterile hot air will be led into the packages. This is necessary to maintain the sterilization medium in gas phase without condensation on the packages. Subsequently, sterile hot air is applied to the packages to remove the sterilization medium. After the sterilization, the remaining H_2O_2 concentration must not exceed 0.5 ppm [3].

Usually, lab-intensive microbiological methods are necessary to monitor the package sterilization. In these microbiological methods test packages are inoculated with highly resistant test organisms. These test organisms have to fulfill special requirements, such as to be highly chemical and heat resistant. For sterility tests, in which H_2O_2 is applied, as sterilization medium, spores of *Bacillus atrophaeus* (DSMZ 675, ATCC 9372, formerly known as *B. subtilis* [4]) are used. Spores of *B. atrophaeus* have demonstrated to be highly resistant against heat and chemical treatment such as H_2O_2 [5–7].

To reduce the laborious microbiological tests different types of calorimetric gas sensors have been developed recently, to monitor gaseous H_2O_2 sterilization processes. With these sensors real-time measurements of the present H_2O_2 concentration, which is important for the sterilization efficiency, were conducted for the first time. Fast process optimizations could be realized by a correlation model between the sensor signal and microbiological tests [8–11]. However, with these sensors it is only possible to detect the H_2O_2 concentration; no information about the microbiological impact is given.

Different sensor structures are common to capture biological activities/processes. One of the most valuable transducer structures are interdigitated electrodes (IDE). IDEs

enable a fast, label-free and sensitive detection method for microbiological cells or biological interactions [12–18]. The transducer structures usually consist of finger pairs and gaps, on which a material under test, such as microbiological samples, can be immobilized. Simulations have demonstrated that the detection limit of such structures is mainly driven by the number of electrodes, the finger width and the interspacing distance [13, 19]. These simulations and impedance analyses have revealed that the electrode geometry should be comparable to the size of the target organism [20].

Several approaches, in which impedance analyses are applied to enumerate/detect bacterial load or growth, have been reported in literature [21, 22]. Also various commercial systems (Bactometer®, Malthus® systems, R.A.B.I.T.®, Bac-Trac®) are available on the market, which are based on impedance measurements to study the bacterial load [23]. However, in all stated systems the measurements are performed in nutrition media or buffers and the impedance change detected by these systems results from the metabolic activity or the increasing number of the organisms during incubation. Hence, to detect the metabolic activity an incubation time of at least half a day is necessary.

In the present work, a novel biosensor set-up will be introduced. The aim is to capture the impact of the sterilization process toward spores immobilized on the sensor surface by an electrical read-out. In this approach, both the measurements and the sterilization have to be performed in gaseous environment. The sensor should be able to allow a "medium-free" evaluation within minutes of measurement.

7.3 Experimental

7.3.1 Microbiological methods

Spores of *Bacillus atrophaeus* (DSMZ 675) have been applied as test organism. A spore suspension with a microbiological spore load of at least 10^8 cfu ml^{-1} (cfu: colony forming units) is usually utilized for sterility tests. The spore suspension was cultivated by the following procedure: a standard plate-count agar (Product No. 1.05463, Merck KGaA, Germany) was applied for initial colony growth and the later enumeration. An initial sample (0.1 ml) of a DSMZ 675 stock solution was surface-plated. After 2 days growth at 30 °C, one colony was transferred into a liquid culture medium (same ingredients as the commercial plate-count media but without agar). To force the sporulation of *B. atrophaeus*, 10 mgl^{-1} of $MnSO_4$ was added to the medium [24]. A shaking incubator was applied for 1 week at 30 °C to cultivate the aerobic bacteria. During this period the bacteria were transformed to spores. Subsequently, centrifugation steps (20 min at 9000 g) were performed to harvest the spores. The supernatant containing living cells and culture medium was removed. Several washing steps with re-suspension in deionized water and centrifugation were done to obtain a pure spore suspension. The suspension was pasteurized in a water bath (20 min at 80 °C). After a final centrifugation step the spore pellet was re-suspended in 70% v/v ethanol. The final spore concentration was determined by serial dilution and surface plating. Whereby, a microbiological load of 10^8 cfu ml^{-1} could be assured.

7.3.2 Sensor design

The biosensor set-up is based on a silicon substrate (3" wafer, SI-MAT, Germany). As transducer structure, a planar interdigitated electrode (IDE) structure has been chosen. In order to capture lethal transformations on microorganisms, the width of each electrode finger and the interspacing between is designed to 5 μm. These parameters are predefined by the spores to be detected and limited by the standard photolithography process. The length of each finger was set to 3.25 mm. With a total number of 614 fingers an active sensing area of about 20 mm^2 can be achieved. The biosensor will operate in a differential set-up, where one of the IDEs will be left blank to serve as a reference. This reference will capture influences of the sterilization process as well as the environment toward the sensing structure. On the second IDE microbiological spores from *B. atrophaeus* will be immobilized. For this immobilization step, micro-fabricated walls are designed on the sensors with a height of about 400 μm. These walls will allow the immobilization of a 10 μl spore suspension by drop-coating on the sensor structure. The amount of 10 μl corresponds to the inoculation volume of conventional package sterilization tests (e.g., count-reduction test). In these conventional evaluation tests the packages will be inoculated by either spraying or drop-coating [25]. The differential sensor set-up ensures to only capture interactions on the spore layer.

To gather additional process informations, temperature-sensing resistance structures were designed below the IDEs.

7.3.3 Sensor fabrication

Fig. 7.1 shows the thin-film fabrication steps: a piranha-cleaned 3" silicon wafer was used as initial substrate. By wet oxidation a 500 nm SiO_2 insulation layer was deposited. TI prime was spin-coated onto the substrate to improve the adhesion of the photoresist and metal layers. Subsequently, a positive-tone photoresist (AZ 5214-E, AZ Electronic Materials GmbH) was spin-coated onto the substrate to enable lithographic patterning. A thickness of 1.4 μm of the photoresist could be achieved by spin-coating at 4000 rpm for 30 s. A prebake of the photoresist layer was conducted at 90 °C for 5 min on a hot plate. In order to obtain the above stated structures, a glass mask has been applied for the photolithography process (Fig. 7.1 c)). The structures from the glass mask were transferred into the photoresist by a mask aligner (Süss MicroTec AG, Germany) with a UV light source (wavelength 365 nm). Development of the structures was done with AZ 326 MIF, as recommended for the photoresist. After the photolithography process two metal layers were deposited by electron-beam evaporation (Univex, Leybold GmbH, Germany). As a first layer, titanium was deposited to serve as an adhesion layer between substrate and electrode structure (layer thickness of 20 nm). The electrode structure itself was deposited from a platinum target (layer thickness of 200 nm) (Fig. 7.1 e)).

During the lift-off process unnecessary parts of the metal layers were removed. Therefore, the wafer was placed in a dimethyl sulfoxide (DMSO) bath. The lower vapor pressure of DMSO compared to acetone prevents a re-adsorption of the lifted metal. The lift-off process was supported by gently applied ultrasonic forces.

A further photolithographic process was done to form cavities; these enable a defined immobilization of microorganisms onto the electrode structure. For this purpose, the

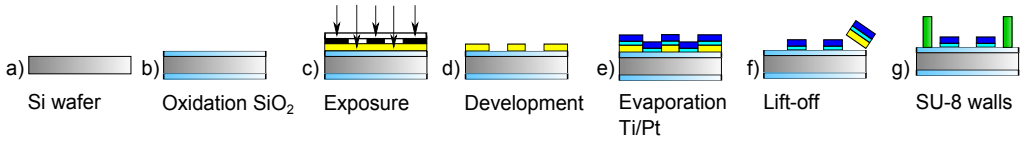

Fig. 7.1: Schematic representation summarizing the thin-film fabrication steps: a) starting with a silicon wafer; b) oxidation to SiO_2 serving as insulation layer; c) photoresist patterning by photolithography; d) photoresist development; e) evaporation of electrode metals; f) lift-off to remove unnecessary metal parts; and g) fabrication of SU-8 walls by photolithography.

high-viscous negative-tone photoresist SU-8 2150 (Microchem, Inc., USA) was applied. The spin-coating was performed at 1400 rpm for 30 s to achieve a layer thickness of about 400 μm. A two-step prebake, to avoid thermal stress of the resulting film, was performed on a hot plate for 7 min at 65 °C and 120 min at 95 °C. Patterning was done with the above stated mask aligner and a film mask. The post-exposure bake was likewise a two-step process, 5 min at 60 °C and 30 min at 95 °C. Developer mr-Dev 600 was used for 30 min to obtain the cavities. A final hard bake was performed for 15 min at 150 °C.

The finished wafer was diced into single chips of 5 x 10 mm^2. Prior to dicing, the electrode structures were protected by a further photoresist coating. The final sensors were received after a subsequent cleaning process in DMSO, isopropanol and DI-water.

A fully processed, impedimetric biosensor chip is shown in Fig. 7.2. The upper part depicts the IDE structures, framed by walls of SU-8 photoresist. In the lower part, the temperature sensors and the contact pads are visible. On one of the IDEs spores of the sterilization test organism *B. atrophaeus* will be immobilized. The applied spore suspension is described in Sec. 7.3.1. The microbiological spores were self-immobilized by drop-coating and a subsequent drying process.

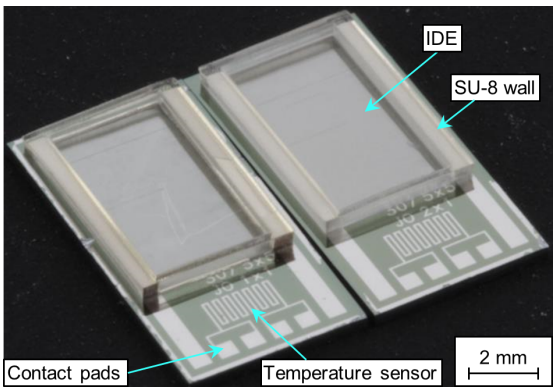

Fig. 7.2: Differential set-up of two 5 x 10 mm^2 chips with interdigitated electrodes and temperature sensors.

7.3.4 Sensor characterization

The following methods were used to characterize the transducer structures as well as the final sensor with the biological spore layer: atomic force microscopy (AFM) and profilometry were performed to analyze the electrode structure and the SU-8 photoresist walls. The sensor surface was additionally characterized by scanning electron microscopy (SEM). Electrical characterizations and all sensor measurements were conducted with an impedance analyzer (Fa. Zahner-Elektrik GmbH, Germany).

7.3.5 Sterilization process

The sterilization process was investigated in a specially designed test-rig, as previously described in Ref. [8]. This test-rig represents the sterilization module of commercial aseptic filling machines. A forced H_2O_2 gas stream was provided with an air stream (10 $m^3\,h^{-1}$) as carrier medium. A LabView-based program was applied to control the H_2O_2 dosage. The resulting air-H_2O_2 mixture was heated in a flow-through vaporizer up to 240 °C. The gaseous H_2O_2 stream was divided onto four outlet nozzles with inner diameters of 15.5 mm. The H_2O_2 concentration within the gas stream can be varied from 0 to 7.5% v/v.

The differential sensor set-up consisting of two IDEs (one with immobilized spores and another blank as reference) was exposed for a defined time of 300 ms. A time-controlled pneumatic sample slide was applied, on which the sensors were directly exposed to the forced H_2O_2 gas stream for a defined time. A distance of 5.5 cm between the gas outlet-nozzle and the sensors was kept constant.

7.4 Results and discussions

7.4.1 Structural characterization

The profilometric scan (Fig. 7.3 a)) captured by an AFM (JPK Instruments AG, Germany) depicts the dimensions of the IDE structures. The gap between each finger is about 4.1 μm, whereas an electrode width of 5.9 μm can be measured. The electrode height is determined to amount 220 nm. Additionally, tear-off edges of up to 300 nm resulting from the lift-off process can be observed. The profilometric scan of the SU-8 wall results in a height of about 400 μm (Fig. 7.3 b)). These walls allow a defined immobilization of 10 μl spore suspension onto the IDEs.

The electrodes were additionally analyzed by means of SEM before and after immobilization of spores (Fig. 7.4). The SEM image of the blank sensor structures depicts also the tear-off edges (Fig. 7.4 a)) as observed by AFM analysis. The second SEM image (Fig. 7.4 b)) elucidates the random distribution of the spores without a certain alignment. The microbiological spores are settled homogeneously on top and between the electrodes.

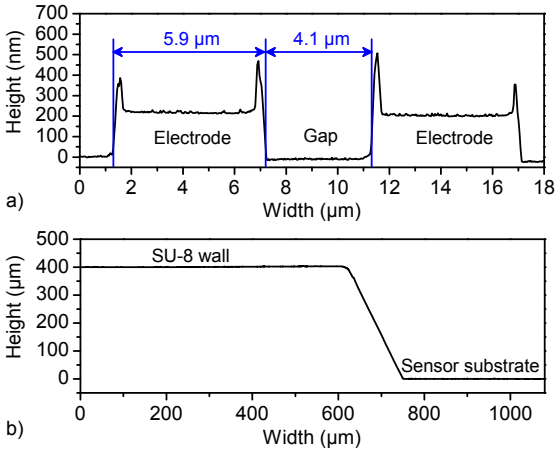

Fig. 7.3: Profilometric scans of: a) an IDE structure; and b) a wall of the SU-8 cavities.

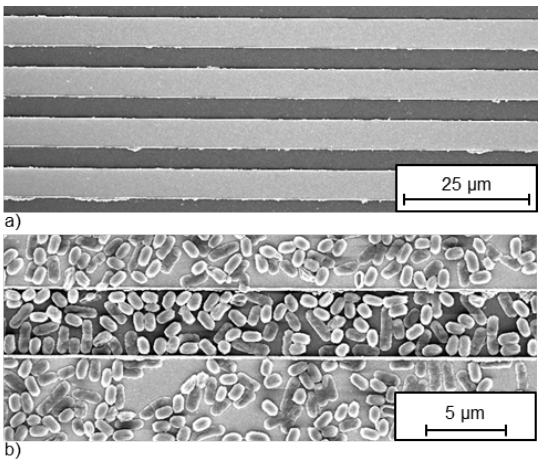

Fig. 7.4: SEM characterization: a) blank transducer structures, light grey defines the electrodes; b) transducer structures with immobilized spores (SEM: Magellan 400, FEI Company, USA).

7.4.2 Impedance characterization of fabricated IDE structures

First, electrical characterization of the sensors was performed by recording the impedance spectra, as shown in Fig. 7.5. An alternating excitation voltage with an amplitude of 20 mV was applied; the polarization voltage was set to 0 V. To determine the impedance and phase of the sensor the resulting current was used. The relation between the applied voltage V, resulting current I, and sensor impedance Z is given in Eq. (7.1) (complex representation). The impedance phase φ_Z is defined by the difference of the imposed voltage phase φ_V and the detected current phase φ_I. The spectra were recorded in a frequency range from 100 Hz to 150 kHz.

$$\underline{Z} = \frac{V \cdot e^{j\varphi_V}}{I \cdot e^{\varphi_I}} = Z \cdot e^{j\varphi_Z} \tag{7.1}$$

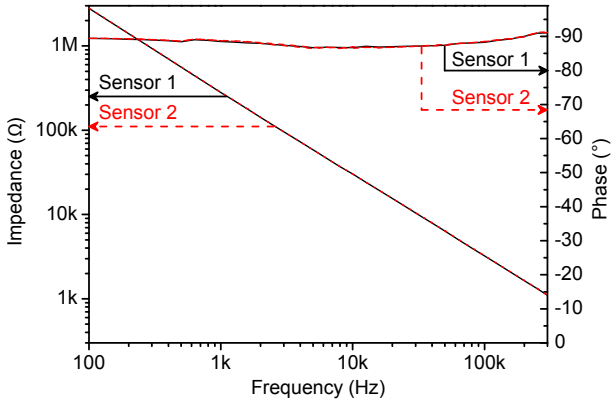

Fig. 7.5: Bode plot of two different IDE sensors. Measurements were conducted in a Faraday cage, wherein the sensors were exposed to air.

The impedance spectra have demonstrated a stable, predominantly capacitive behavior of the sensors (Fig. 7.5). Based on the spectra the capacitance of the whole system (cable impedances, sensor in air, impedance analyzer) can be estimated to be about 520 pF. The strictly capacitive behavior arises from the fact that the electrodes are exposed to air with isolating properties. In contrast, impedance spectra given in literature are often performed within electrolyte. These analyses typically reveal three defined regions depending on the excitation frequency: at low frequencies the double-layer capacitance is predominant. The double-layer capacitance is defined by the transition between electrode and electrolyte. At high frequencies the capacitance resulting from the electrolyte is prevalent. The intermediate range is defined by the resistive characteristics of the electrolyte [13, 19, 26]. In the spectra recorded without electrolyte no differentiation according to the three frequency bands was found.

The impedance analysis of the sensors was realized in air to avoid an additional capacitive signal of the solution [21]. Moreover, solutions were avoided to prevent a detachment of the spores. All sensors have been characterized prior and after microorganism immobilization and after sterilization process with gaseous hydrogen peroxide.

7.4.3 Impedance measurements with immobilized spores

Based on the spectra analysis, a fixed frequency was adjusted to enable impedance measurements over time. These time-dependent measurements were performed with an alternating voltage of 20 mV and the frequency was set to 100 kHz. At this frequency no interferences caused by the environment (e.g., 50 Hz noise) were detected. The impedance of the sensors was analyzed over a time period of at least 10 min to observe drift and signal fluctuations. By means of this method, the immobilization of the microbiological spores can be reported online, as exemplarily depicted in Fig. 7.6. The immobilization of a 10 μl spore suspension containing 10^8 cfu ml^{-1} results in 10^6 cfu per sensor. After applying the spore suspension an immediate impedance change can be observed. This impedance change can be related to the conductivity and dielectric properties of the immobilization solution consisting of a 70% v/v ethanol-water mixture.

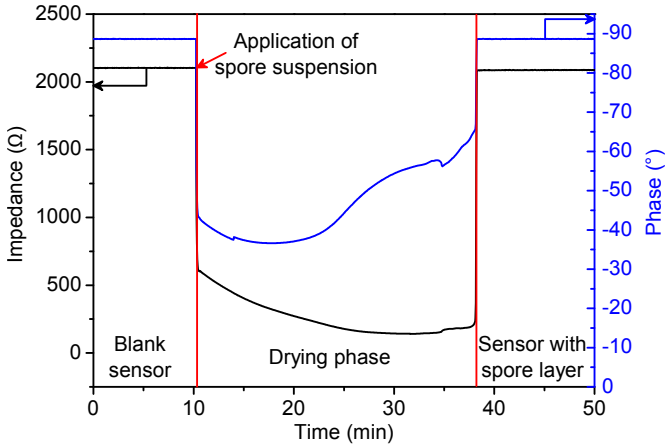

Fig. 7.6: Live immobilization of *B. atrophaeus* spores onto IDE structures (10 μl of an ethanol-based spore suspension: 10^8 cfu ml^{-1}). The measurement was conducted with an excitation voltage of 20 mV, polarization voltage of 0 V, and a frequency of 100 kHz.

Subsequently, further decrease of impedance is registered, which can be related to the evaporation of the solution. This induces an alteration in dielectric properties at the sensor interface. The impedance with spore layer is slightly decreased, in comparison to the blank sensor. This remaining lower impedance results from dielectric and conductive properties of the spore membranes and inner spore substances [27]. It serves as an indicator for successful spore immobilization. The obtained results are different from solution-based impedance measurements, where after cell immobilization an increase of the impedance was observed. The impedance increase can be described by a shielding effect of the electrodes by the microorganisms. This yields a reduced electrode area exposed to the medium resulting in a reduced current between the electrodes [22, 28, 29].

For the solution-free measurements the current flow might be enhanced by the microbiological spores compared to the isolating properties of air. Even though, the spores also possess isolating properties and a low water content of approximately 20% [6, 27].

7.4.4 Impact of the sterilization

For the H_2O_2 gas sterilization the following parameters have been selected: gas temperature of 240 °C, exposure time of 300 ms, H_2O_2 concentration of 7.5% v/v. As described, a differential set-up of two IDE structures was exposed to the sterilization process. The reference structure was used to retrieve impedance changes induced by the harsh process conditions during the H_2O_2 sterilization. By the second IDE the interaction of the sterilization process with the spores will be captured. The resulting impedance values are overviewed in Fig. 7.7. Slight impedance changes for the reference structure were observed (indicated by red dots in Fig. 7.7). The maximum impedance variation between the different measurements is 1.5 Ω. Prior and after the sterilization a deviation of 0.8 Ω is detectable. This indicates that the short exposure of the sensing

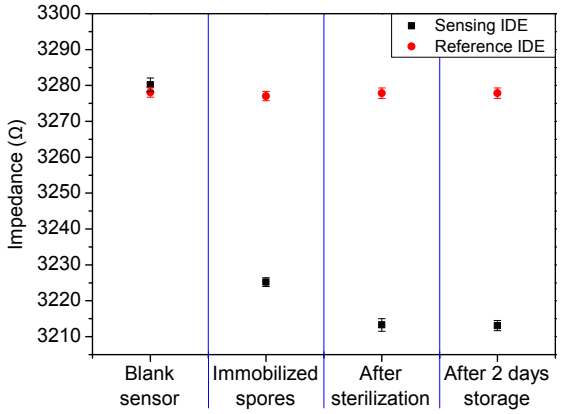

Fig. 7.7: Impedance values of the differential set-up: initial values of blank IDE structures; after immobilization of 10 μl spore suspension (black squares); after sterilization for 300 ms at 7.5% v/v H_2O_2; final measurements after 2 days storage in dry air. Error bars represent measurement fluctuations over 10 min.

structures to hot H_2O_2 vapor causes no distinct interferences. A final measurement was executed after 2 days.

In contrast, for the sensor chip with the immobilized spores a clear impedance drop of 50 Ω can be detected directly after the immobilization procedure. After the sterilization process a further impedance decrease of about 10 Ω was achieved. This impedance decrease can be related to morphological deformations arisen from the interaction of the spores with hydrogen peroxide vapor. Furthermore, it is likely that a rupture of the spores occurs and spore substances will be released [10, 30]. The released spore substances might increase the conductive properties of the spore layer. Subsequently, also collapsing of the spores is favorable. These lethal structural deformations were visualized by the impedimetric sensor. Hereby, a fast evaluation of sterilization processes that induces morphological, lethal alterations on microorganisms is possible.

Conventional microbiological tests, according to Ref. [25], were also applied in order to verify the sterilization efficiency of the performed sterilization scenario. In microbiological terms the sterilization efficiency is defined by the logarithmic reduction rate (Log-rate), which allows a quantitative conclusion. The Log-rate is calculated by the logarithmic ratio of the initial spore load N_0 and the survived colonies N as shown in Eq. (7.2). Sterility is achieved if a six-fold log reduction can be proven [31].

$$Log - rate = log\frac{N_0}{N} \tag{7.2}$$

7.5 Conclusions

In this work, a novel sensor to monitor the sterilization efficiency of gaseous H_2O_2 on microbiological test organisms, namely *B. atrophaeus* spores, has been presented. Silicon-based thin-film technology has been applied for sensor fabrication: interdigitated electrodes were chosen as transducer structures. A high-viscose SU-8 photoresist

was applied to fabricate cavities to enable the defined immobilization of spores from an ethanol-based suspension. The final sensor consists of a differential set-up of two IDEs in order to eliminate effects of the sterilization process onto the sensing structures. The developed sensing structures were characterized by different methods. SEM, AFM, and profilometry were used to analyze the developed structures. Impedance analyses were performed for electrical characterizations. Measurements at a fixed frequency allowed the monitoring of the immobilization process of an ethanol-based spore suspension. The sensor functionality has been demonstrated for the first time by applying a sterilization process with gaseous hydrogen peroxide. The sterilization process itself was adapted to the procedure on commercial aseptic filling machines. In these machines, gaseous H_2O_2 is applied to sterilize packages prior filling of liquid foods. Lethal spore modifications caused by the sterilization were captured by solution-free impedance analyses representing the suitability of the novel biosensor. Future aspects to be investigated are: i) tests at different sterilization scenarios; ii) development of an electrical equivalent model; iii) correlation model between sensor signal and conventional microbiological tests; iv) investigation of different spore loads on the sensor; and v) further transducer optimization.

Acknowledgments

The authors gratefully thank the Federal Ministry of Education and Research (Germany) project "ImpediPack" for financial support. Prof. Dr. J. Bongaerts is acknowledged for offering the lab equipment to run the microbiology studies and Dr. E. Neumann for his technical support concerning the SEM analysis.

References

[1] N. A. Klapes and D. Vesley. "Vapor-phase hydrogen peroxide as a surface decontaminant and sterilant". *Applied and Environmental Microbiology* 56 (1990), 503–506.

[2] P. A. Giguère and I. D. Liu. "Kinetics of the thermal decomposition of hydrogen peroxide vapor". *Canadian Journal of Chemistry* 35 (1957), 283–293.

[3] Food and Drug Administration. *Code of federal registrations: food and drugs: indirect food additives: adjuvants, production aids, and sanitizers*. Code of Federal Regulations (CFR). 2011. URL: `http://www.fda.gov`.

[4] D. Fritze and R. Pukall. "Reclassification of bioindicator strains *Bacillus subtilis* DSM 675 and *Bacillus subtilis* DSM 2277 as *Bacillus atrophaeus*". *International Journal of Systematic and Evolutionary Microbiology* 51 (2001), 35–37.

[5] B. Setlow, C. A. Loshon, P. C. Genest, A. E. Cowan, C. A. Setlow, and P. Setlow. "Mechanisms of killing spores of *Bacillus subtilis* by acid, alkali and ethanol". *Journal of Applied Microbiology* 92 (2002), 362–375.

[6] P. Setlow. "Spores of *Bacillus subtilis*: their resistance to and killing by radiation, heat and chemicals". *Journal of Applied Microbiology* 101 (2006), 514–525.

[7] P. Setlow. "Resistance of bacterial spores". In: *Bacterial Stress Responses*. Ed. by G. Storz and R. Hengge. Monograph, ASM Press. Washington, DC, USA: ASM Press, 2011, 319–332.

[8] P. Kirchner, B. Li, H. Spelthahn, H. Henkel, A. Schneider, P. Friedrich, J. Kolstad, M. Keusgen, and M. J. Schöning. "Thin-film calorimetric H_2O_2 gas sensor for the validation of germicidal effectivity in aseptic filling processes". *Sensors and Actuators B: Chemical* 154 (2011), 257–263.

[9] P. Kirchner, J. Oberländer, P. Friedrich, J. Berger, G. Rysstad, M. Keusgen, and M. J. Schöning. "Realization of a calorimetric gas sensor on polyimide foil for applications in aseptic food industry". *Sensors and Actuators B: Chemical* 170 (2012), 60–66.

[10] P. Kirchner, J. Oberländer, H.-P. Suso, G. Rysstad, M. Keusgen, and M. J. Schöning. "Monitoring the microbicidal effectiveness of gaseous hydrogen peroxide in sterilization processes by means of a calorimetric gas sensor". *Food Control* 31 (2013), 530–538.

[11] N. Näther, H. Henkel, A. Schneider, and M. J. Schöning. "Investigation of different catalytically active and passive materials for realizing a hydrogen peroxide gas sensor". *Physica Status Solidi A* 206 (2009), 449–454.

[12] A. Bratov, J. Ramon-Azcon, N. Abramova, A. Merlos, J. Adrian, F. Sanchez-Baeza, M. P. Marco, and C. Dominguez. "Three-dimensional interdigitated electrode array as a transducer for label-free biosensors". *Biosensors and Bioelectronics* 24 (2008), 729–735.

[13] N. Couniot, D. Flandre, L. A. Francis, and A. Afzalian. "Signal-to-noise ratio optimization for detecting bacteria with interdigitated microelectrodes". *Sensors and Actuators B: Chemical* 189 (2013), 43–51.

[14] N. Couniot, T. Vanzieleghem, J. Rasson, N. van Overstraeten-Schlögel, O. Poncelet, J. Mahillon, La Francis, and D. Flandre. "Lytic enzymes as selectivity means for label-free, microfluidic and impedimetric detection of whole-cell bacteria using ALD-Al_2O_3 passivated microelectrodes". *Biosensors and Bioelectronics* 67 (2015), 154–161.

[15] E. Katz and I. Willner. "Probing biomolecular interactions at conductive and semiconductive surfaces by impedance spectroscopy: routes to impedimetric immunosensors, DNA-sensors, and enzyme biosensors". *Electroanalysis* 15 (2003), 913–947.

[16] P. B. Lillehoj, C. W. Kaplan, J. He, W. Shi, and C. M. Ho. "Rapid, electrical impedance detection of bacterial pathogens using immobilized antimicrobial peptides". *Journal of Laboratory Automation* 19 (2014), 42–49.

[17] A. V. Mamishev, K. Sundara-Rajan, Fumin Yang, Yanqing Du, and M. Zahn. "Interdigital sensors and transducers". *Proceedings of the IEEE* 92 (2004), 808–845.

[18] M. Varshney and Y. Li. "Interdigitated array microelectrodes based impedance biosensors for detection of bacterial cells". *Biosensors and Bioelectronics* 24 (2009), 2951–2960.

[19] M. Ibrahim, J. Claudel, D. Kourtiche, and M. Nadi. "Geometric parameters optimization of planar interdigitated electrodes for bioimpedance spectroscopy". *Journal of Electrical Bioimpedance* 4 (2013), 13–22.

[20] O. Laczka, E. Baldrich, F. X. Munoz, and C. F. J. del. "Detection of *Escherichia coli* and *Salmonella typhimurium* using interdigitated microelectrode capacitive immunosensors: the importance of transducer geometry". *Analytical Chemistry* 80 (2008), 7239–7247.

[21] X. Tang, D. Flandre, J.-P. Raskin, Y. Nizet, L. Moreno-Hagelsieb, R. Pampin, and L. A. Francis. "A new interdigitated array microelectrode-oxide-silicon sensor with label-free, high sensitivity and specificity for fast bacteria detection". *Sensors and Actuators B: Chemical* 156 (2011), 578–587.

[22] L. Yang and R. Bashir. "Electrical/electrochemical impedance for rapid detection of foodborne pathogenic bacteria". *Biotechnology Advances* 26 (2008), 135–150.

[23] M. Zourob, S. Elwary, and A. Turner, eds. *Principles of Bacterial Detection: Biosensors, Recognition Receptors and Microsystems*. 1st ed. New York, NY, USA: Springer Science and Business Media, 2008.

[24] Deutsche Sammlung von Mikroorganismen und Zellkulturen, DSMZ. *Katalog für Mikroorganismen*. GmbH. Braunschweig. 2007. URL: `http://www.dsmz.de`.

[25] Verband Deutscher Maschinen- und Anlagenbau e.V. "Code of practice: filling machines of VDMA hygiene class V: testing the effectiveness of packaging sterilization devices". *VDMA-Fachverbandsschriften* 6 (2008), 1–16.

[26] V. F. Lvovich. *Impedance Spectroscopy: Applications to Electrochemical and Dielectric Phenomena*. Hoboken, NJ, USA: John Wiley & Sons, Inc., 2012.

[27] E. L. Carstensen, R. E. Marquis, S. Z. Child, and G. R. Bender. "Dielectric properties of native and decoated spores of *Bacillus megaterium*". *Journal of Bacteriology* 140 (1979), 917–928.

[28] R. Ehret, W. Baumann, M. Brischwein, A. Schwinde, K. Stegbauer, and B. Wolf. "Monitoring of cellular behaviour by impedance measurements on interdigitated electrode structures". *Biosensors and Bioelectronics* 12 (1997), 29–41.

[29] R. Ehret, W. Baumann, M. Brischwein, A. Schwinde, and B. Wolf. "On-line control of cellular adhesion with impedance measurements using interdigitated electrode structures". *Medical and Biological Engineering and Computing* 36 (1998), 365–370.

[30] H. Shintani, A. Sakudo, P. Burke, and G. McDonnell. "Gas plasma sterilization of microorganisms and mechanisms of action". *Experimental and Therapeutic Medicine* 1 (2010), 731–738.

[31] A. Kramer, O. Assadian, and K. H. Wallhäußer, eds. *Wallhäußers Praxis der Sterilisation, Desinfektion, Antiseptik und Konservierung*. Stuttgart: Georg Thieme Verlag, 2008.

7.6 Supplemental information

The impedance measurements within this chapter are results of a first sensor characterization by applying the Zahner-Elektrik impedance analyzer IM5. Whereas, the measurements performed in all other chapters have been conducted with an Agilent LCR-meter E4980A. Due to this device change the fixed frequency to analyze the sensors has been adjusted from 100 kHz (Ch. 7) to 3 kHz (all other chapters). During further performed sensor analyses by applying the Agilent LCR-meter the impedance change caused by the microbiological layer has been observed to be more pronounced in the lower frequency region. In general, before evaluating the impedance at a single frequency the impedance spectra have been recorded at least between 1 kHz–100 kHz.

8 Surface functionalization for spore-based biosensors with organosilanes (*Electrochimica Acta*, 241, 6 (2017), 237–243)

J. Arreola*, **J. Oberländer***, M. Keusgen, and M. J. Schöning

Published in: *Electrochimica Acta,* Vol. 241, 6 (2017), 237–243.

Submitted: 2017-01-30; Accepted: 2017-04-28; Published: 2017-04-29

* Both authors contributed equally to this work.

8.1 Abstract

In the present work, surface functionalization of different sensor materials was studied. Organosilanes are well known to serve as coupling agent for biomolecules or cells on inorganic materials. 3-aminopropyltriethoxysilane (APTES) was used to attach microbiological spores to an interdigitated sensor surface. The functionality and physical properties of APTES were studied on isolated sensor materials, namely silicon dioxide (SiO_2) and platinum (Pt) as well as the combined material on sensor level. A predominant immobilization of spores could be demonstrated on SiO_2 surfaces. Additionally, the impedance signal of APTES-functionalized biosensor chips has been investigated.

8.2 Introduction

Under stressful environments (e.g., nutrient-limiting conditions), a variety of bacteria of *Bacilli* and *Clostridia* genus produce spores: a dormant (i.e., no detectable metabolism) cell type, that can withstand a wide range of different stresses such as heat, radiation and oxidizing agents [1–3]. During the dormant state, the spores nonetheless are still able to monitor changes in their surroundings, making them suitable for use as sensitive or recognition elements in biosensor systems [4–8].

Recently, a first type of spore-based biosensor was suggested to evaluate sterilization processes in aseptic filling machines [9]. Such biosensor is illustrated in Fig. 8.1. It consists of a glass substrate with temperature sensors and several interdigitated electrodes (IDEs) as transducer elements, where the spores can be immobilized on one of the IDEs due to walls of SU-8 photoresist, whereas the other IDE is utilized as reference sensor (differential set-up measurement).

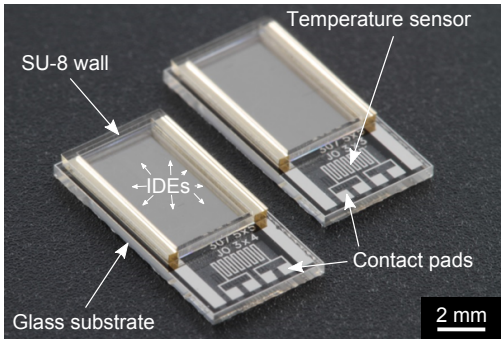

Fig. 8.1: Spore-based biosensor. Differential set-up of two glass chips with temperature sensors and interdigitated electrodes (IDEs).

The principle of the spore-based biosensor is depicted in Fig. 8.2. First, the spores are chemically immobilized (e.g., via silanization) onto the sensor surface to prevent any detachment during the sterilization process. Then, the biosensor is exposed to a vaporized hydrogen peroxide (H_2O_2) hot gas stream (e.g., 240 °C, 10 $m^3\,h^{-1}$) and the sensor signal change (e.g., impedance) before and after sterilization is evaluated. The signal change can be correlated to the morphology deformation of the spores due to the H_2O_2 concentration. In general, the H_2O_2 concentration applied defines the grade of sterilization in aseptic food processes and the dosed H_2O_2 concentration can serve as a sensor signal to monitor the sterilization efficiency [10, 11]. Nonetheless, for industrial standards, additional microbiological challenge test routines, such as end-point test and count-reduction test, are necessary for validation [12]. A reliably functioning spore-based biosensor might enable the combination of both, the standard microbiological tests and H_2O_2 monitoring by chemical gas sensors.

On the other hand, for developing a spore-based biosensor for sterilization processes the immobilization of spores is the most challenging aspect in order to ensure its reliability and reproducibility. Organosilanes have been used previously to functionalize glass substrates to provide moieties suitable for covalent attachment of spores [13, 14]. They are a versatile option as they promote the attachment of molecules through their

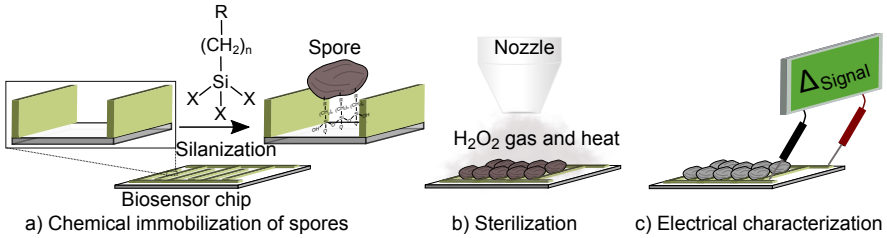

Fig. 8.2: Principle of those spore-based biosensor. a) The spores are chemically immobilized onto the sensor substrate. b) Then, the spore-based biosensor is sterilized with H_2O_2 and heat and c) finally due to the sterilization process, the morphology of the spores is compromised and this causes a change in the sensor signal.

terminal reactive groups (e.g., amines) and show likewise self-assembly behavior [15, 16]. Generally, the silanization process (organosilane formation on a surface) involves four phases: hydrolysis, condensation, hydrogen bond formation and curing [17, 18]. In the first phase, the organosilane groups are hydrolyzed to form highly reactive silanols (Si−OH). During the second phase, the silanols undergo condensation to form siloxanes (Si−O−Si) over the surface. In the third phase, the hydroxyl groups (OH) from the surface interact with the hydrolyzed organosilanes via hydrogen bonding. In the last phase, the silicon of the organosilane and the silicon of the surface are covalently bonded with the associated loss of water molecules by curing.

In the present work, two biosensor substrates (SiO_2, Pt) are functionalized with the organosilane 3-aminopropyltriethoxysilane (APTES) and characterized by means of atomic force microscopy, contact angle measurements and microbiological evaluation tests for the immobilization of *Bacillus atrophaeus* spores (DSM 675). Furthermore, the influence of the silane layer on the biosensors' signal is investigated by means of impedance spectroscopy measurements.

8.3 Experimental

8.3.1 Materials

The following chemicals have been used for the surface functionalization and the microbiological methods: APTES (98% v/v), toluene (99% v/v), ethanol (99% v/v), acetone (99% v/v), isopropanol (99% v/v), Tween® 80 were obtained from Sigma-Aldrich. Plate-count agar (PCA), Ringer solution tablets and manganese (II) sulphate monohydrate were obtained from Merck Millipore. Dry meat extract and peptone from meat were purchased from VWR.

8.3.2 Fabrication of the silicon oxide (SiO_2), platinum (Pt) substrates and sensors

SiO_2 substrates

As initial material a boron-doped silicon wafer (ρ = 1-10 Ω cm, <100>) was chosen with 30 nm of SiO_2 thermally grown by dry oxidation at 1000 °C for 30 min. For the

further functionalization and characterizations, the wafer was diced into 10 x 10 mm^2 pieces and cleaned for 5 min sequentially in ultrasonic bath with acetone, isopropanol and deionized (DI) water, respectively.

Pt substrates

The platinum substrates were fabricated (to characterize the sensor electrode material) as follows: 10 nm of Ti and 100 nm of Pt were deposited on a glass wafer (Borofloat® 33, Schott, Germany) with an e-beam evaporation process (Univex 350, Leybold). In addition, the wafer was diced into 10 x 10 mm^2 pieces and cleaned for 5 min sequentially in ultrasonic bath with acetone, isopropanol and deionized (DI) water.

Sensor fabrication

For the sensor fabrication conventional photolithography methods were applied. The fabrication steps are summarized in Fig. 8.3. In a first step, titanium and platinum were deposited on a glass wafer by an e-beam evaporation process. The thicknesses of these metal layers were chosen as 10 nm and 100 nm, respectively. A negative photoresist AZ 2020 nLOF was applied as masking layer for the subsequent reactive ion-etching (RIE) process. The lithography mask applied to pattern the photoresist layer defines the IDE structures with a finger width and gap of 5 μm. A total number of 614 electrode fingers and a length of 3.25 mm is resulting in a sensing area of about 20 mm^2. The metal layers were patterned by a reactive ion-etching process (RIE, Plasmalab 100, Oxford Instruments plc, United Kingdom) (Fig. 8.3 e)). Oxygen plasma was applied to remove the photoresist masking layer (Fig. 8.3 f)). A SU-8 wall was fabricated to enable a precise immobilization of microbiological samples on the IDE (Fig. 8.3 g)). After these fabrication steps the wafer was diced into single chips size of 5×10 mm^2. The single sensors were cleaned in acetone, isopropanol and DI water prior to further characterization and functionalization procedures.

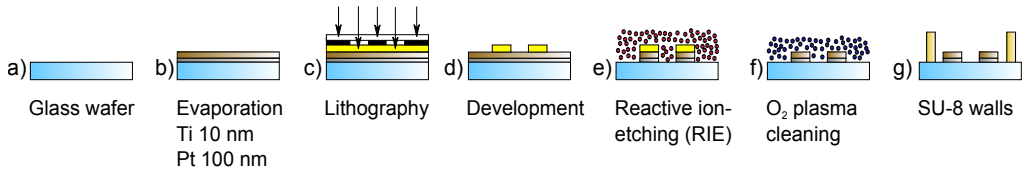

Fig. 8.3: Schematic view of the sensor fabrication steps: a) cleaned glass wafer; b) deposition of the electrode materials; c-d) structuring of a photoresist etching mask; e) transfer of the electrode pattern by reactive ion-etching; f) removal of photoresist mask; g) SU-8 walls to define the sensor-active regions with immobilized spores onto the interdigitated electrodes.

8.3.3 Surface functionalization

Pt, SiO_2 substrates and the sensors were silanized with a modified protocol for the immobilization of bacterial spores developed in [13].

Hydroxylation

The mentioned substrates and sensors were firstly cleaned to remove organic contaminants in a series of ultrasonic baths for 5 min for each step in acetone, isopropanol and DI water, respectively. Subsequently, their surface was activated with hydroxyl groups (hydroxylation) by oxygen plasma treatment (Femto PCCE, Diener electronic GmbH + Co. KG) at 100 W for 2 min.

APTES

For the silanization with APTES the drop-casting method was applied for all substrates and sensors. A solution of 1% APTES in toluene was pipetted onto the surfaces and incubated for 1 h. In order to avoid unwanted reactions (e.g., polymerization) from the organosilane under atmosphere conditions, the silanization has been performed in a glove box under nitrogen atmosphere.

The excess of APTES was washed out from the substrates and sensors with a series of ultrasonic baths in toluene and ethanol for 5 min each step. At the end, a curing process was performed to increase stability of the organosilanes by cross-linking of the silane molecules. The substrates and the sensors were cured at 110 °C for 1 h.

8.3.4 Physical characterization of the SiO_2 and Pt substrates

Contact angle measurements

Contact angle measurements on all substrates were conducted to demonstrate the successful surface functionalization. Therefore, the water contact angles were measured before and after the silanization process. The optical contact angle system OCA (Dataphysics, Germany) was used for the measurements performed at room temperature and the data were analyzed with the software SCA 20.

Atomic force microscopy

The morphology and topology of the samples were analyzed with a BioMat Workstation (JPK Instruments, Germany). The surface roughness was chosen to quantify these analyses. The scans ($2\times2\ \mu m^2$) were performed in tapping mode at 512 pixels per line, scanning at 0.2–0.4 Hz under ambient conditions. Silicon cantilevers (Arrow NCR, NanoWorld AG, Switzerland) with a spring constant of 42 $N\,m^{-1}$ and resonant frequency of 285 kHz were used.

Scanning electron microscopy

Surface characterizations of the functionalized sensor surface have been conducted on a Jeol JSM-7800F (Japan) scanning electron microscope.

Ellipsometry

The thickness of the APTES layer was characterized by spectroscopic nulling ellipsometry (EP3, Accurion GmbH, Germany). The angle of incidence used was 65° over a wavelength range of 360–1002 nm.

8.3.5 Microbiological methods

Bacterial culture, sporulation and spore purification

The strain of *Bacillus atrophaeus* (DSM 675) was purchased from IVV Fraunhofer, Germany. All procedures were performed aseptically under a laminar flow hood. Bacterial culture, sporulation and spore purification were carried out as stated in [13]. *B. atrophaeus* cells were grown at 30 °C in 10 ml of complex medium (3 $g\,l^{-1}$ meat extract dry, 5 $g\,l^{-1}$ peptone) for 24 h. The sporulation was initiated by inoculation of all cells in 200 ml of freshly complex medium with 10 $mg\,l^{-1}$ $MnSO_4$ and an incubation at 30 °C for 7 days. After the incubation, the spores were harvested by centrifugation at 4,000 rpm (A-4-81; Centrifuge 5810R, Eppendorf, Germany) at 20 °C and then resuspended in Ringer solution with 0.01% Tween® 80. After this, the spores were washed at least five times in Ringer solution with 0.01% Tween® 80 and three times in DI water. Subsequently, the spores were pasteurized in a water bath at 80 °C for 20 min, centrifuged and resuspended in DI water. The spore suspension was free of vegetative cells ($> 95\%$). The spore concentration was determined by serial dilutions and plating, resulting in a final concentration of 10^8 $cfu\,ml^{-1}$.

Microbiological evaluation

In order to evaluate the efficiency of the silanization process, the spore recovery method, serial dilutions and spread-plate methods were utilized [13]. For the spore recovery, 10 μl of the main spore suspension of *B. atrophaeus* were inoculated onto different silanized and non-silanized surfaces and dried under a laminar flow hood for 60 min. The immobilized spores were recovered from the surfaces by resuspending them in 10 ml of Ringer solution with 0.01% Tween® 80 and placing them in ultrasonic bath for 10 min. After that, each spore suspension was diluted by serial dilutions, spread-plated on PCA and cultivated at 30 °C for 24 h. The colony forming units (cfu) were counted and a final cell concentration ($cfu\,ml^{-1}$) of the recovered spores was obtained (N_s). The number of spores of the different solutions was compared to the total cell concentration ($cfu\,ml^{-1}$) found in the main spore suspension (N_t). As a result, the ratio (r) between recovered spores (N_s) and the total number of spores from the main suspension (N_t) can be determined by:

$$r = \left(\frac{N_s}{N_t}\right) \cdot 100 \tag{8.1}$$

In Eq. (8.1), the lower the N_s concentration, the better the silanization process (i.e., more spores remained on the substrates or sensors).

8.3.6 Electrical characterization of the sensors

In order to characterize the electrical parameters of the silane layer on the sensors, impedance measurements were performed. All measurements were conducted on a point-probe station with a precision LCR-meter (E4980A, Agilent Technologies, United States). An excitation voltage of 0.02 V without a DC (direct current) bias was applied. The impedance characteristics were monitored over a frequency range between 200 Hz and 200 kHz. In order to avoid effects of air humidity- and temperature variations the measurements were conducted in a vacuum chamber.

8.4 Results and discussions

8.4.1 Physical characterization of APTES on SiO_2 and Pt substrates

Contact angle measurements

Water contact angle measurements were performed to characterize the hydrophilicity or hydrophobicity of the SiO_2 and Pt substrates after silanization with APTES as shown in Tab. 8.1. Control chips were used as a reference and cleaned in a series of ultrasonic baths for 5 min for each step in acetone, isopropanol and DI water, respectively. For SiO_2, a contact angle of 73° was obtained with APTES. This value is in good agreement with amino-terminated films from literature [19, 20]. Furthermore, the contact angle of Pt after APTES was 98°. Water contact angles after silanization on Pt surfaces are similar than that from SiO_2 [21]. In our experiment, the contact angle on Pt was more hydrophobic in comparison with that of SiO_2. This difference may come from the lack of oxide species produced after O_2 plasma (i.e., the less oxide species, the less OH groups available), since no significant differences were found between contact angles before and after O_2 plasma treatments for Pt (data not shown). Therefore, the silanization process might be unfavorably affected for Pt, probably indicating alkyl fragments exposed at the surface [15]. Moreover, the outermost layer of the spore coat (spore surface) is mainly formed from proteins, including CotB, CotC, CotG and CotZ [22, 23]. APTES may bind to these proteins by their N- or C-termini producing a covalent bond by cross-linking due to the nature of the spore deposition (i.e., a droplet of DI water with spores is let dried at the sensor surface). In addition, non-covalent interactions (hydrophobic forces) between the alkyl fragments and the spore's coat may be involved due to the orientation of the silane layer.

Tab. 8.1: Contact angle measurements and roughness of Pt and SiO_2 substrates silanized with APTES.

Material	Silane	Contact angle (°)	Roughness (R_q)(nm)
SiO_2	Control	47	0.11
	APTES	73	0.86
Pt	Control	72	2.72
	APTES	98	6.57

Atomic force microscopy and ellipsometry

The morphology and roughness (R_q) of the silanized SiO_2 and Pt substrates were further characterized with AFM and ellipsometry. Representative images of their surface topography for APTES are shown in Fig. 8.4. Fig. 8.4 a) and 8.4 c) were taken as a reference and were cleaned as described in Sec. 8.3.3. The increase of roughness (R_q) for SiO_2 (0.11 nm compared to 0.86 nm) and Pt (2.72 nm compared to 6.57 nm) silanized with APTES suggest the presence of an organic layer as it can be also seen from Tab. 8.1. In addition, the increases of roughness can be attributed to domains or agglomeration of APTES molecules on the surface of SiO_2 (Fig. 8.4 b)) and Pt (Fig. 8.4 d)). These domain diameters for SiO_2 are in the range from 5 nm to 10 nm and for Pt from 5 nm to 30 nm. Furthermore, the APTES thickness obtained with ellipsometry was 6.1±1.15 nm.

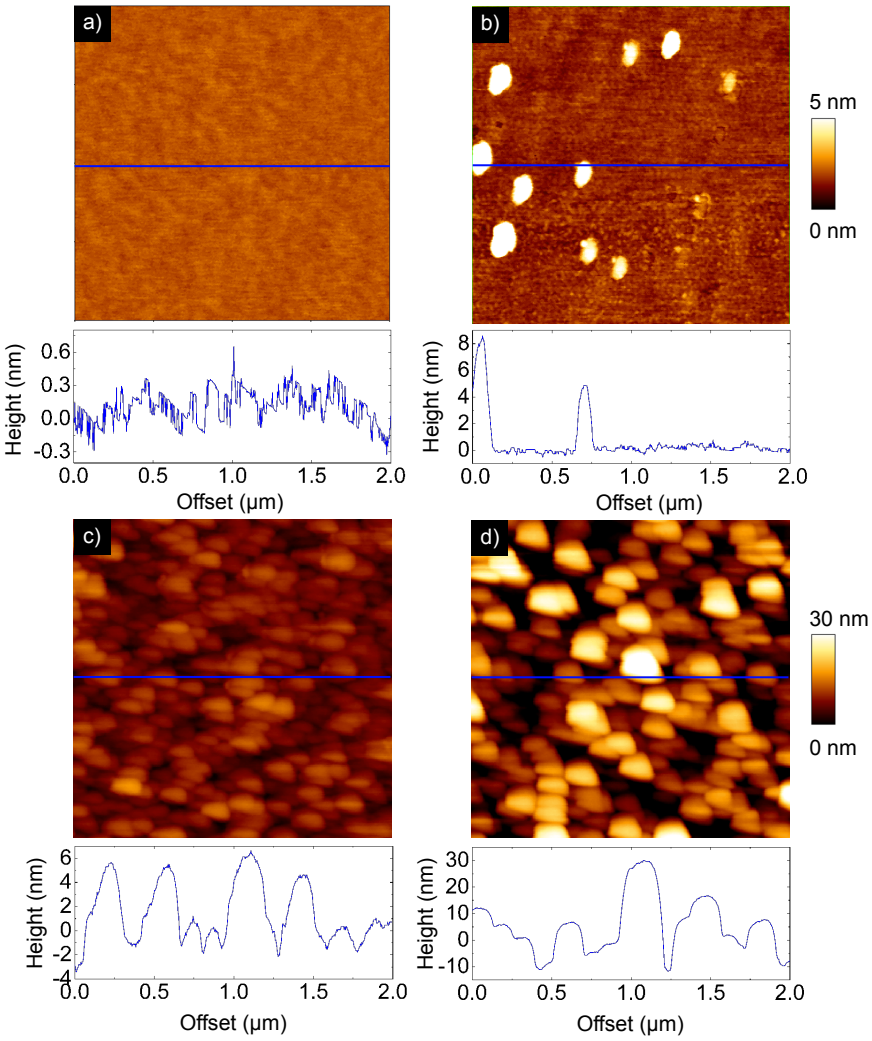

Fig. 8.4: Atomic force microscopy images 2 x 2 μm^2 (height) of the silanization on SiO_2 and Pt substrates with APTES. a) Control SiO_2; b) SiO_2 with APTES, c) control Pt; d) Pt with APTES.

8.4.2 Microbiological evaluation of the SiO_2, Pt substrates and sensors

The results of the immobilization study of spores with APTES on SiO_2, Pt substrates and interdigitated sensor chips are depicted in Fig. 8.5. The control substrates were cleaned as mentioned in Sec. 8.3.3 without further silanization. For SiO_2 and Pt no significant difference could be observed between substrates with a spore recovery of 32% and 33%, respectively. The opposite case was found for the sensor with a spore recovery of 78%. There are several factors that can affect the adhesion strength between the spores and the substrates such as hydrophobic interactions, surface topography or spore's surface [24]. In this case, no difference could be observed between a relatively smooth (SiO_2) and a slightly rough (Pt) surface. However, a combination of both surfaces and a change from a 2D surface to a 3D surface (sensor) showed a substantial decrease of the spore adhesion. Since both materials alone remained almost the same, this may suggest that the decrease of the spore adhesion may be affected by the 3D geometry of the IDEs. Future studies should address this influence in more detail. Moreover, the results exhibit that the best immobilization of spores could be achieved on APTES-functionalized SiO_2 surfaces, as only 2% of the spores could be recovered. In comparison to that of the Pt substrate, 23% of the spores were found in the solution. A reason for the reduced or lower adhesion could be the higher hydrophobicity and roughness of the surface (Sec. 8.4.1) compared to that of the SiO_2 substrates. In combination with the applied method to evaluate the immobilization, the bonding between APTES layer and the Pt surface might be less stable in the buffer solution as for the SiO_2 substrate [25]. As a result, the silane molecules probably detach from the Pt surface at the mentioned conditions. Furthermore, for the sensors, 36% of the spores were decoupled. Since the sensor consists mainly of a combination of both materials (glass (SiO_2) and Pt), it is probably expected that the percentage of detached spores would be between those values. However, the geometry of the IDE structures may play as well an important role in the immobilization of spores due to the spore recovery method.

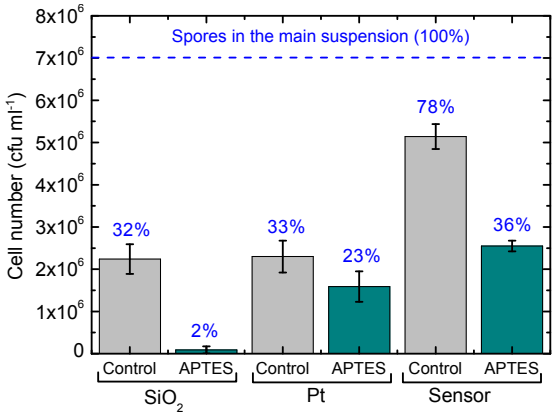

Fig. 8.5: Microbiological evaluation of the immobilization of the spores with APTES on SiO_2, Pt and interdigitated sensor chips. The error bars indicate the standard deviations of four samples for each group.

This may be illustrated in Fig. 8.6; Fig. 8.6 a-c) shows SiO_2, Pt and the biosensor substrates, respectively. In addition, in Fig. 8.6 d-f) spores immobilized on their respective surfaces can be observed. Finally, after the spore recovery method, the spores are detached (Fig. 8.6 g-i)), so they can be found in their respective spore suspension. One of the main differences between the substrates and the biosensor chips is the 3D structure obtained from the IDEs. The spores seem to attach better to the planar surfaces (substrates) compared to their 3D counterparts on the sensor structure. This result can be observed for all the surfaces from the control groups (Fig. 8.5). Therefore, future investigations will explicitly study the influence of the 3D geometry of the IDEs (e.g., thickness of Pt electrodes) with respect to the *B. atrophaeus* attachment on the sensor surface. Nevertheless, APTES has been shown to enhance the attachment of spores for all the investigated substrates distinctly.

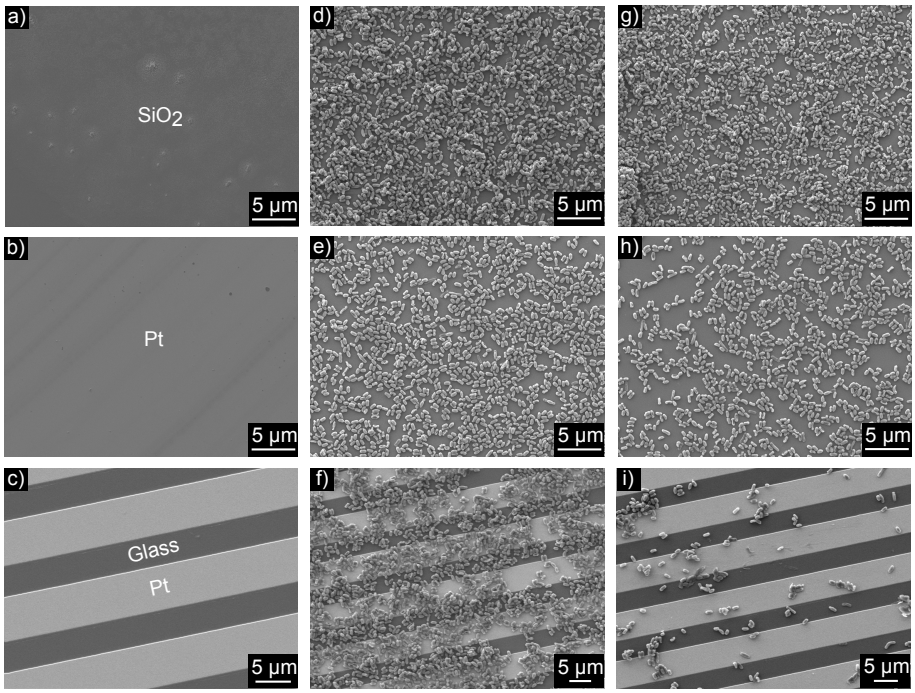

Fig. 8.6: Scanning electron microscope images of the spore recovery method. APTES-functionalized surfaces for: a) SiO_2; b) Pt; and c) biosensor chips with interdigitated electrodes. Immobilized spores on their respective surfaces (d-f). Remaining spores on the sensor surface after the spore recovery method (g-i).

8.4.3 Impedance measurements of the sensors with APTES

To study the influence of APTES on the sensor signal, impedance characterizations were performed before and after the sensor functionalization. As a base line the newly produced and cleaned sensor structures were investigated under vacuum conditions to exclude external disturbing factors such as variations of air humidity and temperature. The resulting impedance signal depicts a capacitive sensor behavior, negative slope of the impedance plot and a phase of about –90° (Fig. 8.7 (black plots) in impedance (top)

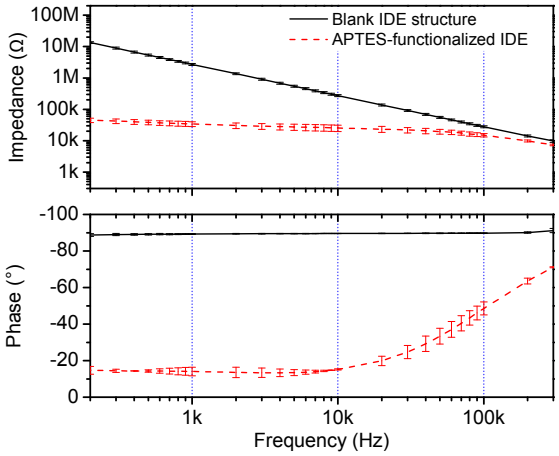

Fig. 8.7: Bode plots of interdigitated electrodes before (black line) and after functionalization with APTES (red-dashed line). The lines represent the mean values of three independent sensors and the error bars indicate the standard deviations.

and phase diagram (bottom)). The Bode diagram shows the mean and standard deviation of three independent IDE structures. After functionalization of the sensor surface with APTES the impedance signal was recorded again (Fig. 8.7). In comparison to the impedance plot of a non-functionalized sensor, it can be observed that the sensor impedance decreased, and a resistive characteristic is present (phase of about –20°). This increase in electrical conductivity can be interpreted by different hypotheses. For instance, the APTES molecules can serve as electron donor on the surface to be functionalized and enhance thereby the electrical conductivity [26–29]. Another possible assumption is that the permittivity between the electrode fingers changes due to the adsorbed APTES monolayer as investigated in [30], whereby the capacitive characteristics are changing at frequencies above 10 kHz. Furthermore, the improved conductivity could also be related to electron tunneling effects occurring in the self-assembled monolayer, as discussed by [31, 32]. The change of electrical properties of the APTES functionalization combined with the microbiological spores at the sensor surface is subject of the ongoing research. Succeeding experiments will focus on signal changes of the immobilized spores as well as in combination with the sterilization process at various process conditions such as different H_2O_2 concentrations.

8.5 Conclusions

In this work, the surface functionalization of transducer chips for biosensors with the organosilane APTES has been investigated. The immobilization of bacterial spores was studied on different materials to be applied in sensor fabrication, namely silicon oxide (SiO_2), platinum (Pt) and the combination on sensor level consisting of glass (SiO_2) and platinum. In a first attempt, the silanization has been proven by analyzing the wettability by means of contact angle measurements. These measurements have demonstrated successful surface modifications. Furthermore, AFM and ellipsometric

analyses have been conducted to study the surface morphology as well as the resulting change in surface roughness (R_q) supporting the successful coupling of APTES.

Moreover, a microbiological evaluation of the immobilization of spores on the substrates (SiO_2, Pt) and sensors with APTES was performed. SiO_2 showed the best immobilization of the spores. In addition, the immobilization of spores on Pt was negatively affected by the high hydrophobicity and roughness of the silane layer. Furthermore, the detachment of the spores was influenced by the geometry of the IDEs as well as by the silanization on the mixture of both investigated materials.

Additionally, electrochemical studies of the sensors have been realized under vacuum conditions. The electrochemical measurements have revealed a change in the impedance spectrum after silanization with APTES. The functionalized sensors demonstrated resistive behavior at low frequencies (200 Hz–10 kHz). In future, electrochemical characterizations combining the APTES functionalization together with the microbiological spores on the sensor surface will be performed.

Acknowledgments

The project was financially supported by the Federal Ministry of Education and Research, Germany, Project: "ImpediPack" (Fund. No.: 03FH012I3). The authors are gratefully thankful to Prof. Dr. P. Siegert and Prof. Dr. J. Bongaerts for access to the microbiology laboratory to conduct microbiological evaluations, Prof. Dr. T. Mang for access to the instrument for contact angle measurements, H. Iken for assisting the fabrication of the spore-based biosensors, D. Rolka for the scanning electron microscopy measurements and L. Breuer for the ellipsometry measurements.

References

[1] W. L. Nicholson, N. Munakata, G. Horneck, H. J. Melosh, and P. Setlow. "Resistance of *Bacillus* endospores to extreme terrestrial and extraterrestrial environments". *Microbiology and Molecular Biology Reviews* 64 (2000), 548–572.

[2] B. Setlow, C. A. Loshon, P. C. Genest, A. E. Cowan, C. A. Setlow, and P. Setlow. "Mechanisms of killing spores of *Bacillus subtilis* by acid, alkali and ethanol". *Journal of Applied Microbiology* 92 (2002), 362–375.

[3] P. Setlow. "Spores of *Bacillus subtilis*: their resistance to and killing by radiation, heat and chemicals". *Journal of Applied Microbiology* 101 (2006), 514–525.

[4] D. G. Allison. "A review: taking the sterile out of sterility". *Journal of Applied Microbiology* 87 (1999), 789–793.

[5] N. Kumar, G. Thakur, H. V. Raghu, N. Singh, P. Sharma, V. K. Singh, A. Khan, M. Balhara, L. R. Avinash, S. Kouser, N. Tehri, R. Gopaul, and S. Arora. "Bacterial spore based biosensor for detection of contaminants in milk". *Journal of Food Processing and Technology* 04 (2013), 1–6.

[6] R. M. La Ragione, G. Casula, S. M. Cutting, and M. J. Woodward. "*Bacillus subtilis* spores competitively exclude *Escherichia coli* O78:K80 in poultry". *Veterinary Microbiology* 79 (2001), 133–142.

[7] M. L. López Rodriguez, C. Benimeli, R. E. Madrid, and C. E. Giacomelli. "A simple *Streptomyces* spore-based impedimetric biosensor to detect lindane pesticide". *Sensors and Actuators B: Chemical* 207 (2015), 447–454.

[8] B. Rotman and M. A. Cote. "Application of a real-time biosensor to detect bacteria in platelet concentrates". *Biochemical and Biophysical Research Communications* 300 (2003), 197–200.

[9] J. Oberländer, A. Bromm, L. Wendeler, H. Iken, M. P. Durán, A. Greeff, P. Kirchner, M. Keusgen, and M. J. Schöning. "Towards a biosensor to monitor the sterilization efficiency of aseptic filling machines". *Physica Status Solidi A* 212 (2015), 1299–1305.

[10] P. Kirchner, Y. A. Ng, H. Spelthahn, A. Schneider, H. Henkel, P. Friedrich, J. Kolstad, J. Berger, M. Keusgen, and M. J. Schöning. "Gas sensor investigation based on a catalytically activated thin-film thermopile for H_2O_2 detection". *Physica Status Solidi A* 207 (2010), 787–792.

[11] P. Kirchner, J. Oberländer, H.-P. Suso, G. Rysstad, M. Keusgen, and M. J. Schöning. "Monitoring the microbicidal effectiveness of gaseous hydrogen peroxide in sterilization processes by means of a calorimetric gas sensor". *Food Control* 31 (2013), 530–538.

[12] Verband Deutscher Maschinen- und Anlagenbau e.V. "Code of practice: filling machines of VDMA hygiene class V: testing the effectiveness of packaging sterilization devices". *VDMA-Fachverbandsschriften* 6 (2008), 1–16.

[13] J. Arreola, M. Mätzkow, M. P. Durán, A. Greeff, M. Keusgen, and M. J. Schöning. "Optimization of the immobilization of bacterial spores on glass substrates with organosilanes". *Physica Status Solidi A* 213 (2016), 1463–1470.

[14] T. J. Park, K.-B. Lee, S. J. Lee, J. P. Park, Z.-W. Lee, S.-K. Choi, H.-C. Jung, J.-G. Pan, S. Y. Lee, and I. S. Choi. "Micropatterns of spores displaying heterologous proteins". *Journal of the American Chemical Society* 126 (2004), 10512–10513.

[15] R. G. Acres, A. V. Ellis, J. Alvino, C. E. Lenahan, D. A. Khodakov, G. F. Metha, and G. G. Andersson. "Molecular structure of 3-aminopropyltriethoxysilane layers formed on silanol-terminated silicon surfaces". *The Journal of Physical Chemistry C* 116 (2012), 6289–6297.

[16] J. Landoulsi, M. J. Genet, K. El Kirat, C. Richard, S. Pulvin, and P. G. Rouxhet. "Silanization with APTES for controlling the interactions between stainless steel and biocomponents: reality vs. expectation". In: *Biomaterials*. Ed. by R. Pignatello. Rijeka, Croatia: InTech, 2011, 99–126.

[17] B. Arkles. "Hydrophobicity, Hydrophilicity and Silanes". *Paint and Coatings Industry* 22 (2006), 114–125.

[18] C. M. Halliwell and A. E. G. Cass. "A factorial analysis of silanization conditions for the immobilization of oligonucleotides on glass surfaces". *Analytical Chemistry* 73 (2001), 2476–2483.

[19] S. E. Asenath and W. Chen. "How to prevent the loss of surface functionality derived from aminosilanes". *Langmuir* 24 (2008), 12405–12409.

[20] J. A. Howarter and J. P. Youngblood. "Optimization of silica silanization by 3-aminopropyltriethoxysilane". *Langmuir* 22 (2006), 11142–11147.

[21] J. C. Chang and B. C. Wheeler. "Pattern technologies for structuring neuronal networks on MEAs". In: *Advances in Network Electrophysiology*. Ed. by M. Taketani and M. Baudry. Boston: Springer Science and Business Media, 2006, 153–189.

[22] A. Iwanicki, I. Piątek, M. Stasiłojć, A. Grela, T. Lęga, M. Obuchowski, and K. Hinc. "A system of vectors for *Bacillus subtilis* spore surface display". *Microbial Cell Factories* 13 (2014), 30–38.

[23] J.-G. Pan, S.-K. Choi, H.-C. Jung, and E.-J. Kim. "Display of native proteins on *Bacillus subtilis* spores". *FEMS Microbiology Letters* 358 (2014), 209–217.

[24] C. Faille, C. Jullien, F. Fontaine, M.-N. Bellon-Fontaine, C. Slomianny, and T. Benezech. "Adhesion of *Bacillus* spores and *Escherichia coli* cells to inert surfaces: Role of surface hydrophobicity". *Canadian Journal of Microbiology* 48 (2002), 728–738.

[25] M. Zhu, M. Z. Lerum, and W. Chen. "How to prepare reproducible, homogeneous, and hydrolytically stable aminosilane-derived layers on silica". *Langmuir* 28 (2012), 416–423.

[26] J. Kong and H. Dai. "Full and modulated chemical gating of individual carbon nanotubes by organic amine compounds". *Journal of Physical Chemistry B* 105 (2001), 2890–2893.

[27] J. Li and N. Wu. *Biosensors Based on Nanomaterials and Nanodevices*. Boca Raton, FL, USA: CRC Press, 2013.

[28] M. Song, J.-W. Kang, D.-H. Kim, J.-D. Kwon, S.-G. Park, S. Nam, S. Jo, S. Yoon Ryu, and C. Su Kim. "Self-assembled monolayer as an interfacial modification material for highly efficient and air-stable inverted organic solar cells". *Applied Physics Letters* 102 (2013), 143303-1–143303-5.

[29] T. H. Tran, J.-W. Lee, K. Lee, Y. D. Lee, and B.-K. Ju. "The gas sensing properties of single-walled carbon nanotubes deposited on an aminosilane monolayer". *Sensors and Actuators B: Chemical* 129 (2008), 67–71.

[30] A. Markov, K. Greben, D. Mayer, A. Offenhäusser, and R. Wördenweber. "In situ analysis of the growth and dielectric properties of organic self-assembled monolayers: a way to tailor organic layers for electronic applications". *ACS Applied Materials and Interfaces* 8 (2016), 16451–16456.

[31] S. Casalini, C. A. Bortolotti, F. Leonardi, and F. Biscarini. "Self-assembled monolayers in organic electronics". *Chemical Society Reviews* 46 (2017), 40–71.

[32] C. S. S. Sangeeth, A. Wan, and C. A. Nijhuis. "Equivalent circuits of a self-assembled monolayer-based tunnel junction determined by impedance spectroscopy". *Journal of the American Chemical Society* 136 (2014), 11134–11144.

9 Spore-based biosensor to monitor the microbicidal efficacy of gaseous hydrogen peroxide sterilization processes (*Biosensors and Bioelectronics*, 104 (2018), 87–94)

J. Oberländer, M. Mayer, A. Greeff, M. Keusgen, and M. J. Schöning

Published in: *Biosensors and Bioelectronics,* Vol. 104 (2018), 87–94.

Submitted: 2017-10-19; Accepted: 2017-12-26; Published: 2018-05-01

9.1 Abstract

In this work, a spore-based biosensor is evaluated to monitor the microbicidal efficacy of sterilization processes applying gaseous hydrogen peroxide (H_2O_2). The sensor is based on interdigitated electrode structures (IDEs) that have been fabricated by means of thin-film technologies. Impedimetric measurements are applied to study the effect of sterilization process on spores of *Bacillus atrophaeus*. This resilient microorganism is commonly used in industry to proof the sterilization efficiency. The sensor measurements are accompanied by conventional microbiological challenge tests, as well as morphological characterizations with scanning electron microscopy (SEM) and transmission electron microscopy (TEM). The sensor measurements are correlated with the microbiological test routines. In both methods, namely the sensor-based and microbiological one, a tailing effect has been observed. The results are evaluated and discussed in a three-dimensional calibration plot demonstrating the sensor's suitability to enable a rapid process decision in terms of a successfully performed sterilization.

9.2 Introduction

Aseptic processing and filling of sensitive food products is a common technology for dairy products or juices. Main advantages of aseptic processing are the extended shelf-life, the product distribution at ambient temperatures and protection of nutritional contents [1]. One key process within this technology represents the sterilization of the packages to be filled with separately sterilized goods. In recent years, the package sterilization with vapor-phase hydrogen peroxide (H_2O_2) at elevated gas temperature has been established [2, 3]. Hydrogen peroxide is known as a strong oxidizer and in combination with heat it possesses microbicidal and sporicidal activity [4, 5]. During the sterilization process at elevated temperature, H_2O_2 decomposes to oxygen and water vapor with intermediates of hydroxyl and hydroperoxyl radicals ($HO^{\bullet}$, $HO_2{}^{\bullet}$) and further reactive species of oxygen and hydrogen, such as $O_2{}^{-}$, $O^{\bullet}$ and $H^{\bullet}$ [6]. Even though, the process of the lethal cell and spore damage is not clarified in detail yet, the generated radicals are proposed to be one of the species to be involved in deoxyribonucleic acid (DNA) damage of spores or bacteria [7]. In case of the more resilient spores, the protecting spore coat and membranes need first to be penetrated [8–10]. The lethal damage of spores by applying H_2O_2 vapor at elevated temperature might be a combined process. In a first step, the molecules of the spore coat are oxidized and heat starts the degradation of proteins [11, 12]. In a next step, the protection mechanism of the DNA, small, acid-soluble proteins bound to the spore DNA, needs to be deactivated by oxidation [13–15]. Finally, the DNA and thereby the reproduction system can be oxidized and damaged irreversibly.

The state-of-the-art methods to evaluate the performance and efficiency of package sterilization processes are laborious and time-consuming microbiological challenge tests (count-reduction test or end-point test) [16–18]. Numerous techniques have been applied to reduce the effort and workload of these challenge tests. Nutrition media with colorimetric pH indicators, for example, have been developed to enable a fast true/false detection of outgrowing microbiological colonies [19]. A further method detects changes of the electrical properties of the growth medium; here, impedance measurements are performed on electrodes immersed into the medium. This technique can be differentiated either as direct or indirect method. The direct method detects directly the metabolic activity of microorganisms by conductivity changes in the growth medium. Metabolic conversions of weakly or uncharged nutrition into highly charged end-products are increasing the media conductivity. For example, the conversion of non-ionized glucose into two molecules of lactic acid increases the media conductivity [20]. The indirect method monitors the metabolic carbon dioxide CO_2 production of the microorganisms. The impedance electrodes are immersed into a potassium hydroxide (KOH) solution, which is in a sealed environment together with the culture medium. The increasing CO_2 concentration results in a conductance decrease of the KOH solution [21]. Both impedimetric detection methods are available in commercial cell analysis systems such as: BacTrac®, SY-Lab GmbH; R.A.B.I.T.®, Don Whitley Scientific Ltd.; Bactometer®, Vitek Systems, Biomérieux, Inc.; Malthus®, Malthus Instruments Ltd. etc. [22]. However, they are not able to monitor alterations on the spore morphology and the resulting spore death, induced by sterilization processes.

A first step into this direction was a recently introduced by an impedimetric sensor to directly monitor the sterilization efficiency by means of detecting the degradation of bacterial spores [23, 24]. This sensor is based on interdigitated electrode structures (IDEs) on which resilient microbiological organisms are immobilized, comparable to conventional challenge tests. Sensors based on interdigitated electrodes are commonly used to monitor chemical or biochemical processes in liquids. Examples are given in [25–28]. Those sensitive electrode structures have also been implemented in gaseous detection systems as well as for particle monitoring in air as described e.g., in [29–32]. In the present work, detailed studies on the development of a spore-based impedimetric biosensor system will be presented and discussed. Especially, investigations of the sensor signal behavior with regard to the sterilization parameters are in focus to implement a parametric calibration matrix describing the sterilization efficacy.

9.3 Materials and methods

9.3.1 Spore suspension, microbiological evaluation

The spore suspension was based on a strain of *Bacillus atrophaeus* (DSM 675) purchased from IVV Fraunhofer, Germany. The preparations of the spore suspension, as well as the sensor functionalization and microbiological reference tests, were performed aseptically under a laminar flow work bench. The spore suspensions were prepared and purified as explained previously [23, 33]. The purified spore suspensions were diluted in deionized (DI) water and stored at 4 °C. The load of the microbial spore suspension was adjusted to a colony count of $1 \cdot 10^9$ cfu ml^{-1} (cfu: colony forming unit). As reference test either the sensor chip itself or sample substrates of glass were investigated with microbiological challenging tests (as industrially applied). The sensors and glass samples were inoculated with an aliquot of 10 μl of spore suspension to achieve a final load of $1 \cdot 10^7$ cfu, which corresponds to conventional microbiological tests in industry. After sterilization process with gaseous hydrogen peroxide, the spores were recovered and resuspended in Ringer's solution with 0.01% Tween® 80 as surfactant combined with ultrasonic treatment for 10 min. The enumeration of the surviving colonies was performed by serial dilutions of the resulting suspensions and spread-plated on plate-count agar (PCA). After incubation time of 5 days at 30 °C the outgrown colonies could be counted. The logarithmic cycle reduction (LCR, see Eq. (9.1)) was determined by the initial number of spores per sample (N_0) and the number of outgrown colonies (N) after the sterilization process. The number of outgrown colonies was calculated by a weighted mean in accordance to [18, 34].

$$\mathrm{LCR} = \log\left(\frac{N_0}{N}\right) \tag{9.1}$$

9.3.2 Sensor fabrication

The investigated sensors were in-house fabricated by means of thin-film technologies. The fabrication procedure is schematically depicted in the supplemental information Fig. 9.8. As substrate a Borofloat® glass wafer (Schott GmbH, Germany) was chosen

with a thickness of 500 μm, which possesses reduced parasitic capacitances compared to conventional silicon wafers with necessary insulation layers. Electron beam evaporation was used to deposit the electrode materials (first layer: 10 nm chromium; second layer: 100 nm gold) on top of the glass wafers. Chromium was used as an adhesion promoter between glass and gold. The subsequent electrode pattern was transferred photolithographically into a spin-coated negative photoresist layer (AZ nLOF 2020, Merck KGaA, Germany). For that, a customized chromium glass mask with interdigitated electrodes was applied. The width and interspacing of the electrodes are designed to be 3 μm and 7 μm, respectively, each electrode finger has a length of 3.25 mm; a total number of 614 fingers captures an area of approximately 20 mm^2. The photoresist layer serves as an etching-mask for the following reactive ion-etching process (RIE, Plasmalab 100, Oxford Inc., UK). A gas mixture of argon at 10 sccm and oxygen at 15 sccm has been applied to transfer the electrode pattern into the metal layers. To finalize the RIE process the photoresist mask has been removed by oxygen plasma treatment. A further lithography process was applied to develop SU-8 walls to enable a defined immobilization of the spore suspension. The final wafer was then diced into single sensor chips of 5×10 mm^2 (a sensor chip without SU-8 walls is shown exemplarily in Fig. 9.1 b).

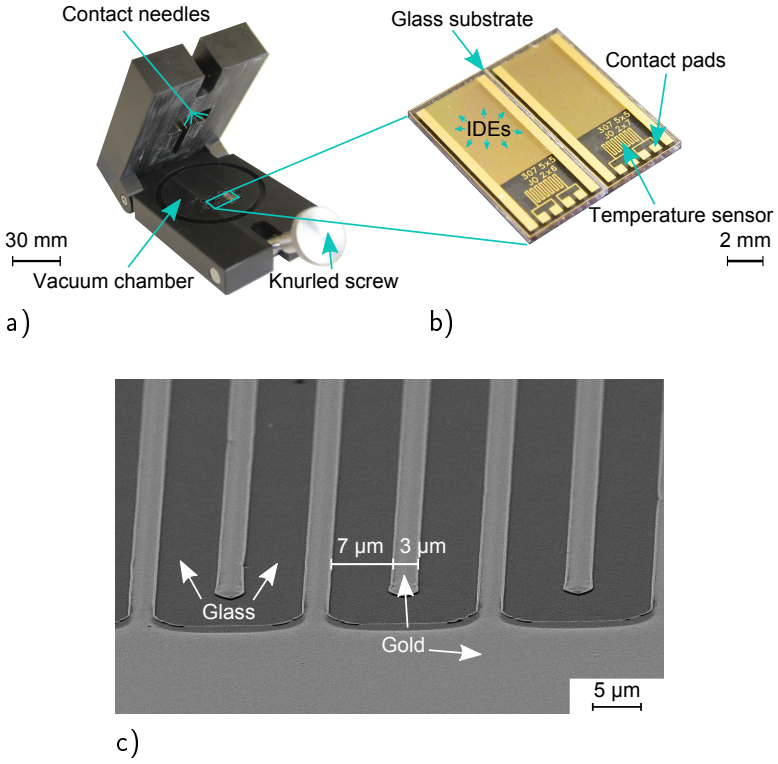

Fig. 9.1: Characterization set-up to evaluate the sterilization process by means of the developed biosensor: a) vacuum measurement chamber; b) differential set-up of two glass-based interdigitated electrodes (IDEs) and temperature sensors, serving as biosensor chip; c) SEM picture of the developed IDE gold structures. Side walls on the electrodes can be recognized caused by the RIE process.

9.3.3 Sensor characterization

The sensor fabrication as well as the microbiological spores have been evaluated by means of scanning electron microscopy (SEM) on a Jeol JSM-7800F. The spores were additionally characterized by transmission electron microscopy (TEM) on a Zeiss Libra® 120.

The developed sensors were electrically investigated by impedance measurements. For all measurements the sensors were placed into a customized measurement chamber as shown in Fig. 9.1 a). The measurement chamber enables the defined connection of the single sensors. Moreover, to maintain a comparable measurement environment (humidity, temperature, pressure) a vacuum pump (Laboport N 86 KN.18, KNF Neuberger GmbH, Germany) was connected during the measurements, adjusting a pressure of 100 mbar (absolute) within the chamber. Gold-covered spring contacts were applied to guarantee a reproducible sensor connection. The spring contacts were connected externally to an Agilent precision LCR-meter (E4980A). The excitation voltage was set to 20 mV with a 0 V DC (direct current) bias. The impedance sweeps were performed in a frequency range between 200 Hz and 200 kHz. Detailed sensor evaluations were performed at a fixed frequency of 3 kHz. Four independent sensors were measured after each step of handling: first, measurement was performed of the blank IDE structures; second, after the immobilization of the spore suspension or drying of pure, deionized (DI) water as reference on the IDE surface; and finally, after the sterilization process with gaseous H_2O_2.

9.3.4 Sterilization process

In this work, all sterilization processes were carried out on a sterilization test-rig that is already described in [35, 36].The process is adapted to the sterilization processes of industrial aseptic filling machines applying gaseous hydrogen peroxide. The test-rig uses pressurized air as carrier gas, which is controlled by a flow meter and regulation valve. Two piston pumps are used as dosage systems for H_2O_2 solution (Interox® 35% w/w, Solvay S.A., Belgium) and for DI water; both media are fed into the carrier gas and can be controlled independently. An evaporation unit consisting of two heating elements is used to transfer the mixture into the gas phase. The power of the heating elements is controlled by the medium temperature at the evaporation unit outlet. The sensors and microbiological samples are exposed to the sterilization processes via a time-controlled hydraulic slide in a defined distance to the gas nozzle of the test-rig, comparable to industrial sterilization processes of composite packages.

The process parameters are chosen according to actual decontamination cycles of aseptic composite packages for liquid food. The gas temperature has been adjusted to 240 °C at a constant air flow of 10 $m^3\,h^{-1}$. Different sterilization scenarios have been investigated by varying the H_2O_2 concentration between 0 and 8.3% v/v. The present H_2O_2 concentration has been logged in addition with one of our previously developed calorimetric H_2O_2 gas sensors [37–39]. The calorimetric gas sensor consists of a differential set-up of a catalytically active and a passive temperature sensor. The exothermal decomposition of H_2O_2 correlates with the present H_2O_2 concentration.

The exposure times of the sensors and microbiological samples are given in the results section.

9.4 Results and discussions

During the sterilization process, the H_2O_2 concentration has been monitored by an additional calorimetric gas sensor. The corresponding measurement plot is shown in Fig. 9.2, where the exposure moments of the biosensor/microbiological samples are indicated, too (see 1. exp. to 6. exp.). The upper part of the diagram represents the temperatures of the catalytically activated (catalyst Pt on Al_2O_3) and the passivated temperature sensor. The resulting H_2O_2 concentration is given in the lower part, determined by the temperature difference of the differential set-up with a sensor's sensitivity of 3.58 °C/(% v/v H_2O_2).

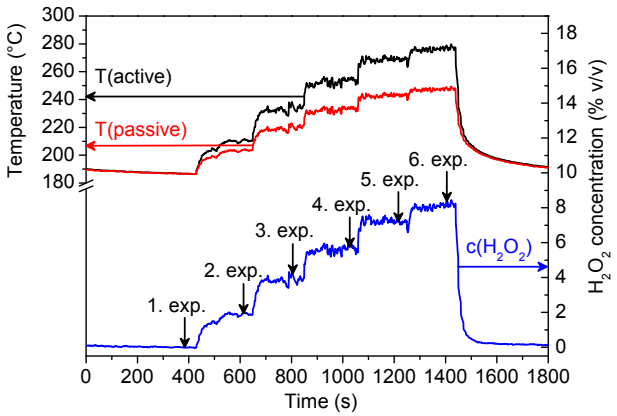

Fig. 9.2: Signal response of the calorimetric H_2O_2 gas sensor, to determine the prevailing H_2O_2 concentration during the subsequent biosensor and sample exposure. The upper part depicts the temperature plots of the calorimetric sensor set-up, one catalytically activated and one passivated. The lower part depicts the resulting H_2O_2 concentration and times of sensor/sample exposures (1. exp. to 6. exp.).

9.4.1 Microbiological kill rate study

As a reference tool to the biosensor-based evaluation (see Sec. 9.4.3), microbiological kill rate studies during the sterilization process were performed. The recovery rate of three non-sterilized samples per run was used to determine the initial load of the microbiological samples, i.e. the glass substrate and sensor chips, respectively (Fig. 9.3 a)), whereby an average value of $9.8 \cdot 10^6 \pm 4.6$ cfu per sample could be obtained. The load number is slightly lower as given in Sec. 9.3.1, which can be related to the applied recovery process: not all spores were resuspended into the solution, remaining spores have been observed on the samples. Nonetheless, the recovery rate can be determined to 98%, that represents an excellent value. The resulting average number has been taken into account to calculate the logarithmic cycle reduction (LCR) for the following experiments.

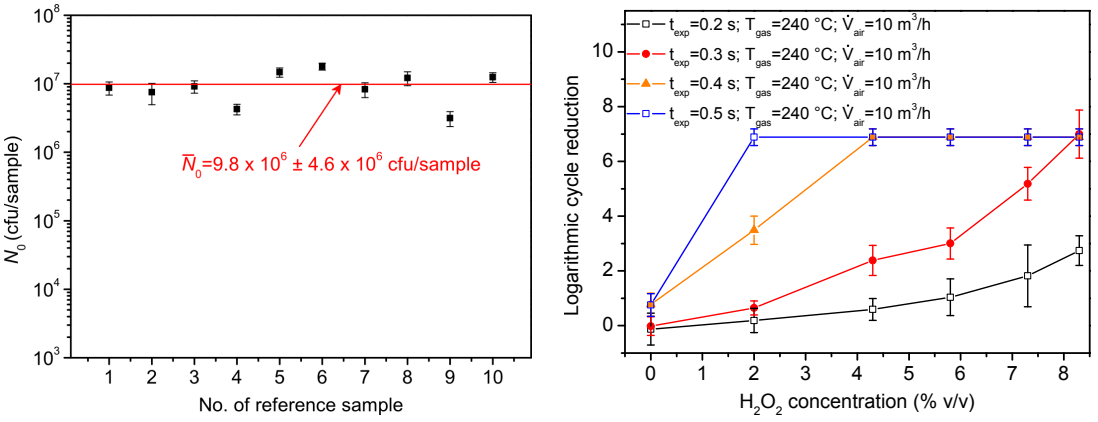

Fig. 9.3: a) Evaluation of the number of microorganisms recovered from reference samples. b) Logarithmic cycle reduction for different exposure times (between 0.2 s and 0.5 s) with varying concentrations (0–8.3% v/v) of gaseous H_2O_2.

In order to determine the dependency between the LCR and the present H_2O_2 concentration, in a first set of experiments the exposure time was varied between 0.2 s and 0.5 s (Fig. 9.3 b)). A correlation between the process at different H_2O_2 concentrations and the LCR can be observed for all exposure times. For short exposure times of 0.2 s, however, a kill rate (logarithmic cycle reduction) of maximum 2.7 is reached, which not fulfills industrial standards (this should be ideally 6 or higher). On the other hand, for exposure times of 0.4 s and 0.5 s, the linear relation between increasing H_2O_2 concentration and logarithmic cycle reduction is only valid for H_2O_2 concentrations up to 4.3% v/v and 2% v/v, respectively. Thereby, to have a linear relationship in the whole H_2O_2 concentration range of interest, an exposure time of 0.3 s has been selected for the further experiments, which will also allow the correlation with the biosensor-based evaluation.

9.4.2 Sensor characterization

Beside the electrical characterization of the sensors the IDE structures were analyzed by SEM. As shown in Fig. 9.1 c), a repetitive pattern of the gold electrodes was produced by use of RIE. The parameters of the electrodes have been analyzed to 3 μm in width and an interspacing width of 7 μm, as predefined by the applied lithography mask. The SEM images further exhibit the topography of the electrodes, which have a slightly elevated side wall. This phenomenon is related to redeposited etching products during the RIE process. The redeposition during the RIE process has been also described by other groups [40, 41]. To overcome this issue the gas constituents and the masking layer should be further adjusted in future experiments. Nonetheless, compared with our previous work, where the lift-off method for electrode patterning was applied [23], the electrode structure now depicts defined edges. This results in a more homogenous distribution of the electric field for the impedimetric measurements (see Sec. 9.4.3).

9.4.3 Biosensor-based evaluation

For each measurement the impedance spectra were recorded in a frequency range between 200 Hz and 200 kHz. The impedance average plot of four sensors is shown in the Bode diagram in Fig. 9.4 a). The first impedance plot was captured from blank IDE structures (Fig. 9.4 a), upper plot, black line, Z(f=3 kHz)=1.12 MΩ). As the measurements were performed in a vacuum atmosphere a strict capacitive behavior can be determined over the whole frequency range, with a phase of about -90° (Fig. 9.4 a), lower plot, black line). After immobilizing and drying of the microbiological spores an impedance decrease can be monitored (Fig. 9.4 a), upper plot, red line, Z(f=3 kHz)=844 kΩ). At low frequencies (200 Hz–10 kHz) the phase shows more conductive behavior, corresponding to the spore layer and the change in permittivity compared to the blank sensor (Fig. 9.4 a), lower plot, red line). A further impedance decrease can be monitored after the sterilization process (Fig. 9.4 a), upper plot, blue line, Z(f=3 kHz)=777 kΩ). This impedance change is related to morphological alterations, such as degradation and rupture of the spores, caused by the sterilization process. The conductivity increase can be explained by the flattened spore structure after sterilization, which enhances the current flow between the electrodes. Furthermore, an additional layer has been formed after the sterilization process, which might be attributed to the release of inner spore substances.

To validate these assumptions and to reveal the morphological effects of the sterilization process and sensing mechanism, surface analyzes were applied after different sterilization scenarios using SEM (Fig. 9.5). It should be declared, some of the effects observed by SEM are related to the characterization at vacuum (10^{-5} Pa) e.g., the shrunken structure. In a comparison between non-treated and treated spores a significant difference can be observed when comparing Fig. 9.5 c), f), i), and l). Non-treated or heat-treated spores show a denser and elliptical structure as spores after sterilization. Even though, also on the reference images already some deformed spores could be found, which could be related to the preparation of the spore suspension. The morphology change after the sterilization could also be seen in transmission electron microscopy studies (s. Fig. 9.6). Furthermore, after the sterilization process some of the spores ruptured and collapsed (Fig. 9.5 k), l), Fig. 9.6 b)). Additionally, a layer between the spores and the electrodes could be observed (Fig. 9.5 k)); similar rupture effects have also been reported after plasma treatment [42]. Both facts are directly related to an enhancement of the conductivity between the electrodes, which leads to a decrease in the impedance signal as achieved in the impedance plot in Fig. 9.4 a).

In order to study the impact of the H_2O_2 concentration toward the sensor signal further impedance investigations were performed. The resulting sensor signal was analyzed at a fixed frequency of 3 kHz. In a first step, the results of the reference sensors (blank sensors and after DI water drying, without spores) will be discussed. The mean impedance value of all blank sensors used in this work (N=48) is evaluated to (1.12±0.26) MΩ (Fig. 9.4 b) orange bar). After drying of 10 μL DI water on the reference sensors (N=24) a mean impedance value of (1.11±0.19) MΩ has been recorded (Fig. 9.4 b) blue bar), which is very close to that of the blank sensors. The reference sensors were also exposed to the harsh environment of the sterilization process, in order to proof their stability

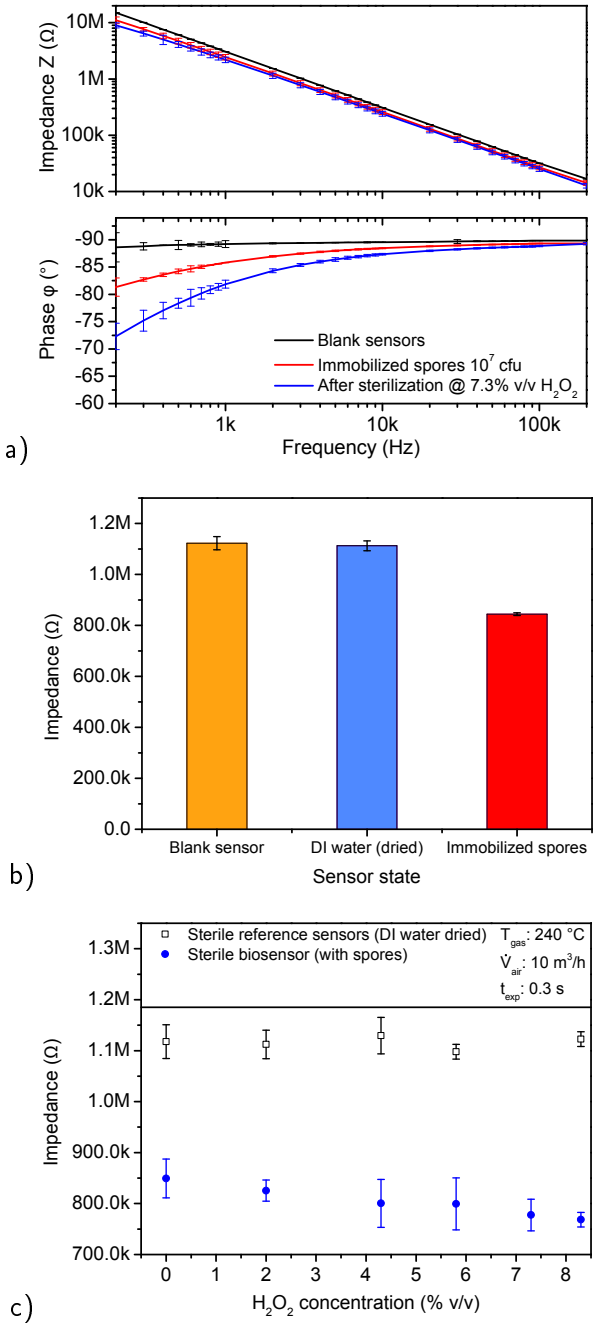

Fig. 9.4: a) Impedimetric biosensor characterizations, Bode plot of biosensor measurements at different states: black line represents mean values of four blank sensor structures; red line corresponds to mean values of four sensors after immobilization of 10^7 cfu; blue line represents mean values of four sensors after sterilization for 0.3 s at 7.3% v/v, temperature 240 °C, air flow 10 $m^3\,h^{-1}$. b) Mean impedance values measured at a frequency of 3 kHz: impedance values of non-sterilized IDE, blank sensors (orange bar, number of sensors N=48); 10 μL DI water dried as reference (blue bar, N=24); with immobilized spores, 10^7 cfu per IDE structure (red bar, N=24). c) Impedance values after sterilization, exposure time 0.3 s: reference sensors (DI water dried) (black open squares, N=4 for each concentration); sterilized biosensor with spores (blue dots, N=4 for each concentration).

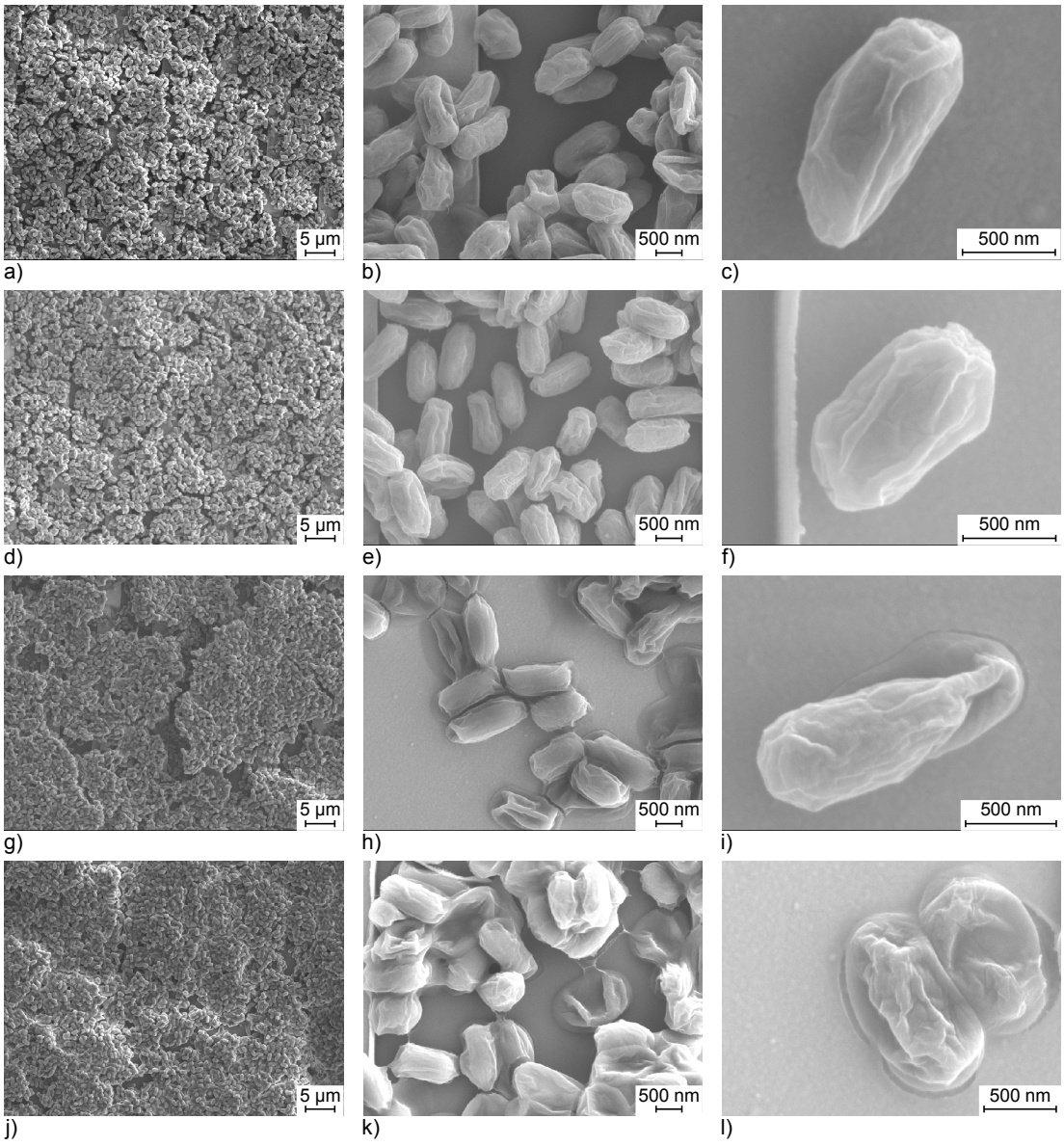

Fig. 9.5: Scanning electron microscopy pictures of spore layers before and after sterilization treatment: a) - c) spore reference no treatment; d) - f) after hot air treatment 0.3 s; g) - i) after sterilization 0.3 s at 4.3% v/v H_2O_2; j) - l) after sterilization 0.3 s at 8.3% v/v H_2O_2; gas parameter: temperature 240 °C, air flow 10 $m^3\,h^{-1}$.

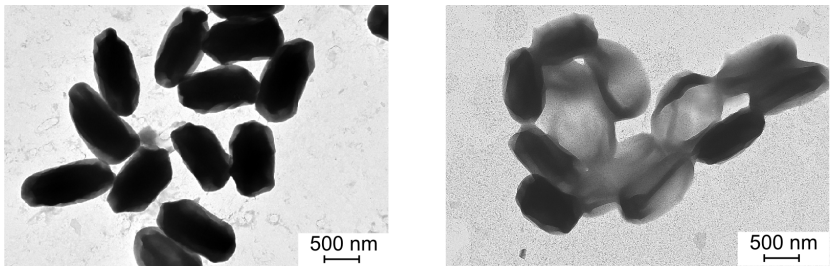

Fig. 9.6: Transmission electron microscopy pictures of spores: a) spore reference, no treatment; b) after sterilization 0.3 s at 8.3% v/v H_2O_2, temperature 240 °C, air flow 10 $m^3\,h^{-1}$.

and possible drift effects. Four independent sensors have been chosen for each H_2O_2 concentration. The measured impedance results versus the particular H_2O_2 concentration are shown in (Fig. 9.4 c) black open squares). The plot reveals small deviations between different sensors, indicated by the error bars and only slight fluctuations of the sensors for different H_2O_2 concentrations. Overall, these characterizations proof that no interactions between the harsh sterilization process and the IDE structure occurs, which ensures the further measured effects are related to the spore layer on top of the sensors.

In Fig. 9.4 b) the mean impedance values, after functionalizing the sensors with a spore layer are evaluated to (844.5±5.2) kΩ (red bar, N=24). The small standard deviation (error bar) depicts a reproducible spore immobilization on top of the sensors.

Again, four independent sensors have been chosen for each H_2O_2 concentration. Compared to the mean value before, a further impedance decrease can be monitored (Fig. 9.4 c) blue, filled dots). Moreover, the impedance decrease is in relation to the present H_2O_2 concentration and thereby to the sterilization efficiency. In order to compare the resulting differences, the normalized sensor signal ($S_{\text{norm signal}}$) as difference between the signals of immobilized spores (Z_{spores}) and after their sterilization (Z_{sterile}) has been calculated using Eq. (9.2):

$$S_{\text{norm signal}} = \frac{Z_{\text{spores}} - Z_{\text{sterile}}}{Z_{\text{spores}}} \tag{9.2}$$

These normalized results of the spore-based biosensor have been combined with the measured H_2O_2 concentrations, presented in Fig. 9.7 a). Overall, a linear relation between the normalized biosensor signal and the present H_2O_2 can be found, see Eq. (9.3) (R^2=0.978).

$$S_{\text{norm signal}} = 0.12\,(\%\ \text{v/v})^{-1} \cdot c(H_2O_2) \tag{9.3}$$

Here, ($S_{\text{norm signal}}$) represents the normalized biosensor signal and $c(H_2O_2)$ denotes the present H_2O_2 concentration.

A signal stagnancy-type behavior can be observed between H_2O_2 concentration of 4.3 and 5.8% v/v, which might be related to partially non-injured spores after the sterilization process. A similar effect has been found during the performed microbiological

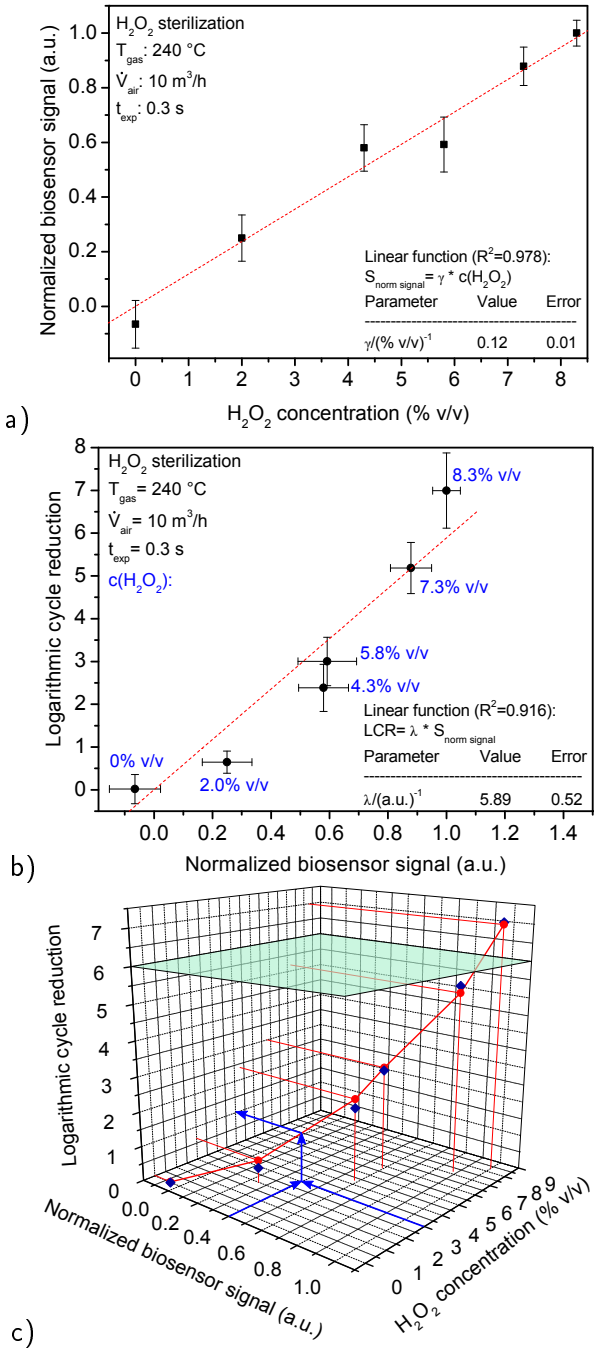

Fig. 9.7: Correlation between sensor signal and process parameters: a) plot of the normalized sensor signal vs. H_2O_2 concentration; b) logarithmic cycle reduction vs. normalized sensor signal; c) parametric, three-dimensional calibration plot: normalized biosensor signal (lower left axis) and measured H_2O_2 concentration (lower right axis) enable a prediction of the resulting logarithmic cycle reduction (vertical axis) (measured values, red dots). The green plane depicts the required LCR value for aseptic packaging. As a control of the derived LCR function (Eq. (9.5)) the resulting values are plotted as blue squares. Blue arrows indicate the graphical method to predict the LCR value by using the resulting value of the biosensor signal and the measured H_2O_2 concentration by the calorimetric gas sensor.

reference tests (Fig. 9.3 b) LCR plot (red line)). In literature, this stagnancy effect has been discussed as tailing effect, which can be related to stacked spore layers at the sample/sensor surfaces, as also observed in our experiments Fig. 9.5 a), d), g), j) [43].

In Fig. 9.7 b), the LCR values of the performed microbiological reference tests have been plotted versus the normalized sensor signals, yielding again a linear relationship. The linear function between the normalized biosensor signal and the LCR values allows a prediction of the sterilization efficiency by the electrical sensor read-out of the biosensor, see Eq. (9.4) (R^2=0.916).

$$\mathrm{LCR} = 5.89\,(\mathrm{a.u.})^{-1} \cdot \mathrm{S_{norm\ signal}} \tag{9.4}$$

Both sensing methods, biosensor set-up and calorimetric H_2O_2 detection, are combined with the LCR values in a three-dimensional parametric calibration plot (Fig. 9.7 c)). A calibration function has been evaluated to Eq. (9.5) (R^2=0.769).

$$\mathrm{LCR} = 0.85\,(\%\ \mathrm{v/v})^{-1} \cdot \mathrm{S_{norm\ signal}} \cdot \mathrm{c(H_2O_2)} \tag{9.5}$$

The combination of both independent sensing principles enables a rapid process evaluation. The resulting biosensor signal and the measured H_2O_2 concentration can be combined with Eq. (9.5), whereby the resulting LCR value is calculated or graphically evaluated as shown in Fig. 9.7 c). The efficacy of the sterilization process can be quantified within 15 min, compared to the conventional, microbiological method, which takes 48 h up to one week until final evaluation. This fast process evaluation leads to an enormous reduction in time and workload, especially during the parameterization of new sterilization systems or testing different process (e.g., gas concentration, air flow). Moreover, an in-field process control would be possible, without extended product storage during incubation of microbiological samples.

9.5 Conclusions

An impedimetric, spore-based biosensor has been introduced to facilitate a rapid control and parameterization of gaseous sterilization processes. The impedimetric measurements were combined with microbiological logarithmic cycle reduction tests. For the first time, the impedimetric biosensor has been applied at different H_2O_2 concentration, depicting a relation between the logarithmic cycle reduction and the H_2O_2 concentration. Both characterizations, the conventional microbiological test routine as well as the biosensor set-up, have shown a tailing effect between 4.3 and 5.8% v/v H_2O_2. Additionally, surface characterizations of the IDE structure, as well as of the microbiological spores at different H_2O_2 concentrations were performed. This study revealed information about the morphological changes of the spores, whereby sensing principles have been proposed. Tab. 9.1 summarizes the advantages and drawbacks of the conventional microbiological and the biosensor-based method, respectively.

In further studies, different sterilization scenarios will be investigated, such as variations in air flow and temperature. In future experiments, the biosensor can be implemented in industrial filling machines, as well as food packages. This might enable a fast process control during initial operation tests, after maintenance or as in-field process

Tab. 9.1: Comparison between the standardized, microbiological evaluation method and the biosensor-based method to evaluate the sterilization efficacy.

Microbiological method	Biosensor-based method
+ Standardized and accepted method (FDA, VDMA)	+ Fast evaluation < 1 hour
– Final result evaluation after 72 hours	+ Electrical read-out signal
– Lab- and time-consuming method	+ In-field application, next to the filling machine
– Costly method	+ Cost reduction, no nutrition medium etc.
– Experienced laboratory personnel necessary	+ Easy application by trained engineers
– High sample number, due to fluctuations of microbiological results	– Non-standardized method until now

FDA: Food and Drug Administration, USA; VDMA: Verband Deutscher Maschinen- und Anlagenbau e.V., Germany.

control, which will reduce the laborious microbiological challenge tests, improve product safety and minimize product recalls.

Acknowledgments

The project was financially supported by the Federal Ministry of Education and Research, Germany, Project: "ImpediPack" (Fund. No.: 03FH012I3). Prof. Dr. J. Bongaerts is acknowledged for offering the lab equipment to run the microbiology studies, H. Iken for assisting the sensor fabrication, D. Rolka for the SEM characterizations, C. Zafiu for the TEM characterizations, C. Hansen for supporting the sensor measurements.

References

[1] B. A. H. von Bockelmann and I. L. I. von Bockelmann. *Long-Life Products: Heat-Treated, Aseptically Packed: A Guide to Quality*. Åkarp, Sweden: B. von Bockelmann, 1998.

[2] R. T. Toledo. "Overview of sterilization methods for aseptic packaging materials". In: *Food and Packaging Interactions: Developed from a Symposium Sponsored by the Division of Agricultural and Food Chemistry at the 193rd Meeting of the American Chemical Society, Denver, Colorado, April 5-10, 1987*. Ed. by J. H. Hotchkiss. Vol. 365. ACS symposium series. Washington, DC, USA: American Chemical Society, 1988, 94–105.

[3] I. A. Ansari and A. K. Datta. "An overview of sterilization methods for packaging materials used in aseptic packaging systems". *Food and Bioproducts Processing* 81 (2003), 57–65.

[4] R. T. Toledo, F. E. Escher, and J. C. Ayres. "Sporicidal properties of hydrogen peroxide against food spoilage organisms". *Applied Microbiology* 26 (1973), 592–597.

[5] S. E. Wallen. "Sporicidal action of hydrogen peroxide". PhD thesis. Ames, IA, USA: Iowa State University, 1976.

[6] G. McDonnell. "The use of hydrogen peroxide for disinfection and sterilization applications". In: *PATAI'S Chemistry of Functional Groups*. Ed. by Z. Rappoport. Chichester, UK: John Wiley & Sons, Ltd, 2009, 1–34.

[7] J. Cadet, T. Delatour, T. Douki, D. Gasparutto, J.-P. Pouget, J.-L. Ravanat, and S. Sauvaigo. "Hydroxyl radicals and DNA base damage". *Mutation Research* 424 (1999), 9–21.

[8] P. J. Riesenman and W. L. Nicholson. "Role of the spore coat layers in *Bacillus subtilis* spore resistance to hydrogen peroxide, artificial UV-C, UV-B, and solar UV radiation". *Applied and Environmental Microbiology* 66 (2000), 620–626.

[9] A. O. Henriques and C. P. Moran. "Structure, assembly, and function of the spore surface layers". *Annual Review of Microbiology* 61 (2007), 555–588.

[10] M. J. Leggett, J. S. Schwarz, P. A. Burke, G. McDonnell, S. P. Denyer, and J.-Y. Maillard. "Mechanism of sporicidal activity for the synergistic combination of peracetic acid and hydrogen peroxide". *Applied and Environmental Microbiology* 82 (2015), 1035–1039.

[11] H. Shintani, A. Sakudo, P. Burke, and G. McDonnell. "Gas plasma sterilization of microorganisms and mechanisms of action". *Experimental and Therapeutic Medicine* 1 (2010), 731–738.

[12] M. Finnegan, E. Linley, S. P. Denyer, G. McDonnell, C. Simons, and J. Y. Maillard. "Mode of action of hydrogen peroxide and other oxidizing agents: differences between liquid and gas forms". *The Journal of Antimicrobial Chemotherapy* 65 (2010), 2108–2115.

[13] B. Setlow and P. Setlow. "Binding of small, acid-soluble spore proteins to DNA plays a significant role in the resistance of *Bacillus subtilis* spores to hydrogen peroxide". *Applied and Environmental Microbiology* 59 (1993), 3418–3423.

[14] P. Setlow. "Spores of *Bacillus subtilis*: their resistance to and killing by radiation, heat and chemicals". *Journal of Applied Microbiology* 101 (2006), 514–525.

[15] G. McDonnell. "Peroxygens and other forms of oxygen: their use for effective cleaning, disinfection, and sterilization". In: *New Biocides Development*. Ed. by P. C. Zhu. Vol. 967. ACS symposium series. Washington, D.C, USA: American Chemical Society, 2007, 292–308.

[16] G. Cerny. "Testing of aseptic machines for efficiency of sterilization of packaging materials by means of hydrogen peroxide". *Packaging Technology and Science* 5 (1992), 77–81.

[17] Food and Drug Administration. *Guide to Inspections of Aseptic Processing and Packaging for the Food Industry*. 2001.

[18] Verband Deutscher Maschinen- und Anlagenbau e.V. "Code of practice: filling machines of VDMA hygiene class V: testing the effectiveness of packaging sterilization devices". *VDMA-Fachverbandsschriften* 6 (2008), 1–16.

[19] Neogen Food Safety. *National food laboratory aseptic validation medium, product information*. 2017. URL: http://www.neogen.com.

[20] P. Silley and S. Forsythe. "Impedance microbiology - a rapid change for microbiologists". *Journal of Applied Bacteriology* 80 (1996), 233–243.

[21] J. D. Owens, D. S. Thomas, P. S. Thompson, and W. Timmerman. "Indirect conductimetry: a novel approach to the conductimetric enumeration of microbial populations". *Letters in Applied Microbiology* 9 (1989), 245–249.

[22] P. Cady, S. W. Dufour, J. Shaw, and S. J. Kraeger. "Electrical impedance measurements: rapid method for detecting and monitoring microorganisms". *Journal of Clinical Microbiology* 7 (1978), 265–272.

[23] J. Oberländer, A. Bromm, L. Wendeler, H. Iken, M. P. Durán, A. Greeff, P. Kirchner, M. Keusgen, and M. J. Schöning. "Towards a biosensor to monitor the sterilization efficiency of aseptic filling machines". *Physica Status Solidi A* 212 (2015), 1299–1305.

[24] J. Oberländer, Z. B. Jildeh, P. Kirchner, L. Wendeler, A. Bromm, H. Iken, P. H. Wagner, M. Keusgen, and M. J. Schöning. "Study of interdigitated electrode arrays using experiments and finite element models for the evaluation of sterilization processes". *Sensors (MDPI)* 15 (2015), 26115–26127.

[25] E. Bianchi, E. Rollo, S. Kilchenmann, F. M. Bellati, E. Accastelli, and C. Guiducci. "Detecting particles flowing through interdigitated 3D microelectrodes". In: *Annual international conference of the IEEE Engineering in Medicine and Biology Society (EMBC), 2012*. Vol. 2012. Piscataway, NJ: IEEE, 2012, 5002–5005.

[26] N. Couniot, A. Afzalian, N. van Overstraeten-Schlögel, L. A. Francis, and D. Flandre. "Capacitive biosensing of bacterial cells: analytical model and numerical simulations". *Sensors and Actuators B: Chemical* 211 (2015), 428–438.

[27] P. van Gerwen, W. Laureyn, W. Laureys, G. Huyberechts, M. op de Beeck, K. Baert, J. Suls, W. Sansen, P. Jacobs, L. Hermans, and R. Mertens. "Nanoscaled interdigitated electrode arrays for biochemical sensors". *Sensors and Actuators B: Chemical* 49 (1998), 73–80.

[28] F. Lisdat and D. Schäfer. "The use of electrochemical impedance spectroscopy for biosensing". *Analytical and Bioanalytical Chemistry* 391 (2008), 1555–1567.

[29] T. A. York, I. G. Evans, Z. Pokusevski, and T. Dyakowski. "Particle detection using an integrated capacitance sensor". *Sensors and Actuators A: Physical* 92 (2001), 74–79.

[30] M. Carminati, L. Pedalà, E. Bianchi, F. Nason, G. Dubini, L. Cortelezzi, G. Ferrari, and M. Sampietro. "Capacitive detection of micrometric airborne particulate matter for solid-state personal air quality monitors". *Sensors and Actuators A: Physical* 219 (2014), 80–87.

[31] A. Weiss, M. Bauer, S. Eichenauer, E. A. Stadlbauer, and C.-D. Kohl. "Impedance spectroscopy characterization of an interdigital structure for continuous particle measurements in wood-driven heating systems". *Journal of Sensors and Sensor Systems* 4 (2015), 37–44.

[32] R. Blue and D. Uttamchandani. "Chemicapacitors as a versatile platform for miniature gas and vapor sensors". *Measurement Science and Technology* 28 (2017), 22001–22024.

[33] J. Arreola, J. Oberländer, M. Mätzkow, M. Keusgen, and M. J. Schöning. "Surface functionalization for spore-based biosensors with organosilanes". *Electrochimica Acta* 241 (2017), 237–243.

[34] M. R. Adams and M. O. Moss, eds. *Food Microbiology*. 3rd ed. Cambridge, UK: Royal Society of Chemistry, 2008.

[35] N. Näther, L. M. Juárez, R. Emmerich, J. Berger, P. Friedrich, and M. J. Schöning. "Detection of hydrogen peroxide (H_2O_2) at exposed temperatures for industrial processes". *Sensors (MDPI)* 6 (2006), 308–317.

[36] P. Kirchner, B. Li, H. Spelthahn, H. Henkel, A. Schneider, P. Friedrich, J. Kolstad, M. Keusgen, and M. J. Schöning. "Thin-film calorimetric H_2O_2 gas sensor for the validation of germicidal effectivity in aseptic filling processes". *Sensors and Actuators B: Chemical* 154 (2011), 257–263.

[37] P. Kirchner, J. Oberländer, P. Friedrich, J. Berger, G. Rysstad, M. Keusgen, and M. J. Schöning. "Realization of a calorimetric gas sensor on polyimide foil for applications in aseptic food industry". *Sensors and Actuators B: Chemical* 170 (2012), 60–66.

[38] P. Kirchner, J. Oberländer, H.-P. Suso, G. Rysstad, M. Keusgen, and M. J. Schöning. "Monitoring the microbicidal effectiveness of gaseous hydrogen peroxide in sterilization processes by means of a calorimetric gas sensor". *Food Control* 31 (2013), 530–538.

[39] J. Oberländer, P. Kirchner, M. Keusgen, and M. J. Schöning. "Strategies in developing thin-film sensors for monitoring aseptic food processes: theoretical considerations and investigations of passivation materials". *Electrochimica Acta* 183 (2015), 130–136.

[40] G. Franz, R. Kachel, and S. Sotier. "Residual free reactive ion etching of the Bell contact Ti/Pt/Au". *Materials Science in Semiconductor Processing* 5 (2002), 45–50.

[41] A. Aydemir and T. Akin. "Prevention of sidewall redeposition of etched byproducts in the dry Au etch process". *Journal of Micromechanics and Microengineering* 22 (2012), 074004–074009.

[42] X. Deng, J. Shi, and M. G. Kong. "Physical mechanisms of inactivation of *Bacillus subtilis* spores using cold atmospheric plasmas". *IEEE Transactions on Plasma Science* 34 (2006), 1310–1316.

[43] K. Warriner, G. Rysstad, A. Murden, P. Rumsby, D. Thomas, and W. M. Waites. "Inactivation of *Bacillus subtilis* spores on packaging surfaces by UV-excimer laser irradiation". *Journal of Applied Microbiology* 88 (2000), 678–685.

9.6 Supplemental information

The developed biosensor has been in-house fabricated by means of thin-film technologies. Fig. 9.8 summarizes the different processing steps: a) starting with a cleaned glass wafer (Borofloat®, Schott GmbH); b) sequentially deposited layers of chromium (10 nm) and gold (100 nm) by e-beam evaporation; c)-d) photo lithographical structuring of a masking layer photoresist (AZ2020 nLOF) masking layer; e) transfer of the pattern by a RIE process; f) O_2 plasma cleaning to remove the photoresist layer; g) deposition and lithographic structuring of SU-8 side walls.

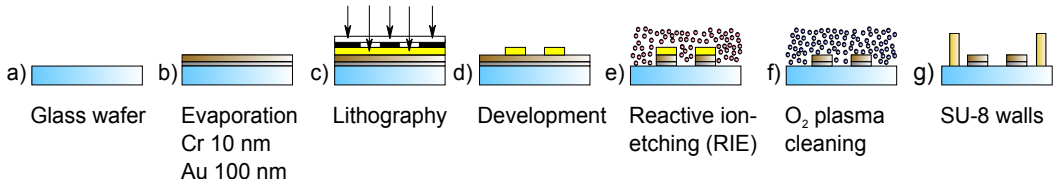

Fig. 9.8: Schematic representation of the thin-film fabrication steps: a) cleaned glass wafer; b) deposition of the electrode materials chromium (Cr) and gold (Au); c-d) patterning of the photoresist etching-mask; e) pattern transfer into the metal layer by reactive ion-etching; f) removal of photoresist mask; g) SU-8 walls to define active regions with immobilized spores.

10 Concluding remarks and perspectives

In aseptic food processes, the sterilization of food packages is an essential step to produce and deliver consumer-safe products, which are microbiologically stable with a guaranteed long shelf-life. During the aseptic packaging process, the packaging material and food products are sterilized separately. Heat treatment is a common method to sterilize food products. Whereas, the packaging material is commonly sterilized by chemical agents. In a favored industrial procedure, a hot gas mixture containing H_2O_2 is used to sterilize composite packages for milk, juice and other food. The application of gaseous H_2O_2 at elevated temperatures (up to 300 °C) facilitates an efficient sterilization process within a short exposure time (less than 2 s). Nowadays, monitoring of the critical packaging sterilization process is performed by recording various machine parameters and by applying conventional, laborious microbiological tests. In previous works, different sensor approaches to monitor the gaseous H_2O_2 sterilization process have been proposed [1–3]. One of the developed sensors is based on the calorimetric detection of gaseous H_2O_2. The suitability of such calorimetric gas sensor to monitor the industrial package sterilization process has been demonstrated. However, up to now, there is no commercial set-up for industrial application available.

The present thesis has been divided into two parts. The aim of the first part (Chapters 3-4) was to conduct further characterizations and studies of the previously developed calorimetric gas sensor. The catalytically active and passivation materials have been investigated. Additionally, the calorimetric gas sensor has been theoretically described by applying analytical expressions. The aim of the second part (Chapters 5-9) of this thesis was to develop and characterize a novel sensor set-up to evaluate the impact of the gaseous H_2O_2 sterilization process towards an industrially applied microbiological test organism.

In Chapter 3, the catalytically active material of the previously established calorimetric H_2O_2 gas sensor was in focus of research. Material analyses of the catalytically active material MnO_2 were performed by applying XPS. The catalytic layer of MnO_2 has been characterized after different fabrication steps as well as after the exposure to gaseous H_2O_2 at a gas temperature of 240 °C. These investigations have pointed out that the MnO_2 layer is initially covered by a thin layer of the polymer. The coverage of the MnO_2 results from the polymeric adhesion matrix. The characterization by XPS has evidenced that the thin layer is removed after the exposure to gaseous H_2O_2. Further XPS analyses of the catalytic layer have revealed a change in the oxidation state of the catalytic layer due to the exposure to gaseous H_2O_2. The change in oxidation state results in a partly transformation of MnO_2 to MnO and Mn_3O_4, with a major portion of MnO_2. The results of the XPS analyses have been concluded by describing

a reaction pathway of the decomposition of gaseous H_2O_2 on the catalytic sensor layer MnO_2. The reaction pathway has been derived by reviewing the H_2O_2 decomposition process on MnO_2 described in literature, where only few information has been found for the process conditions in aseptic filling machines such as elevated temperature and H_2O_2 concentration up to 10% v/v.

In Chapter 4, the calorimetric H_2O_2 gas sensor has been described by analytical expressions. These theoretical considerations have been derived for different sensor scenarios (steady-state process, gas diffusion process and convective gas flow) to evaluate the theoretical temperature rise. The theoretical findings have been compared with sensor measurements with variations of the gas flow rate. Different aspects have been discussed regarding the difference between the theoretical thermochemical considerations and the sensor's sensitivity such as heat conduction between the sensing elements or reduced activity of the catalyst. Thereby, additional tasks arose to further study the sensor. In future works, the catalyst's activity should be included into theoretical analyses. The sensor performance could also be improved by studying adaptations of the sensor housing, e.g., including a thermal barrier between the two temperature-sensing elements. In addition to the theoretical considerations of the sensor, further characterization methods were applied to examine the effect of H_2O_2 on the sensor passivation materials. The examined materials were three types of polymers, namely two Teflon derivatives PFA and FEP, and the epoxy-based photoresist SU-8. Thermal characterizations by DSC and TGA have been performed to analyze the thermal stability of the polymers with regard to the sensor application. The Teflon derivatives pointed out a thermal stability until 268 °C (FEP) and 309 °C (PFA), determined by the melting temperature. For SU-8 no distinct melting point could be observed during the DSC analysis up to 320 °C. The TGA of SU-8 has depicted that a degradation starts at 393 °C. These analyses verify the thermal suitability of the polymer layers. Surface characterizations of the polymers have been examined by applying ATR-FTIR. The characterizations of the polymers have been performed before and after exposure to the process gas containing H_2O_2 at a temperature of 240 °C. The transmission spectra of the polymers have been used to analyze the overall resistance (thermally and chemically) against the sterilization process. The results of the Teflon derivatives highlighted that the process gas doesn't interfere with the deposited layers. Whereas, the analyses of the SU-8 depict slight variations after the exposure to gaseous H_2O_2. These variations could be assigned to further hardening of the epoxy-based polymer. These characterizations were necessary to proof the resistance against the process conditions during sensor measurements and to guarantee long-term stability and reproducible results. As an overall result of the polymer characterization, the three materials have demonstrated their stability against the harsh conditions of sensor application.

These two previously discussed chapters are succeeding experiments of the work of Dr. P. Kirchner [2].

Perspectives for the calorimetric gas sensors are to further optimize the long-term stability of the catalytic material within the harsh environment of the sterilization process. Industrial studies have already shown the suitability for inline monitoring the

sterilization process of food packages. In future, the sensor integration into aseptic filling machines and test packages should be focused. Therefore, the calorimetric gas sensor needs to fulfill regulatory requirements, e.g., no product contamination is allowed by sensor parts. This could be circumvented by developing suitable sensor housings with respect to maintain the sensor performance. Additionally, further applications could be envisaged where monitoring of H_2O_2 is necessary, e.g., sterilization processes of medical equipment or pharmaceutical isolators. In which, the sterilization processes with H_2O_2 are performed in a vacuum atmosphere. Preliminary tests have already demonstrated the sensor's functionality even at these conditions. Thereby, the lack of oxygen within this atmosphere will not inhibit the decomposition reaction of H_2O_2 at the sensor's catalyst, as for conventional combustible gas sensors.

In the second part of this work (Chapters 5-9), a new biosensor set-up to monitor the efficacy of the gaseous H_2O_2 sterilization process has been developed and characterized. The biosensor is based on interdigitated electrodes as transducer structure, which have been in-house developed and fabricated by thin-film technologies. Physical characterizations of the transducer structure were performed by means of SEM, AFM, and electrically, by impedance spectroscopy. As microbiological test organism industrially applied spores of *Bacillus atrophaeus* are used and immobilized on the IDEs. The impedance of the IDE has been captured before and after the immobilization, as well as after various sterilization scenarios. Remaining signal changes have been attributed to alterations of the spores and a relation between the sterilization process and the sensor signal has been found.

In Chapter 5, the procedure to fabricate the IDE by means of thin-film technologies has been described. Impedimetric characterizations of the IDE-based sensors with and without the microbiological spore layer as well as after the gaseous H_2O_2 sterilization process have been performed. As an approach to describe the sensor set-up, analytical expressions have been reviewed and refined. FEM-based numerical simulations of the IDE structure have been applied to gather information about the electric field distribution. The numerical model geometry of the sensor set-up has been systematically simplified by applying periodicity and symmetry of the electrode structure. Thereby, the computational time has been distinctly reduced. The results of theoretical considerations (analytical and numerical) have been analyzed and discussed in comparison with impedimetric characterizations of the developed sensor. The FEM-based model has been refined by applying a profilometric scan of the IDE, which reduces the relative error between impedimetric and FEM-based simulation from 12.4% to 9.2%. This FEM model can be applied in future to study the influence of the IDE geometry (electrode width, interspacing and length) and number of electrode fingers. Additionally, the FEM simulation can be applied to gather information of the electrical properties (relative permittivity and electrical conductivity) of a substrate and a material deposited on top or between the IDE.

In Chapter 6, a follow up work of the previous FEM-based simulation has been presented. The FEM-based simulations have been combined with sensor measurements.

Thereby, material properties (relative permittivity and electrical conductivity) of the sensor substrate and the microbiological spores at different states have been evaluated. The FEM model has been validated by applying experimental data of the blank sensor and by determining the relative permittivity of the glass substrate. The resulting value corresponds to the value given by the manufacturer of the substrate (relative error 2%). The validated FEM model has been further adapted to determine electrical properties of the spore layer at different states (immobilized spores and sterile spores). In future studies, these simulation models can be applied to perform theoretical analyses and evaluations before final development and fabrication of transducer structures, in order to improve the tailoring of the transducer structure in accordance to the substance or material of interest. These studies can comprise geometrical variations of IDEs (electrode width, interspacing and length) as well as the number of electrode fingers. Moreover, the simulation of the spore layer might be enhanced by incorporating a more realistic geometrical model of the spores, which can also include the spore deformation by the sterilization process.

The FEM-based simulations within these previous chapters have been performed in cooperation with Zaid B. Jildeh.

In Chapter 7, the design and fabrication of the spore-based biosensor has been introduced. Characterizations of the IDE geometry and the immobilized spore layer have been performed by applying SEM and profilometry. The immobilization of the spores from an ethanol-based suspension onto the IDE structure have been captured by impedance analyses. Further impedance measurements have demonstrated impedimetric detection of spore modifications caused by the gaseous H_2O_2 sterilization process. Whereas, the impedance of a reference IDE (without spores) was not affected by the sterilization process. Within this chapter the first proof-of-concept experiment of the spore-based biosensor has been demonstrated. This chapter with initial investigations highlighted further research topics, e.g., sensor tests at different sterilization scenarios, development of an electrical equivalent model of the sensor, correlation between sensor signal and microbiological tests, optimization of the transducer structure, and investigation of different spore loads on the sensor.

In Chapter 8, a method to enhance the spore immobilization onto the transducer structure has been suggested. The transducer structure has been pretreated by an organosilane (APTES), thereby N- or C-termini are available at the surface, which enable covalent bonding between proteins of the spore coat and the functionalized surface. Analyses of the immobilization strategy have been performed by AFM, SEM, microbiological methods and impedance spectroscopy. Further research should involve the influence of the 3D sensor geometry towards the attachment of the spores, as the study revealed differences between the planar surfaces and the sensor structure. Moreover, the change of electrical properties of the applied organosilane in combination with the spores needs to be studied in detail.

The strategy to immobilize the microbiological spores onto sensor surfaces has been developed by Julio Arreola, further research on this topic are also subject of the work by Julio Arreola. The author of the present thesis has fabricated and charac-

terized the sensor structure and conducted the experiments together with Julio Arreola.

In Chapter 9, further studies of the spore-based biosensor have been examined. Within this study the impact of gaseous H_2O_2 has been evaluated in more detail. Microbiological count-reduction tests have been conducted to enumerate the efficacy of the sterilization process. Moreover, physical characterizations of the spores by means of TEM and SEM have been performed to evaluate the morphological alterations. In order to facilitate a controlled environment studying the alterations of the spores a measurement chamber has been developed. The measurement chamber enables the connection of a differential pair of two sensors within a vacuum or low pressure environment. During the performed analyses a constant pressure of 100 mbar (absolute) has been applied to reduce the sensor interference by variations in humidity or air pressure. The spore-based biosensor has been subjected to different H_2O_2 concentrations. The present H_2O_2 concentration has been evaluated by one of the previously discussed calorimetric gas sensors. Sensor-based measurements (biosensor and calorimetric gas sensor) and results of the microbiological count-reduction test have been concluded in a 3D calibration plot, which facilitates the evaluation of the sterilization process by using two independent sensing principles.

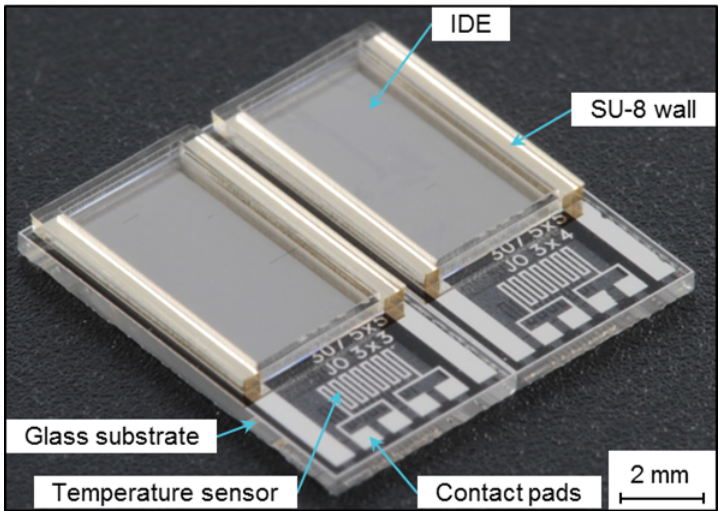

Fig. 10.1: Micrograph of the developed spore-based biosensor, depicting the IDE structure surrounded by SU-8 walls; the lower part shows temperature sensors and contact pads.

The developed biosensor (Fig. 10.1) enables a rapid process control to evaluate the efficacy of gaseous H_2O_2 sterilization processes compared to conventional methods. The sensor-based evaluation can be performed without additional nutrition media or laborious sample preparation. Table 10.1 summarizes the advantages and drawbacks of the developed biosensor in comparison to standardized microbiological methods. An additional drawback of the sensor might be the unspecific detection of environmental interactions with the immobilized microorganisms. Thereby, the operator needs to be aware of the sensor's history. The reduced evaluation time is an enormous benefit to

minimize the storage of packaged food products during microbiological sample analysis. Thereby, the delivery time of the food products to customers can be shortened. The sensor-based evaluation will also reduce time and workload during parameterization of new sterilization systems. Within Chapter 9 an initial calibration between the two sensor-based methods (calorimetric and impedimetric biosensor) and the microbiological method has been described by $\mathrm{LCR} = 0.85\,(\%\ \mathrm{v/v})^{-1} \cdot \mathrm{S_{norm\ signal}} \cdot \mathrm{c}(\mathrm{H_2O_2})$. Here, the resulting logarithmic count reduction (LCR) can be derived by the normalized sensor signal of the developed biosensor ($\mathrm{S_{norm\ signal}}$) and the present H_2O_2 concentration ($\mathrm{c}(\mathrm{H_2O_2})$), measured by the calorimetric H_2O_2 gas sensor.

Further analyses and evaluations are necessary to establish this method as standardized evaluation method. These analyses should comprise different sterilization scenarios e.g., at varying gas flow and gas temperature. In future, the nowadays applied microbiological test strips, with pre-defined spore load, might be replaced by the biosensor-based evaluation method.

Tab. 10.1: Comparison between the standardized, microbiological evaluation method and the biosensor-based method to evaluate the sterilization efficacy [4].

Microbiological method	Biosensor-based method
+ Standardized and accepted method (FDA, VDMA)	+ Fast evaluation $<$ 1 hour
– Final result evaluation after 72 hours	+ Electrical read-out signal
– Lab- and time-consuming method	+ In-field application, next to the filling machine
– Costly method	+ Cost reduction, no nutrition medium etc.
– Experienced laboratory personnel necessary	+ Easy application by trained engineers
– High sample number, due to fluctuations of microbiological results	– Non-standardized method until now
	– Unspecific detection of environmental interactions

FDA: Food and Drug Administration, USA; VDMA: Verband Deutscher Maschinen- und Anlagenbau e.V., Germany.

In conclusion, the present work has demonstrated that an electrical read-out signal can be used to analyze the efficacy of the sterilization process within minutes by means of the developed biosensor. In general, the conventionally applied microbiological challenge tests take at least 72 hours to incubate samples and are laborious in preparation and evaluation. In contrast, the established biosensor set-up possesses an essential time-benefit. Moreover, beside a method to measure the prevalent chemical concentration, the interaction between microbiological samples at the biosensor surface and the sterilization process can be directly assessed. Both measurement principles (calorimetric gas sensing and impedimetric biosensor) have been combined in a miniaturized sensor system to characterize the efficacy of the gaseous H_2O_2 sterilization process.

The developed spore-based biosensor has been subjected to a set of sterilization parameters by varying the H_2O_2 concentration. Nonetheless, further studies should involve additional sterilization parameters such as variations in air flow and gas temperature, which will also affect the efficiency of the gaseous H_2O_2 sterilization process. Further sensor studies should also be performed in food packages to evaluate different

positions and sterilization parameters as industrially applied.

As a perspective of this biosensor, further high-resolution lithography or nano-imprint lithography can be employed in order to develop sub-micron IDEs. Thereby, characterization of a single microbiological spore, before and after the sterilization process, might be possible. Moreover, other kinds of resilient microorganisms can be studied with respect to the sterilization process. In a further extend, there might be other sterilization processes, especially gaseous, at which the sensor can be applied. For example, sterilization processes applying gas plasma have demonstrated to result also in deformations of the microorganism. A detailed electrical equivalent model of the sensor and especially of the spores or spore layer could be developed to reveal more information about the sensing principle. This will also further unravel the interactions of the sterilization process with the microbiological spores.

References

[1] N. Näther. "Entwicklung eines H_2O_2-Messverfahrens für die Überwachung der mikrobioziden Wirksamkeit bei der Sterilisation aseptischer Verpackungen". PhD thesis. Marburg, Germany: Philipps-Universität Marburg, 2009.

[2] P. Kirchner. "Thin-film calorimetric gas sensors for hydrogen peroxide monitoring in aseptic food processes". PhD thesis. Marburg, Germany: Philipps-Universität Marburg, 2013.

[3] S. Reisert. "Novel strategies for evaluating the effectiveness of aseptic sterilization processes by means of a multi-sensor set-up". PhD thesis. Hasselt, Belgium: Hasselt University, 2014.

[4] J. Oberländer, M. Mayer, A. Greeff, M. Keusgen, and M. J. Schöning. "Spore-based biosensor to monitor the microbicidal efficacy of gaseous hydrogen peroxide sterilization processes". *Biosensors and Bioelectronics* 104 (2018), 87–94.

11 Zusammenfassung

Ein wesentlicher Prozessschritt bei der Herstellung von aseptisch verpackten Lebensmitteln ist die Sterilisation der Packstoffe. Diese ist notwendig, um eine Rekontamination der Lebensmittel mit Mikroorganismen zu verhindern und dem Verbraucher ein sicheres und lang haltbares Produkt zur Verfügung zu stellen. Für die Sterilisation der Packstoffe wurde in den letzten Jahren vermehrt gasförmiges Wasserstoffperoxid bei erhöhter Gastemperatur eingesetzt. Dieses erzielt eine hohe Sterilisationswirkung innerhalb einer kurzen Expositionszeit. Derzeit wird dieser kritische Prozess industriell lediglich über die Erfassung der Maschinenparameter sowie mittels zeit- und kostenintensiver mikrobiologischer Verfahren überwacht. Ziel dieser Arbeit war es daher, Sensor-basierte Methoden zu entwickeln und zu charakterisieren, um die Wirksamkeit des Sterilisationsprozesses zeitnah beurteilen zu können.

Hierzu wurden im ersten Teil dieser Arbeit Sensoren nach dem kalorimetrischen Sensorprinzip untersucht und weiterentwickelt. Materialanalysen des eingesetzten Katalysators Manganoxid wurden durchgeführt, um den Reaktionsmechanismus mit dem Prozessgas Wasserstoffperoxid zu beschreiben. Hierzu erfolgten Oberflächenuntersuchungen des Katalysators mit der Röntgenphotoelektronenspektroskopie. Hierbei konnten Veränderungen der Oxidationsstufe des Katalysators nachgewiesen werden. Weitere Materialanalysen wurden an Polymeren durchgeführt, diese werden zur Passivierung der entwickelten Sensorstrukturen eingesetzt. Diese Materialien wurden hinsichtlich ihrer Beständigkeit gegenüber den harschen Prozessbedingungen untersucht. Hierzu wurden insgesamt drei Polymere charakterisiert: ein Epoxy-basierter Photoresist (SU-8), sowie zwei Teflon-Derivate PFA (Perfluoralkoxy) und FEP (Fluorethylenpropylen). In thermischen Analysen konnte der Einsatzbereich der Polymere hinsichtlich der maximalen Temperaturen abgegrenzt werden. Zusätzlich fanden Oberflächencharakterisierungen vor und nach der Exposition im Sterilisationsprozess statt; hier zeigten die untersuchten Materialien ihre Beständigkeit gegenüber gasförmigem Wasserstoffperoxid. Im Weiteren wurden mittels analytischer Methoden theoretische Betrachtungen des kalorimetrischen Gassensors durchgeführt. Hierzu wurden thermodynamische Beziehungen des Wärme- und Massetransportes aufgestellt und mit experimentellen Messungen abgeglichen.

In Zukunft könnten noch weitere Optimierungen hinsichtlich der Langzeitstabilität des Katalysators erfolgen. In industriell durchgeführten Untersuchungen konnte bereits die Einsatzfähigkeit des Sensors gezeigt werden; hier könnten nun weitere Einsatzfelder, z.B. bei der Sterilisation von Medizinprodukten im Vakuum, anvisiert werden. Hierzu bietet die Detektion von H_2O_2 einen wesentlichen Vorteil gegenüber konventionell eingesetzten Pellistor-Gassensoren, da für die Umsetzung von H_2O_2 kein atmosphärischer Sauerstoff notwendig ist.

Dieser erste Teil der vorliegenden Arbeit basiert auf den Sensorentwicklungen einer früheren Doktorarbeit von Dr. P. Kirchner.

Im zweiten Teil dieser Arbeit wurde ein neuartiger Biosensor entwickelt und charakterisiert. Dieser basiert auf Interdigitalelektroden (IDE), welche auf einem isolierenden Substrat, z.B. Glas, unter Anwendung von Dünnschichttechnologien hergestellt wurden. Diese IDE wurden physikalisch mit REM, AFM charakterisiert, die elektrische Charakterisierung erfolgte mit Hilfe der Impedanz-Spektroskopie. Auf diese IDE wurden widerstandsfähige Mikroorganismen (Sporen des Typs *Bacillus atrophaeus*) immobilisiert; diese werden in der Industrie bei mikrobiologischen Challenge-Tests zur Evaluierung des Sterilisationsprozesses eingesetzt. Mittels Impedanz-Spektroskopie wurde die Impedanz der IDE vor und nach der Immobilisierung, sowie nach dem Sterilisationsprozess, erfasst. Nach jedem dieser Schritte konnten Änderungen in Impedanz und Phase detektiert werden. Insbesondere die Impedanzänderungen nach der Sterilisation wurden in Beziehung mit morphologischen Veränderungen der Sporen gebracht, welche wiederum in Korrelation zur H_2O_2-Konzentration des Sterilisationsprozesses standen. Die morphologischen Veränderungen wurden mit physikalischen Methoden (REM und TEM) nachgewiesen.

Numerische Simulationen der IDE-Strukturen wurden eingesetzt, um die Verteilung des elektrischen Feldes zu analysieren. Darüber hinaus konnten elektrische Eigenschaften, wie relative Permittivität und elektrische Leitfähigkeit, der Sensormaterialien sowie der biologischen Sporen analysiert werden. In weiteren Entwicklungen könnten die erstellten Modelle eingesetzt werden, um die Sensoreigenschaften zu verbessern. So könnte eine Zeitersparnis erzielt werden, um z.B. die Elektroden an die zu charakterisierenden Substanzen oder Materialien anzupassen. Hierzu könnten Analysen an der IDE-Geometrie durchgeführt werden, wie z.B. Fingerlänge, Breite und Abstände der Elektroden, sowie Anzahl der Finger. Darüber hinaus könnte zusätzlich ein geometrisches Modell der Sporen eingebunden werden, welches ebenfalls die Deformation berücksichtigt. Diese FEM-basierten Simulationen wurden in Kooperation mit Zaid B. Jildeh durchgeführt.

Um eine adäquate Immobilisierung der Sporen auf den IDE zu gewährleisten, wurde eine Behandlung der Sensoroberfläche mit dem Organosilan APTES untersucht. Diese Funktionalisierung stellt Stickstoff- oder Kohlenstoffendgruppen bereit, um eine kovalente Bindung zwischen Spore und Oberfläche zu erzielen. Im Weiteren könnte der Einfluss der 3D-strukturierten Sensoroberfläche hinsichtlich der Sporenhaftung genauer untersucht werden, da in den aufgeführten Studien eine geringere Haftung an den 3D-Oberflächen gegenüber den planen Oberflächen festgestellt wurde. Ebenso sind noch weitere Untersuchungen hinsichtlich der elektrischen Eigenschaften des genutzten Organosilans notwendig. Diese Strategie zur Immobilisierung der Sporen auf der Sensoroberfläche wurde von Julio Arreola entwickelt; weitere Untersuchungen und Beschreibungen erfolgen im Rahmen der Arbeit von Julio Arreola.

In dieser Arbeit wurde ein Sporen-basierter Biosensor erfolgreich entwickelt und charakterisiert. Dieser ermöglicht eine zeitnahe Evaluierung des Sterilisationsprozesses innerhalb von Minuten, verglichen mit konventionellen mikrobiologischen Methoden, bei denen eine Auswertung in der Regel erst nach 72 Stunden möglich ist. Der Biosensor erfasst dabei nicht nur Parameter wie H_2O_2-Konzentration und Temperatur, sondern direkte Auswirkungen an mikrobiologischen Testkeimen. Die Kombination von beiden Messverfahren, kalorimetrischer Gassensor und impedimetrischer Biosensor, ermöglicht eine detaillierte Abbildung des Sterilisationsprozesses.

List of publications

Publications in peer-reviewed journals

[1] F. Vahidpour, J. Oberländer, and M. J. Schöning. "Flexible calorimetric gas sensors for detection of a broad concentration range of gaseous hydrogen peroxide: a step forward to online monitoring of food-package sterilization processes". *Physica Status Solidi A* (2018), 1800044 (1–7). DOI: 10.1002/pssa.201800044.

[2] Z. B. Jildeh, J. Oberländer, P. Kirchner, M. Keusgen, P. H. Wagner, and M. J. Schöning. "Experimental and numerical analyzes of a sensor based on interdigitated electrodes for studying microbiological alterations". *Physica Status Solidi A* (2018), 1700920 (1–9). DOI: 10.1002/pssa.201700920.

[3] Z. B. Jildeh, J. Oberländer, P. Kirchner, P. H. Wagner, and M. J. Schöning. "Thermocatalytic behavior of manganese(IV) oxide as nanoporous material on the dissociation of a gas mixture containing hydrogen peroxide". *Nanomaterials (MDPI)* 8 (2018), 262 (1–16).

[4] J. Oberländer, M. Mayer, A. Greeff, M. Keusgen, and M. J. Schöning. "Spore-based biosensor to monitor the microbicidal efficacy of gaseous hydrogen peroxide sterilization processes". *Biosensors and Bioelectronics* 104 (2018), 87–94.

[5] Z. B. Jildeh, P. Kirchner, J. Oberländer, A. Kremers, T. Wagner, P. H. Wagner, and M. J. Schöning. "FEM-based modeling of a calorimetric gas sensor for hydrogen peroxide monitoring". *Physica Status Solidi A* 214 (2017), 1600912 (1–9).

[6] J. Arreola, J. Oberländer, M. Mätzkow, M. Keusgen, and M. J. Schöning. "Surface functionalization for spore-based biosensors with organosilanes". *Electrochimica Acta* 241 (2017), 237–243.

[7] J. Oberländer, Z. B. Jildeh, P. Kirchner, L. Wendeler, A. Bromm, H. Iken, P. H. Wagner, M. Keusgen, and M. J. Schöning. "Study of interdigitated electrode arrays using experiments and finite element models for the evaluation of sterilization processes". *Sensors (MDPI)* 15 (2015), 26115–26127.

[8] J. Oberländer, A. Bromm, L. Wendeler, H. Iken, M. P. Durán, A. Greeff, P. Kirchner, M. Keusgen, and M. J. Schöning. "Towards a biosensor to monitor the sterilization efficiency of aseptic filling machines". *Physica Status Solidi A* 212 (2015), 1299–1305.

[9] J. Oberländer, P. Kirchner, M. Keusgen, and M. J. Schöning. "Strategies in developing thin-film sensors for monitoring aseptic food processes: theoretical considerations and investigations of passivation materials". *Electrochimica Acta* 183 (2015), 130–136.

[10] J. Oberländer, P. Kirchner, H.-G. Boyen, and M. J. Schöning. "Detection of hydrogen peroxide vapor by use of manganese(IV) oxide as catalyst for calorimetric gas sensors". *Physica Status Solidi A* 211 (2014), 1372–1376.

[11] P. Kirchner, J. Oberländer, H.-P. Suso, G. Rysstad, M. Keusgen, and M. J. Schöning. "Monitoring the microbicidal effectiveness of gaseous hydrogen peroxide in sterilization processes by means of a calorimetric gas sensor". *Food Control* 31 (2013), 530–538.

[12] P. Kirchner, J. Oberländer, H.-P. Suso, G. Rysstad, M. Keusgen, and M. J. Schöning. "Towards a wireless sensor system for real-time H_2O_2 monitoring in aseptic food processes". *Physica Status Solidi A* 210 (2013), 877–883.

[13] P. Kirchner, J. Oberländer, P. Friedrich, J. Berger, G. Rysstad, M. Keusgen, and M. J. Schöning. "Realization of a calorimetric gas sensor on polyimide foil for applications in aseptic food industry". *Sensors and Actuators B: Chemical* 170 (2012), 60–66.

[14] P. Kirchner, J. Oberländer, P. Friedrich, J. Berger, H.-P. Suso, A. Kupyna, M. Keusgen, and M. J. Schöning. "Optimization and fabrication of a calorimetric gas sensor built up on a polyimide substrate for H_2O_2 monitoring". *Physica Status Solidi A* 208 (2011), 1235–1240.

Patent applications

[1] J. Oberländer, M. Gast, M. Ohneberg, and M. J. Schöning. "Vorrichtung zur Messung von Sterilisationsparametern". DE 10 2017 222 804.0. 2017.

[2] P. Kirchner, J. Oberländer, and M. J. Schöning. "Biosensor". DE 10 2013 217 359 A1. 2013.

[3] P. Kirchner, J. Oberländer, and M. J. Schöning. "Verfahren für einen Gassensor oder Sensor in der Gasphase". DE 10 2012 221 436 A1. 2012.

Proceedings

[1] J. Arreola, J. Oberländer, M. Keusgen, and M. J. Schöning. "Viability analysis of spore-based biosensors in sterilization processes". *Proceedings (MDPI)* 1 (2017), 789.

[2] J. Oberländer, J. Arreola, C. Hansen, A. Greeff, M. Mayer, M. Keusgen, and M. J. Schöning. "Impedimetric biosensor to enable fast evaluation of gaseous sterilization processes". *Proceedings (MDPI)* 1 (2017), 435.

[3] J. Oberländer, Z. B. Jildeh, P. Kirchner, L. Wendeler, A. Bromm, H. Iken, P. H. Wagner, M. Keusgen, and M. J. Schöning. "Experimental and numerical evaluation of interdigitated electrode array for monitoring gaseous sterilization processes". In: *12. Dresdner Sensor-Symposium*. Ed. by AMA Service GmbH. Wunstorf, Germany, 2015, 163–168.

[4] J. Oberländer, P. Kirchner, M. Keusgen, and M. J. Schöning. "Flexible polyimide-based calorimetric gas sensors for monitoring hydrogen peroxide in sterilization processes of aseptic filling machines". In: *Sensoren und Messsysteme 2014*. Ed. by VDI/VDE-Gesellschaft Mess- und Automatisierungstechnik. Vol. 250. ITG-Fachbericht. Berlin: VDE-Verlag, 2014.

[5] J. Oberländer, S. Reisert, P. Kirchner, M. Keusgen, P. H. Wagner, and M. J. Schöning. "Kalorimetrische Gassensoren zur H_2O_2-Detektion in aseptischen Sterilisationsprozessen". In: *11. Dresdner Sensor-Symposium*. Ed. by AMA Service GmbH. Wunstorf, Germany, 2013, 234–238.

Oral and poster presentations

[1] J. Oberländer, J. Arreola, C. Hansen, A. Greeff, M. Mayer, M. Keusgen, and M. J. Schöning. *Impedimetric biosensor to enable fast evaluation of gaseous sterilization processes.* Eurosensors 2017. Paris, France. 03. - 06.09.2017.

[2] J. Oberländer, Z. B. Jildeh, P. Kirchner, T. Wagner, P. H. Wagner, M. Keusgen, and M. J. Schöning. *Experimental and numerical analyzes of a sensor based on interdigitated electrodes for studying microbiological alterations.* Engineering of Functional Interfaces. Marburg, Germany. 28. - 29.08.2017.

[3] J. Oberländer, J. Arreola, C. Hansen, A. Greeff, M. Mayer, M. Keusgen, and M. J. Schöning. *Functionalized spore-based biosensor to evaluate gaseous sterilization processes.* European Biosensor Symposium. Potsdam, Germany. 03. - 05.03.2017.

[4] J. Oberländer, A. Bromm, T. Kerschgens, A. Greeff, M. Mayer, M. Keusgen, and M. J. Schöning. *Sensor-based determination of sporicidal mechanisms of gaseous sterilization processes in food industry.* International Meeting on Chemical Sensors. JeJu Island, South Korea. 10. - 13.07.2016.

[5] J. Oberländer, A. Bromm, T. Kerschgens, A. Greeff, M. Mayer, M. Keusgen, and M. J. Schöning. *Customized impedance analyzer to evaluate sensors for sterilization processes.* Engineering of Functional Interfaces. Wildau, Germany. 03. - 05.07.2016.

[6] J. Oberländer, Z. B. Jildeh, P. Kirchner, L. Wendeler, A. Bromm, H. Iken, P. H. Wagner, M. Keusgen, and M. J. Schöning. *Experimental and numerical evaluation of interdigitated electrode array for monitoring gaseous sterilization processes.* Dresdner Sensor-Symposium. Dresden, Germany. 07. - 09.12.2015.

[7] J. Oberländer, Z. B. Jildeh, P. Kirchner, L. Wendeler, A. Bromm, H. Iken, P. H. Wagner, M. Keusgen, and M. J. Schöning. *Study of interdigitated electrode array using experiments and FEM models for evaluation of sterilization processes.* Engineering of Functional Interfaces. Hannover, Germany. 06. - 07.07.2015.

[8] J. Oberländer, J. Arreola, A. Bromm, L. Wendeler, H. Iken, M. Palomar Durán, A. Greeff, M. Bäcker, M. Keusgen, and M. J. Schöning. *Überwachung von Sterilisationsprozessen in der Lebensmittelindustrie mittels einer Biosensor-Lösung.* 9. Deutsches BioSensor-Symposium. München, Germany. 11. - 13.03.2015.

[9] J. Oberländer, A. Bromm, L. Wendeler, H. Iken, M. Palomar Durán, A. Greeff, P. Kirchner, M. Keusgen, and M. J. Schöning. *Towards a biosensor to monitor the sterilization efficiency of aseptic filling machines.* Engineering of Functional Interfaces. Jülich, Germany. 14. - 15.07.2014.

[10] J. Oberländer, P. Kirchner, M. Keusgen, and M. J. Schöning. *Flexible Polymid-basierte kalorimetrische Gassensoren zur Detektion von Wasserstoffperoxid in Sterilisationsprozessen aseptischer Abfüllanlagen.* Sensoren und Messsysteme. Nürnberg, Germany. 03. - 04.06.2014.

[11] J. Oberländer, P. Kirchner, M. Raue, T. Mang, M. Keusgen, and M. J. Schöning. *Investigation of polymers as passivation materials for H_2O_2 gas sensors.* International Meeting on Chemical Sensors. Buenos Aires, Argentina. 16. - 19.03.2014.

[12] J. Oberländer, P. Kirchner, S. Reisert, and M. J. Schöning. *Kalorimetrische Gassensoren zur H_2O_2-Detektion in aseptischen Sterilisationsprozessen.* Dresdner Sensor-Symposium. Dresden, Germany. 07. - 09.12.2013.

[13] J. Oberländer, P. Kirchner, H.-G. Boyen, and M. J. Schöning. *Detection of hydrogen peroxide vapor by use of manganese(IV) oxide as catalyst for calorimetric gas sensors.* Engineering of Functional Interfaces. Hasselt, Belgium. 08. - 09.07.2013.

[14] J. Oberländer, P. Kirchner, S. Reisert, and M. J. Schöning. *Intelligente, Sensor-gestützte Qualitätskontrolle bei Lebensmittelverpackungen im Bereich Aseptik-Food.* Nano auf dem Teller? Saarbrücken, Germany. 12. - 13.06.2013.

Acknowledgments

This work would not have been successful without the support of a number of people.

My deepest gratitude belongs to Prof. Dr. Michael J. Schöning to give me the opportunity for this PhD project. His willingness to correct the numerous publications, abstracts, posters, presentations and the final version of this thesis. For a lot of professional discussions as well as conversions with some cold beers. Moreover, to give me the chance to travel and present my results all over the world. It was a pleasure to be part of your team at the Institute of Nano- and Biotechnologies.

Prof. Dr. Michael Keusgen I would like to express my gratitude for his support during the PhD project and to be an interested supervisor. His valuable advice and great support pushed this work to success. Additionally, I would like to thank him for the opportunity for this PhD thesis.

Prof. Dr. Arno Förster is acknowledged for supporting the impedance analyzes and providing laboratory equipment at the laboratory of technical physics.

Prof. Dr. Petra Siegert and Prof. Dr. Johannes Bongaerts is acknowledge for supporting the microbiological experiments.

My special thanks belongs to Prof. Hans-Gerd Boyen for his support performing the XPS analyzes and his willingness to answer all open questions and his interest in this work.

I would like to thank Marlena Mayer and Anton Greeff for the support throughout the project and their interest in this work.

I am very grateful to Dr. Patrick Kirchner to push my scientific curiosity, starting from my bachelor thesis. His never-ending interest in this work and many scientific discussions also with some beers in Norway after extensive measurement days.

I would like to thank all my colleagues I have worked with at the Institute of Nano- and Biotechnologies. In particular, Prof. Dr. Arshak Poghossian and Prof. Dr. Torsten Wagner for their interest and scientific advise. Denise Molinnus for fruitful scientific coffee-discussions and being a friendly, open-minded person. Heiko Iken for technical support during the sensor development and fabrication. David Rolka for his support performing SEM analyzes. Dr. Farnoosh Vahidpour for scientific discussions and her interest in this work. Julio Arreola as project partner and "officemate". Former and current PhD students and colleagues, Dr. Christina Huck, Dr. Matthias Bäcker, Dr. Sebastian Schusser, Dr. Frederik C. Werner, Dr. Steffen Reisert, Melanie Jablonski and René Welden.

Many thanks to Zaid B. Jildeh for his enthusiasm during project and paper discussions, and giving inside into Jordan's food culture.

I would like to thank all the students for their valuable contributions and scientific discussions throughout the project. Many thanks to: Kshitij Thurakia, Luisa Wendeler,

Christina Hansen, Alexander Bromm, Tobias Kerschgens, Rishabh Shrivastava, for your great support.

Finally, I like to thank my family and friends for their support during my student and PhD time, this work would not have been possible without you.

Thank you all for your individual support!

This present thesis would not have been possible without financial support. Hence, I express my gratitude to:
The German Federal Ministry of Education and Research (BMBF) for financial support of the project: "ImpediPack" (Fund. No.: 03FH012I3).
The European Union and the Ministry of Economic Affairs, Energy and Industry of the State of North Rhine-Westphalia for support of the project "EfficientSterile" (Fund. No.: EFRE-0800079) within the operational program EFRE.NRW 2014-2020.
The FH Aachen for financial support in the frame of promotion of PhD students.

Curriculum vitae

The curriculum vitae is not part of the online version.

The curriculum vitae is not part of the online version.